Radiobiology
and
Radiation Safety

Radiobiology

and

Radiation safety

TABLE OF CONTENTS

RADIOGENIC BREAST CANCER RISK PROJECTION FOR THE GEORGIAN FEMALE POPULATION

*Giorgi. Ormotsadze[1,2], Tamar. Sanikidze[2,1], Alla. Zedginidze[1], Levan Ormotsadze[1]

[1] [2]Beritashvili Center of Experimental Biomedicine, Laboratory of Radiation Safety Problems
[2] Tbilisi State Medical University

*Corresponding author: g.ormotsadze@lifescience.org.ge

ABSTRACT: *This paper presents the results of the initial stage of the research cycle, aimed at adapting the methodology for assessing radiogenic risk to the specifics of the Georgian population. This adaptation aims to equip practicing radiologists, medical workers, and nuclear and radiation safety regulators with appropriate theoretical and methodological bases. Data from the National Center for Disease Control and Public Health of Georgia for 2017-2019, regarding the age structure of breast cancer incidence among the female population of Georgia, and demographic data from the National Statistical Office of Georgia for 2017-2019, were used. Comparative analysis utilized data from The Surveillance, Epidemiology, and End Results (SEER) Program of the National Cancer Institute (NCI) of the USA and Cancer Statistics in Korea. Competing risk methodology was employed to estimate the age-conditional and lifetime baseline risk (LBR) of developing breast cancer. The US National Cancer Institute's DevCan 6.9.0 software was used for computation.*

The methodology described in the 2006 report of the National Academies of Sciences' BEIR VII Committee was used to estimate the age-conditional and Lifetime Attributable Risk (LAR) of radiogenic breast cancer. US National Cancer Institute software RadRat (version 4.3.1) and the R package for lifetime attributable risk estimation (LARisk) were used for computation. Monte Carlo simulation techniques were applied to estimate uncertainties in risk and subjective uncertainties under various assumptions. It was revealed that the lifetime baseline cancer risk for the hypothetical population of Georgia is 6.5% (95% CI: 6.2%-6.9%), for the US white non-Hispanic female population is 14.1% (95% CI: 13.99%-14.23%), and for the Korean female population, it is approximately 4.2%. For women in Georgia, the United States, and Korea irradiated with a dose of 10 mGy, the lifetime attributable risk is approximately the same, varying between 120-140 cases per 100,000 persons. The Lifetime Fractional Risk (LFR), defined as the ratio of lifetime attributable risk to lifetime baseline risk, is 3.5 times higher in the American white non-Hispanic female population than in Korea, and 2 times higher than in the female population of Georgia.

Key words*: Radiogenic breast cancer risk, Georgian female population, Radiation Protection

INTRODUCTION

Implementing the scientific support system (risk management) for decision-making in the health sector is the main priority of the 2022-2030 national strategy in the healthcare field (Resolution #230 of the Government of Georgia dated May 2, 2022). The strategy's implementation in the medical exposure field started in 2022 [1].

The International Commission on Radiological Protection stated that the intended effective dose should be used as a principal protection quantity for establishing radiological protection guidance. However, it should not be used to assess risks of stochastic effects in retrospective situations for exposures in identified individuals and epidemiological evaluations of human exposure [2,3]. In these cases, an age- and sex-specific radiogenic carcinogenic risk assessment methodology should be used. The population-specific, age- and sex-dependent radiogenic risk assessment methodology was initially developed by the National Research Council (US) Committee on the Biological Effects of Ionizing Radiation (BEIR) of the National Academy of Sciences of the United States of America [4]. This methodology is based on a study of long-term radiation-related health effects in Japanese atomic bomb survivors and US demographic and health data. At the modern stage, different modifications of this methodology have been developed under various assumptions and approximations for the populations of the USA, Great Britain, France, South Korea, Japan, and others [2,5,6,7]. To fulfill its mandate to provide consultations and assistance to public health during radiation emergencies, the medical consequences of the Fukushima nuclear incident were evaluated using this methodology by the expert group of the World Health Organization [9]. This paper presents the results of the initial stage of the research cycle, aimed at adapting the methodology for assessing radiogenic risk to the specifics of the Georgian population. This adaptation aims to equip practicing radiologists, medical workers, and nuclear and radiation safety regulators with appropriate theoretical and methodological bases.

MATERIALS AND METHODS

Data from the National Center for Disease Control and Public Health of Georgia for 2017-2019 on the age structure of breast cancer incidence among the female population of Georgia, and demographic data of the population of Georgia for 2017-2019 from the National Statistical Office of Georgia, were used. Data from The Surveillance, Epidemiology, and End Results (SEER) Program of the National Cancer Institute (NCI) of the USA and Cancer Statistics in Korea [15] were used for comparative analysis. Competing risk methodology was used to estimate the age-conditional and lifetime baseline risk (LBR) of developing breast cancer. The US National Cancer Institute's DevCan 6.9.0 software was used for computation. The methodology described in the 2006 report of the National Academies of Sciences' BEIR VII Committee was used to estimate the age-conditional and lifetime attributable risk (LAR) of radiogenic breast cancer. US National Cancer Institute software RadRat (version 4.3.1) and the R package for lifetime attributable risk estimation (LARisk) were used for computation. Monte Carlo simulation techniques were used to estimate uncertainties in risk and subjective uncertainties under a range of assumptions.

Results: First, let's consider the basic provisions of the BEIR VII approach to make clear all the assumptions and approximations that the methodology is based on. In general, in the direct assessment of health risk in the exposed population, two models are considered: excess absolute risk - $EAR(t) = \lambda_E(t) - \lambda_U(t)$, which is a difference in cancer incidence rates of the exposed and unexposed populations, and excess relative risk, which is defined as: - $ERR(t) = [(\lambda_E(t)/ \lambda_U(t)) -1]$; The incidence rates of the exposed and unexposed population in this case are related by the equation

$$\lambda_E(t) = \lambda_U(t) \{1 + ERR(t)\}$$

In terms of the mechanisms of radiation carcinogenesis, the first model reflects the nature of radiation as a cancer initiator, and the second as a cancer promoter.

BEIR VII methodology is based on statistical approximation of existing experimental and epidemiological data with classes of functions based on the most general regularities of radiation carcinogenesis. Based on Radiobiological considerations, it is postulated that for low doses of radiation with low LET (linear energy transfer), the risk of disease for a person exposed to dose d depends on a linear or linear-quadratic function of the form: $f(d) = \alpha_1 * d + \alpha_2 * d^2$ where α1 and α2 are parameters to be estimated from the epidemiological data. In linear approximations, the dose-effect function of cancer incidence in the experimental population is described by the expressions:

$$\lambda(s, a, d) = \lambda(s, a) + [1 + \beta_S^{ERR} * ERR(e, a) * d]$$

$$\lambda(s, a, d) = \lambda(s, a) + \beta_S^{EAR} * EAR(e, a) * d$$

where $\lambda(s, a)$ - sex-dependent baseline cancer incidence rate, βs - sex-dependent coefficient determining dose-effect dependence. The influence of dose-effect modifying factors - age at irradiation (e) and attained age (a) is described by the expressions:

$$ERR(e, a) \text{ or } EAR(e, a) = \exp(\gamma e) * a^\eta$$

Coefficients γ and η are empirical and based on epidemiological and statistical principles [18]. In BEIR VII approach the lifetime attributive risk (LAR), for each cancer sites, is the main measure of risk.

$$LAR^J(d, e) = \int_{e+L}^{100} M^J(d, e, a) * S(a)\Big/ S(e) * da$$

where *S(a)* is the probability of surviving to age a, and L is the minimum latency period of developing cancer. Index J-corresponds to either the EAR or ERR model, and accordingly:

$$M^{EAR}(d, e, a) = \beta_S^{EAR} * EAR(e, a) * d$$

$$M^{ERR}(d, e, a) = \beta_S^{ERR} * ERR(e, a) * d * \lambda(s, a)$$

Coefficients βs, γ, and η for each individual sex and each individual cancer site were calculated from health data of Japanese atomic bomb survivors. [18].

The key issue in risk assessment is the legality of applying the estimates obtained based on the study of a specific population, to other populations that may have different genetic characteristics and lifestyles, as well as different baseline cancer risks. In this regard, it should

be noted that the BEIR VII methodology does not take into account the interpopulation radiosensitivity factor and the possible causal relationship between radiogenic and baseline carcinogenesis mechanisms, and adapting the results obtained in Japanese atomic bomb survivors to the specificity of the United States population (risk transport) performs by combining EAR and ERR models with appropriate weighting coefficients (w):

$$LAR(d,e) = w * LAR^{ERR}(d,e) + (1-w) * LAR^{EAR}(d,e)$$

From the positions above, for the assessment of LAR and age-conditional risk for the population of Georgia, it is necessary to bring the demographic data of the population of Georgia and the *cancer statistics* under the requirements of the methodology.

Demographic data

As it was clear from the above discussion, for population-specific risk assessment, the degree of detailing of demographic data and population morbidity is of principal importance, this primarily concerns the age-dependent intensity of population mortality, according to which life tables are calculated. As it was clear from the above discussion, for population-specific risk assessment, the degree of detailing of demographic data and population morbidity is of principal importance, this primarily concerns the age-dependent intensity of population mortality, according to which life tables are calculated. Life tables are currently constructed using age-specific central mortality rates derived from vital statistics and census data. Over the age of 85, the reliability of mortality rates is compromised by incorrect age reporting and lack of birth records for extremely elderly people.

The life tables of the population published by the National Statistical Service of Georgia, as well as the life tables of many other countries, closed with the category 85 years, while in Georgia approximately 30-35% of the female population survives beyond the age of 85 years. Consequently, a life table inadequately describes the mortality structure of a significant proportion of the population. To expand the open age interval of the life table of the Georgian population to 100 years, we used the procedure developed by Coale and Kisker [10], which predicts mortality by extrapolating mortality in a range close to 85 years. The developed model has a well-founded theoretical basis [13,14] and has been verified on the populations of the United States and Canada [11,12]. The procedure relies upon a function called the age-specific rate of mortality change with age (k_x). By definition,

$$k_x = ln(m_x) - ln(m_{x-1}) (1)$$

m_x - central death rate by x age interval.

The first important assumption is that k above 85 years should be linear,

$$k_x = k_{85} + (x-85) * s   (2)$$

Where s denotes the slope of the change in k_x.

By combining these formulas, we get the expression:

$$m_x = m_{84} * exp\left[\sum_{y=85}^{x} (k_{85} + (y-85)*s) (3)\right]$$

through which it is possible to calculate m_x for any x>85 age interval if k_{85} and s are known. k_{85} is calculated from the central mortality rate in age intervals close to x=85

$$k_{85} = (1/4) * log[m_{86}/m_{82}] (4)$$

s - Calculated from the expression (3),

$$s = \left(-1/325\right) * [log(m_{84}/m_{110}) + 26 * k_{85}] (5)$$

where m_{110} denotes the cut-off age for the given population. According to the assumption of Coale and Kisker, the cut-off age is determined to be about 110 years, while m_{110} is considered equal to 1 for men and 0.8 for women.

For the 2017-2019 population of Georgian women, the parameters estimated by the above procedure have the following values: $k_{85} = 0.1$; $m_{84} = 0.1132$; s=-0.002. It should be noted that the values of s for US White end US Black Females, estimated based on demographic data and verified by Medicare Data are equal respectively −0.00243 and −0.00151 [11],

Figure 1. and Figure 2. presents the age structure of the central mortality rate of the female populations of Georgia, the United States, and South Korea, and the survival rate estimated by the method of [10].
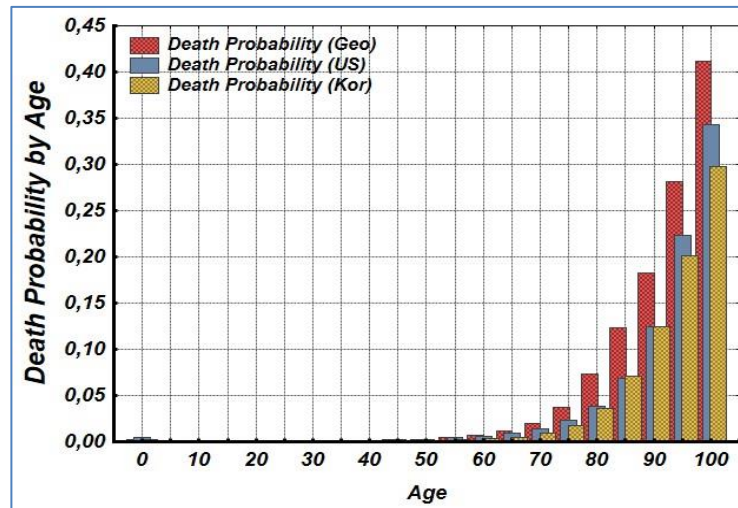
Figure 1. Mortality probability of the female populations of Georgia, the United States, and South Korea. (2015-2019 US white non-Hispanic women, Georgian 2015-2019 women's populations, and South Korea 2010 women's populations.)
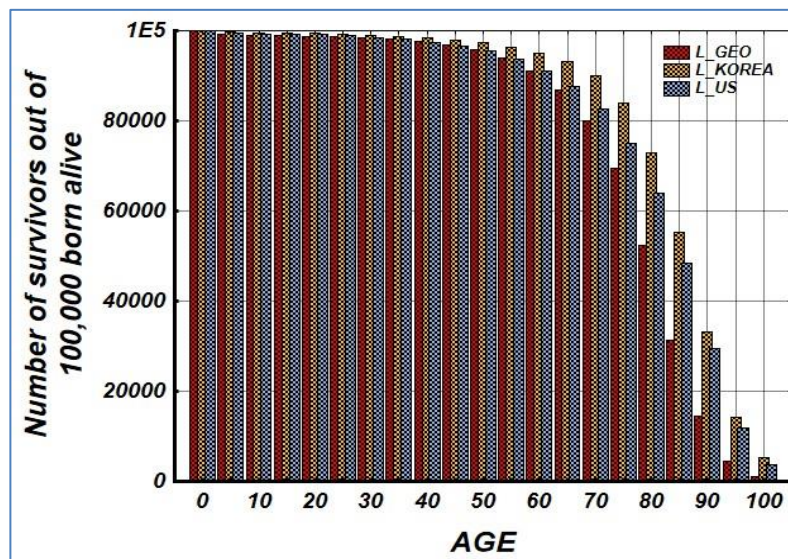
Figure 2. The survival rate of the female populations of Georgia, the United States, and South Korea. (2015-2019 US white non-Hispanic women, Georgian 2015-2019 women's populations, and South Korea 2010 women's populations.)

As can be seen from the graph, the central mortality rate in the female population of Georgia is significantly higher than in the female population of the United States and especially South Korea, this is reflected in the survival rate as well. The threshold age of the female population of Georgia is about 100 years, this allows the use of the last closed interval in the calculations, which significantly simplifies the calculations and reduces the level of uncertainty in the estimates.

Baseline Breast Cancer Risk

The baseline breast cancer risk is not directly factored into the formulas for lifetime and age-conditional radiogenic cancer risk. However, it is important to examine how these indicators vary between different populations concerning radiation-related cancer risk. This analysis helps clarify the mechanisms of radiation-induced carcinogenesis and the population-based predisposition of cancer. To estimate lifetime and age-conditional probabilities of developing breast cancer in a hypothetical cohort for the Georgian population, we use methodology [19] which is currently used by the US National Cancer Institute to review cancer statistics from the Surveillance, Epidemiology, and End Results (SEER) program [https://seer.cancer.gov/];

In this approach the probability of getting a first cancer in the age interval [t_0, t] given alive and cancer-free until just before t_0 is:

$$P(t_0, t) = \left. \frac{\int_{t_0}^{t} \lambda_c(u)S(u)du}{} \right/ S(t_0) \quad (6)$$

Where $\quad S(u) = exp\left\{-\int_0^u [\lambda_c(a) + \lambda_o(a)]da\right\}$

λ_c (a) is the rate of first cancer per person-years alive and cancer-free at age **a** and λ_o (a) is the rate of deaths per person-years alive *and cancer free* at age **a.** If we take into account that $exp\left\{-\int_0^u [\lambda_c(a)]da\right\} \approx 1$ and to a crude approximation ignore it, then S(u) essentially coincides with survival rate and the meaning of the probability functions P(t_0,t) becomes clear. Figure 3. and Figure 4. present the distributions of Baseline age-conditional and lifetime baseline breast cancer risk (LBR) *.
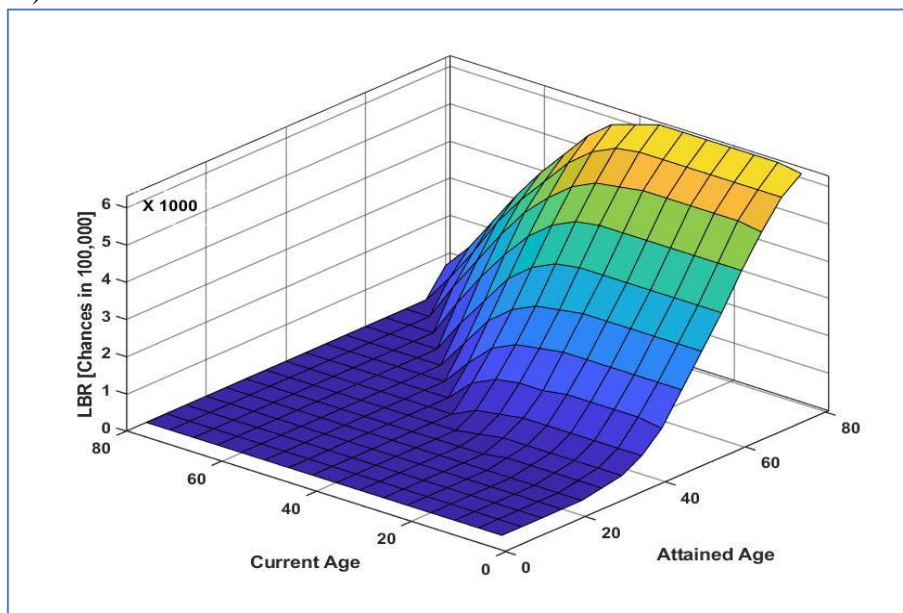
Figure 3. Age-conditional probabilities of developing breast cancer in the hypothetical cohortfor Georgian population
* Number of individuals in the hypothetical cohort, diagnosed with cancer to the end of the expected lifetime (100 years), given nndiagnosed at current Age.
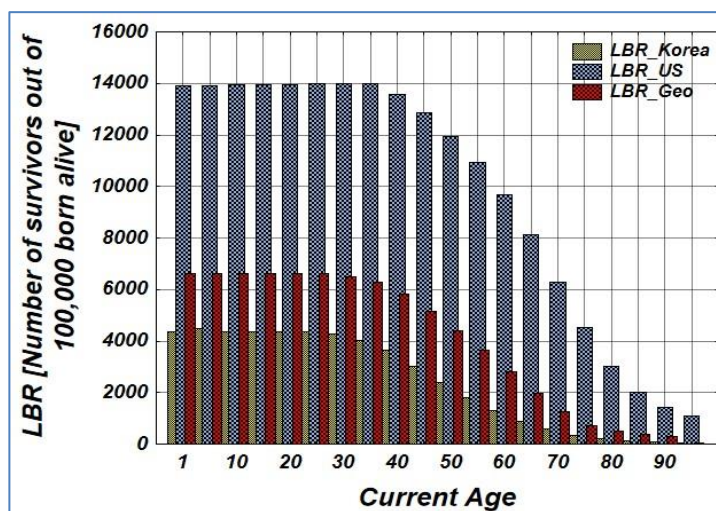
Figure 4. Lifetime baseline risk in 2015-2019 US white non-Hispanic women, Georgian 2015-2019 women's populations, and South Korea 2010 women's populations.

As can be seen from the distribution, lifetame baseline cancer risk for the hypothetical population of Georgia is equal to 6.5%, 95%CI (6.2%-6.9%) , and for the population of American women is equal to 14.1% 95%CI (13.99%-14.23%), lifetame baseline cancer risk for the Korean female population is smaller and equal to about 4.2%.

As can be seen from the expression (6), lifetime baseline risk depends on both the survival rate and the level of cancer incidence in a specific population, although the main determining factor is the incidence, which can be easily confirmed by a joint analysis of lifetime baseline risk (Figure 4.), Survival rate and Age-conditional cancer incidence rate in populations (Figure 5). From these positions, the identification of the factors that determine the level of cancer incidence in the population acquires both theoretical and practical relevance. A comparative analysis of the patterns of oncology in the American and Korean populations can give us some insight into the factors responsible for the practically two-fold difference in the risk of developing breast cancer in the Georgian and American women's populations;
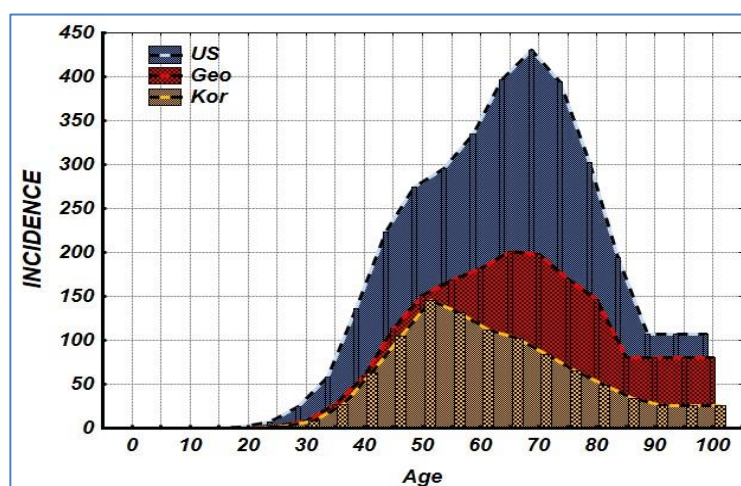
Figure 5. Age-conditional cancer incidence rate in 2015-2019 white non-Hispanic women, Georgia 2015-2019, and South Korea 2010 female populations

The incidence of cancer has been studied in white and black Americans, Korean immigrants, and native Koreans [15,16,17]. Data from the Surveillance, Epidemiology, and End Results (SEER) program and the International Agency for Research on Cancer were used. It was revealed: that in men the risk of stomach, liver, gallbladder, larynx, and esophageal cancer has sharply declined in Korean-American men compared with their native counterparts while prostate, colon, and rectum cancer risk has increased. In women, there was a decrease in stomach, liver, gallbladder, and cervical cancers, and breast, lung, colon, rectum, and endometrial cancers increased. It is worth noting that the incidence of breast cancer among Korean immigrant women, although increasing, remains at a much lower level than among white Americans; Age-adjusted cancer rates in Koreans are equal to 50.7, while in white Americans their value reaches 152.9 [16,17]. These studies highlight the leading role of nutritional diet and environment, as well as social factors in the risk of several cancer site, although the role of genetic factors in breast localization is also clearly defined.

Radiogenic Breast Cancer Risk

For breast cancer, the BEIR VII Committee used only an EAR model to quantify risk. The model was based on a pooled analysis of eight cohorts, including the LSS cohorts [18]. The parameterized function of EAR has the following form:

$$EAR(d,e,a) = \beta * d * exp\left[\frac{\gamma(e-25)}{10}\right]\left(\frac{a}{50}\right)^{\eta}$$

where $\beta = 10$; $\gamma = -0.50$; $\eta = 3.5$ for $a < 50$ and 1.1 for $a \geq 50$.

For the irradiated population, the dependence of lifetime attributable risk on age-at-exposure and radiation dose was calculated using the following expression:

$$LAR^{Breast}(d,e) = \beta * d * \int_{e+L}^{100} exp\left[\frac{\gamma(e-25)}{10}\right]\left(\frac{a}{50}\right)^{\eta} * \frac{S(a)}{S(e)} * da$$

The latency period L was assumed as 5 years.
For the populations of women in Georgia, the United States, and Korea irradiated with a dose of 10 mGy, the lifetime attributable risk is approximately the same within the margin of error and varies between 120-140 cases in a cohort of 100,000 persons. Small inter-population differences in lifetime attributable risk estimates are explained by differences in inter-population survival rates [20] (Figure 6.)
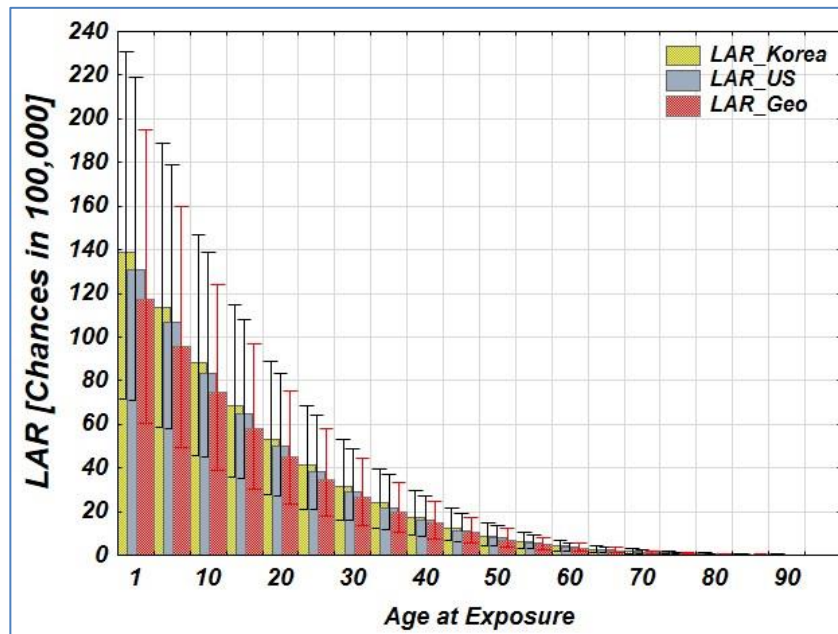
Figure 6. Distributions of lifetime attributable risk for female populations of Georgia, the United States, and Korea irradiated at a dose of 10 mGy. Whiskers - uncertainty range (95% CI)

We get a completely different picture if we consider the Lifetime Fractional Risk (LFR), which is defined as the ratio of lifetime attributable risk and lifetime baseline risk [21] – in the American white non-Hispanic female population is 3.5 times higher than that of Korea, and 2 - times higher than in the female population of Georgia (Figure 7.).
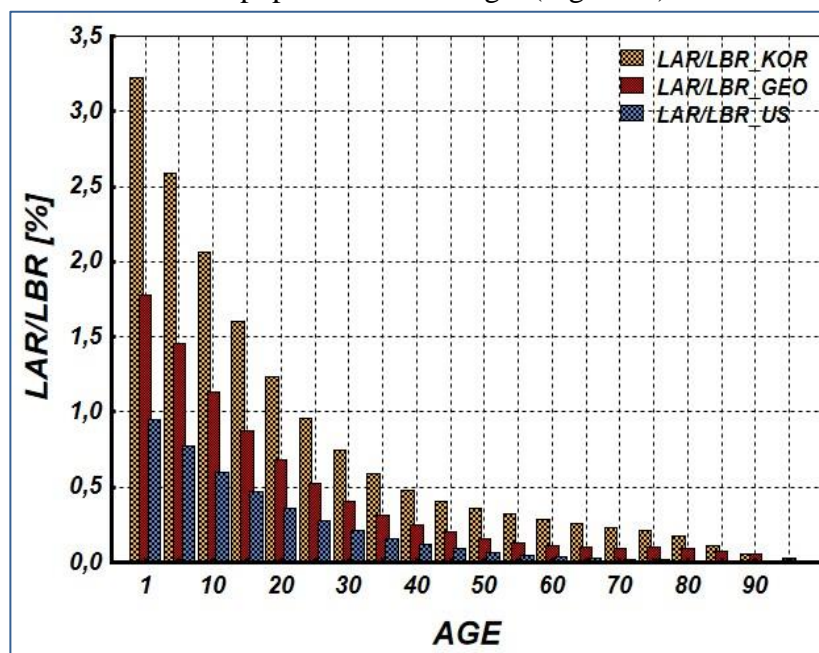
Figure 7. Distributions of lifetime fractional risk (LFR) for female populations of Georgia, the United States, and Korea irradiated at a dose of 10 mGy.

DISCUSSION

We will discuss those assumptions and approximations that can modify the results, uncertainties related to them, and possible ways to minimize these uncertainties for the population of Georgia. First of all, it should be noted that the main sources of uncertainties considered in the BEIR VII methodology, and its various modifications include:

1. Coefficients of ERR and EAR models
2. Dose and dose rate factor (DDREF)
3. The latent period of cancer development in the post-radiation period
4. Radiation dose and dose power
5. Factors related to the quality of medical statistics and demographic data
6. Risk transport coefficient

The algorithmic base and software used in this work for uncertainty estimation use the Monte Carlo method and values of parameter variability obtained at the modern stage in radiation epidemiology.

o The main dose-effect factor β - 10.00 (7.00–14.20) is considered with its variability ranges, while the corresponding coefficients of the modifying factors; $\gamma = -0.50$ (irradiation age) and $\eta = 3.50$ (attained age) are considered as fixed quantities and therefore do not contribute to the uncertainty.

o The distribution of DDREF is described by log-normal distribution (mean= 1.5, std=1.35)

o The latent period of breast cancer development usually represents an S-shaped curve with a parameter in the center of the S-shaped function and a range of variability from 2.5 to 7.6 years.

o Radiation dose uncertainty can be applied to a fixed value

o Uncertainties related to demographic data and medical statistics: the software we use does not provide for the analysis of uncertainties related to medical statistics and demographic data, especially the analysis of time trends of these data, which is especially important in the case of long-term prognosis. From this point of view, it is appropriate to develop new software that ensures the consideration of the uncertainties related to the demographic and medical statistics of Georgia in the risk assessment.

The subject of detailed consideration is the analysis of the uncertainty associated with the weight coefficient (w) of the ERR and EAR models, which are used for interpopulation risk transfer., and determine the contribution of age-dependent and age-independent members of risk to LAR. As mentioned above, the conceptual basis of the BEIR VII methodology is the assumption that the sex-specific main component of the dose-effect (β) is invariant for different populations, which implies that the inter-population difference in radiosensitivity is leveled in the dose-effect relationship, although it is somewhat reflected in the high range of its uncertainty, but as it is known, populations differ in the basic (background) level of cancers of

different sites, therefore, the generalizability of radio-epidemiological- data obtained in Japanese LSS cohorts to other populations depends on:

1) Are there correlations between background and radiogenic carcinogenesis risks, that is, if we formulate it differently, is there a causal relationship between genetic predisposition to cancer and genetic susceptibility to radiogenic cancer;

2) What is the share of endogenous (genetics, age, sex) and exogenous (chemical factors, diet, lifestyle, etc.) factors in the background level of cancer incidence and its age structure in a specific population? The latter has an independent scientific and practical value in terms of developing a national cancer prevention strategy for any country [22-25]

The issue is particularly relevant in terms of the prognosis of radiogenic breast cancer because it is modeled only based on the EAR model (WEAR=1), which completely excludes the contribution of the population-specific factor of onco-incidence and therefore a certain correction of the risk according to the population specificity. This assumption was mainly based on the study of Preston and colleagues [18], where the age structure of radiogenic breast cancer in the American and Japanese populations was comprehensively analyzed (it should be noted that the background level of breast cancer in the American population almost twice as high as in the Japanese population). It was revealed that the β estimated by the ERR model was equal to 1.44 for the LSS cohorts, and 0.51 for the American cohorts, and the level of the LAR estimated by the EAR model was identical for all four studied cohorts. Based on the opinion that the increase in cancer incidence in different populations irradiated with the same doses should be identical, the use of the EAR model was considered more correct. At that time, this argument was considered sufficient, however, the study of genetic susceptibility to radiation tumorigenesis is ongoing and is still the subject of intensive research. Based on these studies, the recommendations of the International Commission on Radiological Protection #103 of 2007 conclude that; "Although the Commission recognizes that weakly expressing variant cancer genes may, in principle, be sufficiently common to impact upon population-based estimates of radiation cancer risk, the information available is not sufficient to provide a meaningful quantitative judgment on this issue".

The same position is shared by The Advisory Group on Ionising Radiation (UK), of the AGIR report (AGIR, 2013, www.gov.uk)), „Although theoretical and empirical considerations suggest that individuals differ in their response to radiation exposure, no strong and consistently validated biomarkers of either tissue or stochastic effects have been identified to date. Studies of functional assays and candidate SNPs have been largely inconclusive"

The United Nations Scientific Committee on the Effects of Atomic Radiation 2020/2021 report [26] indicates that such modifiers of low dose effects as Genomic instability, bystander effects, adaptive response, which can be considered as possible mechanisms of individual radiosensitivity in the range of small doses, are still not clear and are insufficiently coherent to adopt for risk assessment purposes.

On the other hand, in the last period, solid evidence has been obtained that questions the correctness of using the EAR model for breast cancer risk assessment [21], in particular, the incidence of breast cancer among the Japanese population is constantly increasing. As a result, in the Life Span Study (LSS) of Japanese atomic bomb survivors, the ERR model currently

predicts similar dose-dependent increases among different birth cohorts, whereas the EAR model predicts different dose-dependent increases among different birth cohorts. This contradicts the findings of Preston and colleagues [18]. These circumstances point to the need for further elaboration and development of radiogenic carcinogenic risk models.

CONCLUSION

Considering the level of uncertainty in modern concepts of individual and interpopulational radiosensitivity mechanisms, as well as the problems that have recently been revealed in methodological approaches to interpopulational transport of radiogenic breast cancer risk, we consider it appropriate to consider the issue of using Lifetime fractional risk as an additional criterion for decision-making and regulatory control in medical exposure, understanding the problems related to the ethical aspects of the issue.

REFERENCES
[1]. Resolution No. 226 of 2022 of Georgian Government on Radiation Safety Requirements in Medical Settings
[2]. The 2007 Recommendations of the International Commission on Radiological Protection, PUBLICATION 103, Annals of the ICRP, 2007
[3]. Radiation Protection in Medicine, ICRP PUBLICATION 105, Annals of the ICRP, 2007
[4]. National Research Council. 2006. Health Risks from Exposure to Low Levels of Ionizing Radiation: BEIR VII Phase 2. Washington, DC: The National Academies Press.
[5]. EPA Radiogenic Cancer Risk Models and Projections for the U.S. Population, U.S. Environmental Protection Agency Office of Radiation and Indoor Air, April 2011, 1200 Pennsylvania Ave., NW Washington, DC 20460
[6]. Amy Berrington de Gonzalez at all, RadRAT: A Radiation Risk Assessment Tool for Lifetime Cancer Risk Projection, J Radiol Prot. 2012 September; 32(3):
[7]. Juhee Lee at all, LARisk: An R package for lifetime attributable risk from radiation exposure, **doi:** https://doi.org/10.1101/2022.02.21.22271307
[8]. Health risk assessment from the nuclear accident after the 2011 Great East Japan Earthquake and Tsunami based on a preliminary dose estimation. World Health Organization; 2013. (http://www. who.int/ionizing_radiation/pub_meet/fukushima_risk_assessment_ 2013/en)
[9]. International Atomic Energy Agency. Emergency preparedness and response. In: Joint radiation emergency management plan of the international organizations. EPR-JPlan 2013. Vienna: IAEA. (http://www-pub.iaea.org/MTCD/publications/PDF/EPRJplan2013 _web.pdf)
[10]. Coale AJ, Kisker EE. Defects in data on old-age mortality in the United States: New procedures for calculating mortality schedules and life tables at the highest ages. Asian and Pacific Population Forum 1990; 4(1): 1-31.
[11]. Method for Constructing Complete Annual U.S. Life Table, U.S. Department of health and human services Centers for Disease Control and Prevention National Center for Health Statistics, Hyattsville, Maryland December 1999
[12]. Life Tables Canada, Provinces and Territories 1995-1997, Statistics Canada Health Statistics Division, 2002

[13]. Horiuchi S, Wilmoth JR. Deceleration in the age pattern of mortality at older ages. Demography. 35:391–412. 1998.

[14]. Horiuchi S, Wilmoth JR. Age patterns of the life table aging rate for major causes of death in Japan, 1951–1990. Journal of Gerontology: Biological Sciences. 52A:B67–B77. 1997.

[15]. Mee Joo Kang at all, Cancer Statistics in Korea: Incidence, Mortality, Survival, and Prevalence in 2020, Cancer Res Treat. 2023;55(2):385-399

[16]. Joanne Lee, at all, Cancer incidence among Korean-American immigrants in the United States and native Koreans in South Korea, Cancer Control, 2007 Jan;14(1):78-85

[17]. Korean americans & cancer health brief, Asian & Pacific Islander American Health Forum 450 Sutter Street, Suite 600, San Francisco, 2009

[18]. Preston DL, A Mattsson, E Holmberg, R Shore, NG Hildreth, JD Boice Jr. 2002b. Radiation effects on breast cancer risk: a pooled analysis of eight cohorts. Radiat Res 158: 220-235.

[19]. Michael P. Fay, at all, Age-conditional probabilities of developing cancer, Stat Med. 2003 June 15; 22(11): 1837–1848

[20]. FrancisA. Cucinotta1* & Premkumar B. Saganti2, Race and ethnic group dependent space radiation cancer risk prediction, Scientific Reports (2022) 12:2028 | https://doi.org/10.1038/s41598-022-06105-x.

[21]. L. Walsh et al, A Framework for Estimating Radiation-Related Cancer Risks in Japan from the 2011 Fukushima Nuclear Accident, Radiation research 182, 556–572 (2014)

[22]. G Kvaratskhelia, E Tikaradze, M Buleishvili, G Sharashenidze, G Ormotsadze, The structure and risk of chronic morbidity in some villages of the upper Imereti region of West Georgia and their molecular and cytogenetic markers, Georgian Medical News, Issue 283, 97-103, 2018

[23]. Ekaterine Tikaradze, Tamar Sanikidze, G Ormotsadze at all, bayesian sample size determination for cytogenetic studies in a population, Georgian Medical News, Issue 300, 124-128, 2020

[24]. Ekaterine Tikaradze, Tamar Sanikidze, G. Ormotsadze, at all, bayesian modelling and inference of mixtures of distributions of micronuclear buccal cells in the population of sachkhere district's villages. Georgian Medical News, Issue 316-317, 154-158, 2021

[25]. Ekaterine Tikaradze, Tamar Sanikidze, G Ormotsadze at all, Complex study of Cancer Morbidity and Inflammatory Markers, Presented in the Blood Serum of the Rural Population of Sachkhere District of Georgia, Asian Pacific Journal of Cancer Prevention: APJCP, vol 23, issue 6, 2022

[26]. Sources, effects and risks of ionizing radiation, United Nations Scientific Committee on the Effects of Atomic Radiation, UNSCEAR 2020/2021 Report to the General Assembly, New York, 2021

[27]. Chris Kalman & Deborah Oughton, Ethical considerations related to radiosensitivity and radiosusceptibility, International journal of radiation biology 2020, Vol. 96, No. 3, 340–343

NUCLEOLAR DYNAMICS: REARRANGEMENT OF NUCLEOLUS ASSOCIATED CONDENSED CHROMATIN UNDER DNA DAMAGE INDUCED BY DIFFERENT DOSES OF γ-IRRADIATION
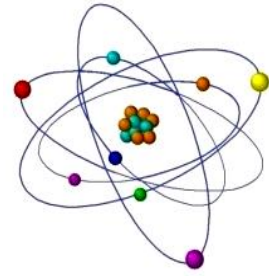
[1,2]Lili Nadaraia, [1]Vera Okuneva, [3]Mikheil Gogebashvili, [3]Nazi Ivanishvili, [1]Pavel Tchelidze*

[1]Carl Zeiss Education and Scientific Center, New Vision University, Georgia
[2]Republic Center of Structure Research, Georgian Technical University, Georgia
[3]I.Beritashvili Center of Experimental Biomedicine,
Laboratory of Radiation Safety Problems, Georgia

*Corresponding author: pavel.tchelidze@univ-reims.fr

ABSTRACT: *The nucleolus, a vital nuclear compartment, orchestrates ribosome biogenesis by producing polycistronic transcripts. It integrates gene-rich chromosomal domains, forming nucleolus-associated DNA (naDNA) or nucleolus-associated chromatin (NAC). The nucleolus hosts molecular machinery that guides the transcription of ribosomal genes (r-genes), pre-rRNA processing, and ribosome assembly. These are organized into nucleolar components (NCs). NAC, consisting of intra-nucleolar condensed chromatin (ICC) and peri-nucleolar condensed chromatin (PCC), is less studied, and its functional significance in establishing and maintaining the global nucleolar structure still needs to be elucidated. Previous studies demonstrated the spatiotemporal reorganization of NAC by inhibiting rRNA synthesis with DNA intercalating compound - actinomycin D (AMD), leading to profound changes in ICC and PCC. This study explores the structural reorganization of NAC under severe DNA damage induced by γ-irradiation. The focus is on ICC and PCC to investigate whether physically damaged naDNA retains the ability to move/contract, similar to the chemical inhibition observed with AMD. Histone H2B-GFP permanently transfected He-La cells were utilized for their stability and suitability for time-lapse imaging. γ-Irradiation was applied at 10 Gy (Gray) and 30 Gy doses, followed by post-irradiation imaging for 24-72 hours. Two approaches were employed: post-irradiation LSM imaging of fixed and living cells (time-lapse LSM). The structural organization of NAC, ICC network, and PCC shell were analyzed to understand the spatial changes induced by γ-irradiation. The study reveals that γ-irradiation-induced NAC inactivation dynamics mirror changes observed with AMD-induced rRNA synthesis inhibition. Under both regimes (10 Gy and 30 Gy) of γ-irradiation, ICC structures coalesce, forming more significant and more prominent clumps that migrate toward the PCC shell. This research provides insights into the dynamics of nuclear and nucleolar changes induced by severe DNA damage. The observed similarities between chemical inhibition and γ-irradiation effects on nucleolus-associated chromatin emphasize its significance in nucleolar organization. The study contributes to understanding the spatial changes in nucleolar structure under different modes of cellular stress.*

Key words: Nucleolus – Nucleolar Components – Nucleolus Associated Chromatin – γ-Irradiation

INTRODUCTION

The nucleolus, a key nuclear compartment, drives ribosome biogenesis by generating polycistronic transcripts, namely the 47S precursor or pre-rRNA. Through cleavage during processing, it yields the final forms of rRNAs - 18S, 5.8S, and 28S, while their maturation and assembling processes lead to the formation of pre-ribosomal sub-particles. Integrating gene-rich chromosomal domains, it forms giant tandems of eukaryotic rDNA loops comprising numerous r-gene repeats. This process, facilitated by accessory protein factors, forms naDNA domains known as NAC. The nucleolus houses extremely compact yet highly active molecular machinery orchestrating ribosomal r-genes transcription, pre-rRNA processing, and pre-ribosomal assembling [1-13].

In the nucleolar realm, molecular machinery intricately orchestrates ribosome biogenesis within tightly coordinated NCs, functional sub-compartments discernible in light and transmission electron microscopes (LM and TEM). These NCs, marked by specific protein signatures, structurally organize transcription and processing machinery into three major NCs. This tripartite nucleolar structure is exceptionally identifiable in TEM by its distinct ultra-structural appearance and electron density. Transcriptionally active, non-nucleosomal ribosomal chromatin (r-chromatin) takes the form of pale-stained fibrillar centers (FCs), recognized as an interphase counterpart of mitotic nucleolus organizing regions (NORs). Two additional NCs, the dense fibrillary (DFC) and the granular component (GC), represent early and late processing sub-compartments. Here, 47S pre-rRNA molecules undergo maturation steps, leading to the generation of 40S and pre-60S particles containing precursors to 18S, 28S, 5.8S, and 5S rRNAs. The transitional area between r-genes transcription foci—termed transcriptionally active r-genes territory - is situated between the FC surface and the surrounding DFC [1-13]. In active nucleoli, the products of pre-rRNA synthesis, processing, and pre-ribosome assembly cluster around numerous r-chromatin transcription foci, thus shaping the multifocal global organization of the nucleolus.

Meanwhile, naDNA or NAC domains, though less explored and not determined by the genome map, likely contain more than just r-genes [9-22]. Therefore, these chromatin-associated NCs, with undefined roles in nucleolar organization, are intriguing. NAC manifests as a shell of PCC (PCC shel) extending into strands of ICC (ICC network). ICC is observed in EM-light zones known as nucleolar vacuoles (NVs). On ultrathin sections, ICC and PCC, constituting 10-30 nm thick nucleosomal fibrils, form a single interstitial/vacuolar network system. 3D reconstruction reveals that FCs are intricately linked via ICC clumps [23-26]. Previous studies using the rRNA synthesis inhibitor AMD showcased NAC spatiotemporal reorganization. AMD selectively blocks rRNA synthesis in low concentrations (0.05 µg/ml), causing giant FCs, DFC zones, and large ICC clumps. This approach demonstrated the inactivation dynamics of rRNA synthesis, revealing stepwise gathering and fusion of FCs and NAC. This concerted contraction mobilizes nucleolar components. The tight link between FC and DFC, displaced by selective r-genes transcription block, resembles FC/DFC assembly movement. Time-lapse imaging elucidates FC/DFC assembly dynamics, attributed to progressive NAC condensation in response to r-genes transcription inactivation.

The physical bond between FCs and ICC propels the movement of the FC/DFC complex,

aligning with NAC constituent inactivation dynamics [27].

Having explored NAC inactivation dynamics through chemical r-genes transcription inhibition, we now delve into the structural reorganization of NAC under severe DNA damage by physical factor γ-irradiation that induces single-strand breakages [28-34]. Focusing on ICC and PCC, we investigate if physically damaged naDNA exhibits similar movement to that induced chemically. Our preferred model involves possible post-γ-irradiation (10 Gy and 30 Gy) nucleolar inactivation monitoring changes in He-La cells permanently expressing histone H2B-GFP over 24-72 hours. We utilize LSM 2D imaging and LSM time-lapse analysis to scrutinize how nuclear and nucleolar structures, including naDNA, adapt to large-scale DNA damage. Based on chemical inhibition studies, our hypothesis posits that γ-irradiation induces classical spatial changes akin to NCs segregation [27, 35-39]. Indeed, our findings demonstrate NAC inactivation during γ-irradiation mirroring those observed with AMD-induced rRNA synthesis inhibition. Both regimes (10 Gy and 30 Gy) show the ICC network gradually coalescing before migrating towards the PCC, eventually fusing and forming more significant, more pronounced ICC clumps.

MATERIAL AND METHODS

1.Cell Culture

In our investigation of NAC distribution changes during irradiation, we utilized histone H2B-GFP transfected He-La cells obtained from Prof. O. Piot (University of Reims Champagne-Ardenne, France). The choice of this cell line was based on:

o **Stability:** The nuclear fluorescence of these cells demonstrated high stability, crucial for obtaining brightly fluorescent, reliably transfected cells, especially during time-lapse imaging of post-radiated cell dynamics.
o **Intra-nucleolar Fluorescence:** These cells exhibited prominent intra-nucleolar fluorescence, identified as nucleosomal domains with the ultrastructural appearance of ICC. This characteristic was vital for our study.
o **Distinct Features:** He-La cells are known for their large FCs associated with prominent DFC zones, aiding in the discrimination of nucleolar sub-territories involved in r-gene transcription and pre-rRNA processing.

Cell Maintenance: Stock cultures were maintained in 40 ml flasks containing DMEM (Gibco, UK) supplemented with 10% calf serum and 1% penicillin/streptomycin mixture. Regular reseeding occurred 2-3 times per week based on the cell monolayer reaching late pre-confluent or early confluent stages. Monthly tests for mycoplasma detection were conducted.

Preparation for Post-Irradiation Imaging: To study ICC dynamics during γ-irradiation-induced nucleolar remodeling, we prepared He-La cells expressing histone H2B-GFP. We ensured cultures remained sub-confluent after 48-72 hours of post-irradiation incubation and/or post-irradiation acquisition of living cell images.

2. Cell Seeding Methods

Method (1): The collagen-coated glass surface of Ø35 mm "MatTek" Petri dishes, featuring 14 mm wells as the growth area (MatTek, USA), was pre-conditioned by pouring a few drops of media at 37°C for 15-30 minutes. The exact amount of meticulously homogenized cell suspension was added. Cell density and distribution were checked using a phase-contrast regime after incubation at 37oC for 15-30 min. The satisfactory density of cells within the growth area was obtained by dilution that yielded ~10.000-15.000 cells/ml. Medium (1.5-2 ml) was added by pouring on the wall of Petri dishes to avoid disturbing the attached cells. Cells can be repeatedly re-homogenized inside the well using a 1.0 ml pipette/syringe. Using this concentration, we regularly achieved a dispersion of ready-to-work cultures after 48 hours of incubation. Following these conditions, we obtained cultures showing attached/flattened cells gathered in small groups distributed sparsely enough to stay sub-confluent after 72 h.

Method (2): This method yielded a less dispersed pattern, yet suitable for maintaining sub-confluence after 72 hours. The collagen-coated glass surfaces were pre-conditioned, as described above. 1.5-2.0 ml of a properly homogenized cell suspension (~10.000-15.000 cells/ml) was poured into wells. Desired dispersion was achieved by agitation for 5 minutes. Repeated resuspension with a 1 ml pipette/syringe provided better dispersion.

Both methods ensured the availability of isolated cellular groups suitable for post-irradiation incubation and imaging. After 24-48 hours of incubation, cells were briefly rinsed with PBS and prepared/submitted for γ-irradiation by incubating in a fresh medium at 37°C for 2-3 hours.

3. Experimental Procedures for Time-Lapse Imaging,
Data Analysis and Visualization γ-Irradiated Cells

Before being submitted to γ-irradiation, cells were briefly rinsed with PBS (3 times during 5 min), immersed in fresh medium, and the dishes were delivered to "GUPOS" γ-installation. Irradiation of cells was conducted directly in Petri dishes at a temperature of 35+/- 2°C. As a source of γ-irradiation, the Cs^{137} isotope with a dose of 1.1 Gy/min has been utilized. After irradiation, cells were washed in PBS (3x5 min), returned to the cultivation media, and then s γ-installation subjected to time-lapse imaging during 0-72 h using Carl Zeiss (Germany) LSM 900 microscopes equipped with Axio Observer Z1/7 inverted microscope and AiryScan 2 augmented resolution device. All procedures, including post-irradiation behavior observation, were conducted on cultures directly in Petri dishes. The imaging was performed at 37°C in a CO_2-enriched atmosphere using a special microscope plate holder with a sealed box. Microscopy details included using various objectives at optical zooms of 100x, 200x, and 630x. Hence, images were registered at low and high magnifications using objectives with corresponding numerical apertures. We used Plan-Neofluar/10x with 0.3 M27 numerical aperture and Plan-Apochromat/20x/0.8 M27 for low magnification, including a time-lapse approach. By imaging objects at high magnification, including time-lapse mode, we used Plan-Apochromat/63x/1.4 Oil DIC M27. The time-lapse imaging setup involved capturing images every 10 minutes for every 24 h post-irradiation imaging time (i.e., 0-24h, 24-48, and 48-72 h), simultaneously in phase contrast and fluorescence regimes.

Histone H2B-GFP fluorescence was induced and recorded using a Colibri 7 laser device at 488 nm excitation light, while emission light was 517 nm. As a control, we used high-magnification

LSM imaging conducted before γ-irradiation treatment. For time-lapse analysis and visualization behavior of living cells damaged by γ-irradiation, obtained time series were transformed into 2D movies using ZEN3.0 software. Significant points from the dataset were extracted to visualize the changes in nuclear/nucleolar quantitative and structural parameters, as well as the movement and coalescence of ICC clumps during γ-irradiation.

RESULTS

1. Exploring γ-Irradiation Induced Nuclear/Nucleolar Changes in Histone H2B-GFP He-La Cell: Fixed Cell Imaging and 2D Time-Lapse Dynamics

The He-La culture, expressing histone H2B-GFP, was selected for its bright, UV-resistant nucleoplasm and intra-nucleolar fluorescence, enabling extended LSM observations with minimal photo-bleaching for up to 24 hours. This resistance proved crucial for living cell observations. Notably, the nuclear chromatin and ICC exhibit early apoptosis-associated changes, making this culture suitable for cellular stress experiments induced by chemical and/or physical factors. By targeting the entire nucleoplasm and ICC, which express histone H2B-GFP fluorescence indicative of condensed chromatin, we investigated structural modifications during the 2D-time series. Therefore, these cells serve as a convenient model to assess the potential drastic effects of γ-irradiation on cell viability, morphology, and physiology.

LSM images displayed in Figure 1. and Figure 2. reveal the structural organization of histone H2B-GFP He-La cell nuclei in fixed control cells. Typically, 2D observations show mononuclear cells, as revealed by merging of phase contrast and fluorescent images (Figure 1. a). Predominantly nuclei have roundish or ovoid shape with smooth contours, while an average diameter ranged between ~14-18 µm (Figure1. b-d). Abundant dividing cells being at different stages of mitosis and occasional apoptotic cells (Figure 1. d) are also seen (Figure 1. a, b, d). Brightly fluorescent nucleoplasm, ICC, and PCC are prominently featured. Nucleoli, are well recognizable as roundish dark zones that have a diameter ranging from ~4-6.5 µm. Even at low magnification, it became obvious that nucleoli contain histone H2B-GFP positive structures of different sizes and appearances attributed to ICC. ICC inclusions have slightly less intense labeling than chromatin fluorescence (Figure 1. a-d).

These features become evident by analyzing various individual/random 2D sections at higher magnification. Therefore, Figure 2. displays the 2D structure, sizes, and localization of the ICC network and the closely adjacent PCC ring. The ICC zones are prominent and vary in size, appearing in individual sections as distinct clumps or extended anastomosing cords. PCC consistently exhibits higher fluorescence than ICC, forming around confines of the nucleolar territory quite thick, solid, or locally disrupted "ring" of ~0.25- 0.55 µm" in thickness (Figure 2. a-d). Therefore, high-magnification images confirm the persistent presence of numerous ICC inclusions and ring-shaped PCC in all observed cells. ICC is either visible as discrete entities or forming well-recognizable network-like structures (Figure 2. c). Furthermore, the analysis at higher magnification confirmed that PCC is organized into a locally open ring. However, it covers a significant part of the nucleolar territory. In addition, these images provide definitive evidence confirming the direct physical link between the PCC ring and ICC clumps as reported

earlier from observations on random ultrathin sections, including those treated for preferential demonstration of NAC [23-25]. Indeed, 2D information presented in Figure 2. b-d reveals multiple cord-like structures emanating from the PCC ring. These "off springs" protrude inside the nucleolar territory, sometimes creating the impression of discrete ICC clumps on individual sections. These findings strongly support the existence of a united ICC network that is continuous with the PCC ring, representing protrusions of the latter.
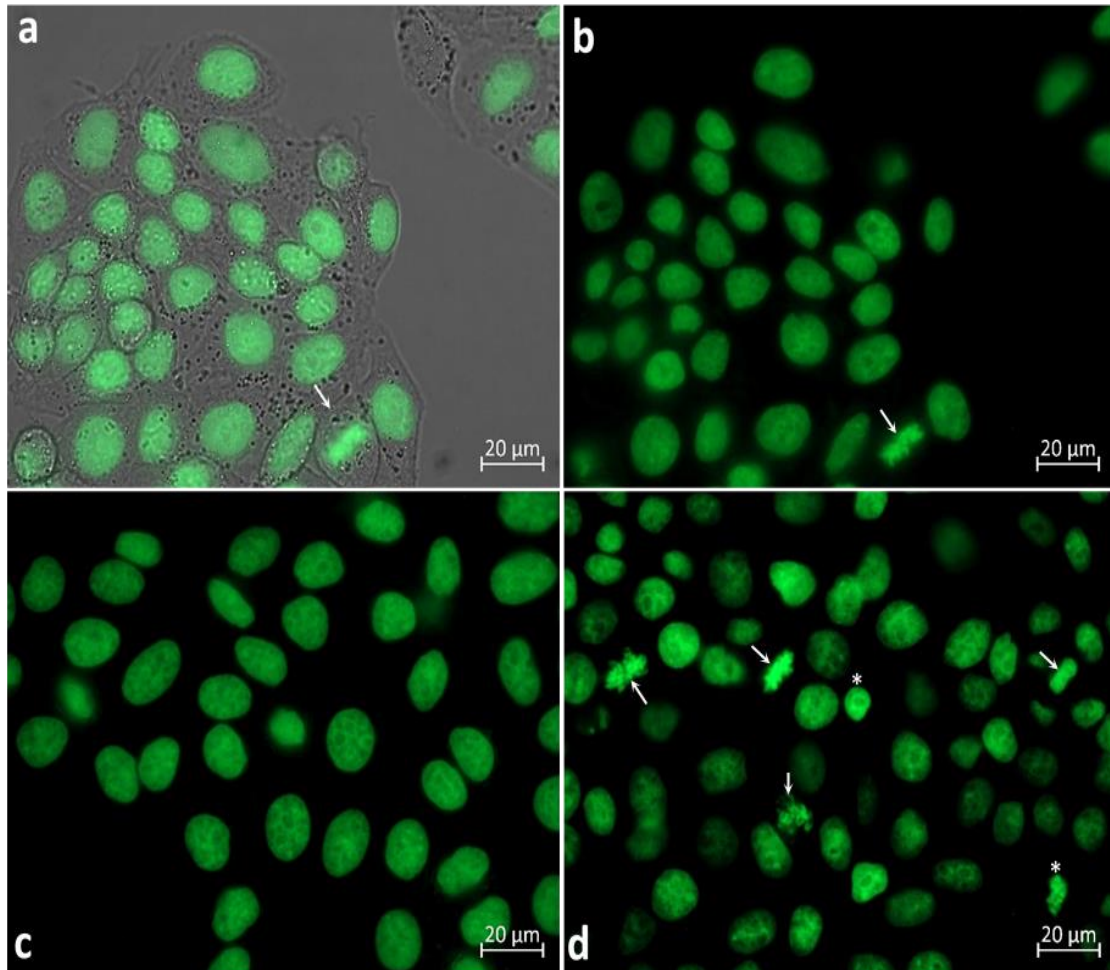
Figure 1. Gallery of images displaying general morphology of fixed cultured He-La cells permanently expressing histone H2B-GFP fused protein. Images were taken at low magnification using phase contrast and fluorescent imaging; a – overlay of phase contrast and fluorescent images demonstrated in order to discriminate mono- and polynuclear cells. All registered cells are mononuclear; b-d – predominantly roundish and/or ovoid shape as well as nearly smooth nuclear contours are better recognizable by fluorescent regime. Nucleolar territory appears in form of roundish or elongated intra-nuclear zone with obviously less intense fluorescence. Even at low magnification it become visible that nucleolar territory is surrounded by ring of PCC, while intra-nucleolar fluorescence is conditioned by presence of worst recognizable ICC structures. Mitotic cells are abundant (Figure 1. a, b, d, arrows) while occasional apoptotic cells are also present (Figure 1. d, marked by stars).

Meanwhile, fixed cells lost about 25%-30% of their initial volume, likely due to shrinkage resulting from PAF fixation. Therefore, we performed time-lapse imaging to capture the 2D dynamics of the NAC, consisting of a PCC ring in continuity with ICC strands in native state (Figure 3.). Analysis of random 2D sections obtained during time-lapse imaging replicated the observed fixed cell pattern, with minor differences in sizes of structures of interest (SOI) between fixed and living cells (Figure 3. a, b) However, we noted that average diameter of nuclei in living He-La cells is higher than in fixed ones and ranged between 17-21 μm. In addition, SOI in fixed cells exhibited fluorescence comparable to or slightly less intense than that in living cells. Random 2D images of living cells prominently revealed all SOI, namely ICC and PCC (Figure 3. c, d). Nucleolar sizes were also slightly higher than in fixed cells, reaching 6.25-8 μm. Living cells were rich in discrete histone H2B-GFP-positive labeling within the nucleolar territory. As expected, ICC appeared as larger clumps or anastomosing cords that form network-like structures (Figure 3. c, d). Accordingly, we can conclusively state that the native structure of ICC is network-like. The extensively branched ICC network consists of anastomosing cord-like protrusions emanating from the PCC shell. Meanwhile, the PCC resembles a highly compacted part of the juxta-nucleolar nucleoplasm, forming a ring delineating the nucleolar territory.
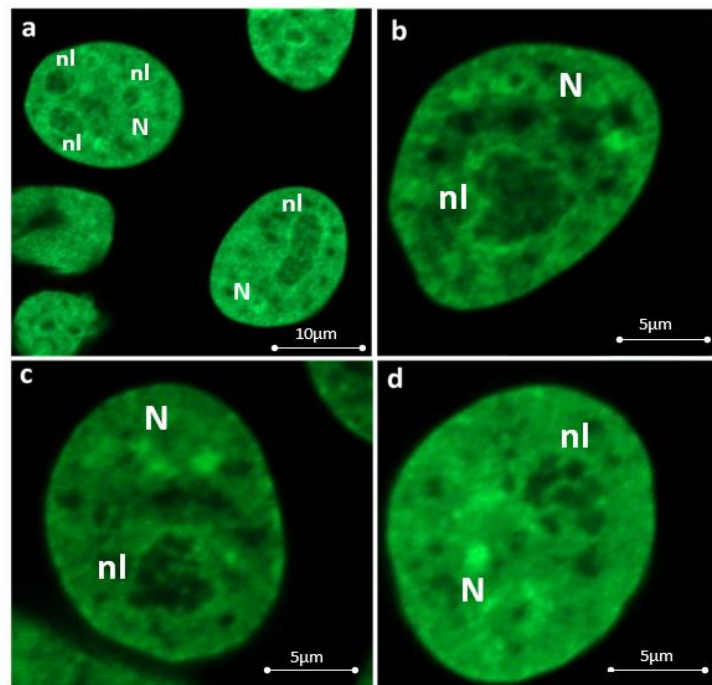
Figure 2. Morphology of nuclei in fixed histone H2B-GFP permanently transfected He-La cells taken at higher magnification; a – medium magnification, general view; note abundant intra-nucleolar GFP-positive inclusions revealing network-like appearance. Note also profound PCC surrounding nucleolus in form of solid ring; b-d – undoubtedly at higher magnification ICC structure became much more prominent, showing either network-like organization (Figure 1. b) or looking as clumps (Figure 1. c). In all samples one can recognize cords of different thickness emanating from prominent PCC ring. This phenomenon is especially well pronounced on Figure 2. d, where interconnected with PCC coarse ICC cords are clearly seen. N –nucleus; nl - nucleolus
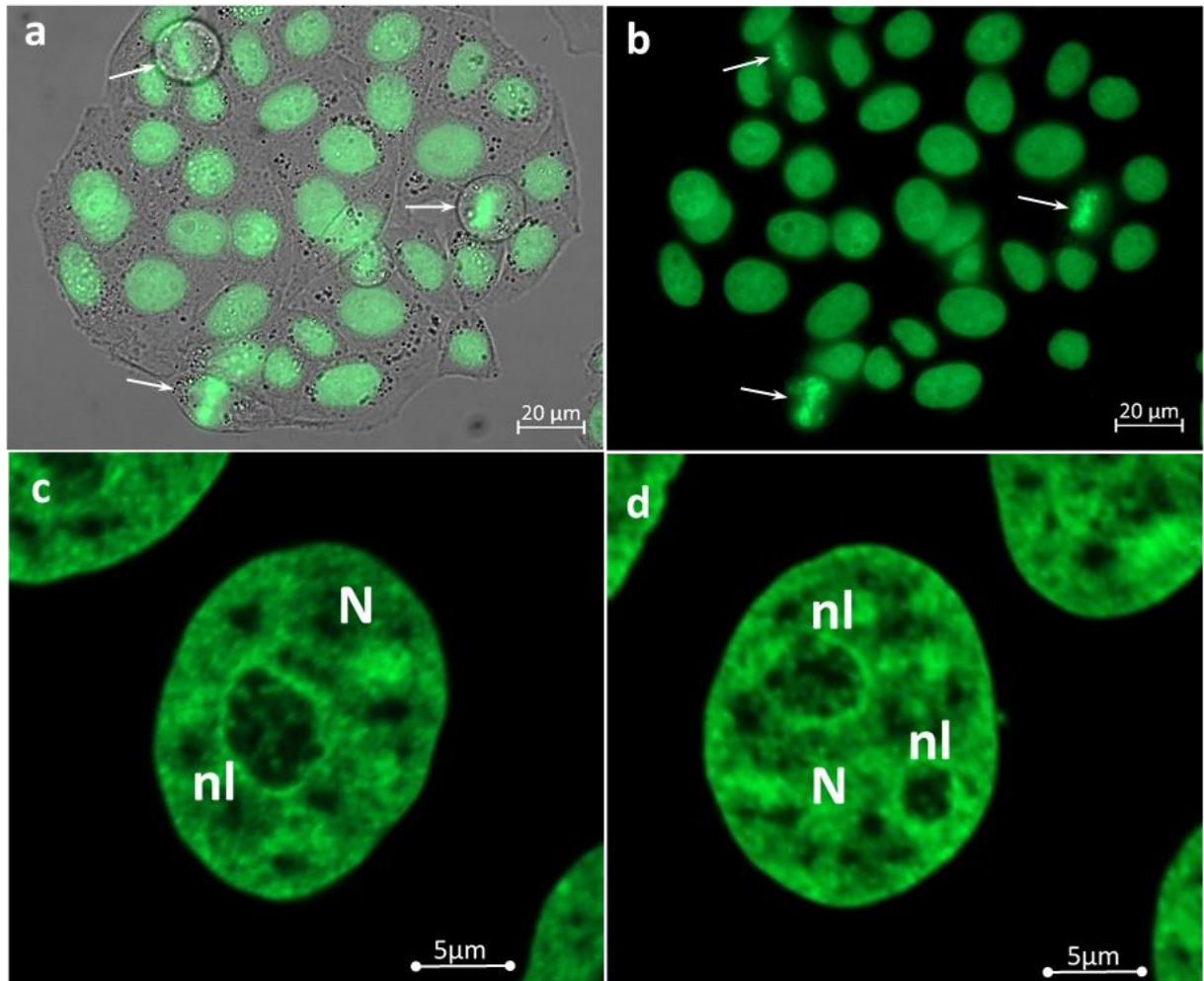
Figure 3. Morphology of cells and nuclei in living histone H2B-GFP permanently transfected He-La cells taken at low (Figure 1. a-b) and high (Figure 1. c, d) magnification; a, b – general view; a - overlay of phase contrast and fluorescent images to reveal mono- and polynuclear cells. All cells are mononuclear and predominantly roundish and/or ovoid. Note abundant mitoses (Figure 3. a, b, arrows); c-d – similarly to fixed cells at high magnification intra-nucleolar GFP-positive inclusions revealing network-like appearance. Note also profound PCC surrounding nucleolus in form of solid ring and emanating from PCC ICC cords. N –nucleus; nl - nucleolus

1.1. Visualizing Nuclear/Nucleolar, ICC and PCC Dynamics: Time-lapse Imaging of He-La Cells Under γ-Irradiation

Time-lapse imaging of He-La cells expressing histone H2B-GFP was conducted to study the dynamics of DNA-containing SOI under γ-irradiation at 10 Gy and 30 Gy. This approach facilitated simultaneous imaging of whole nuclei and nucleoplasm, allowing for 2D analysis of modifications over time. Time series images registered at various time points were used to create galleries of random/individual sections.
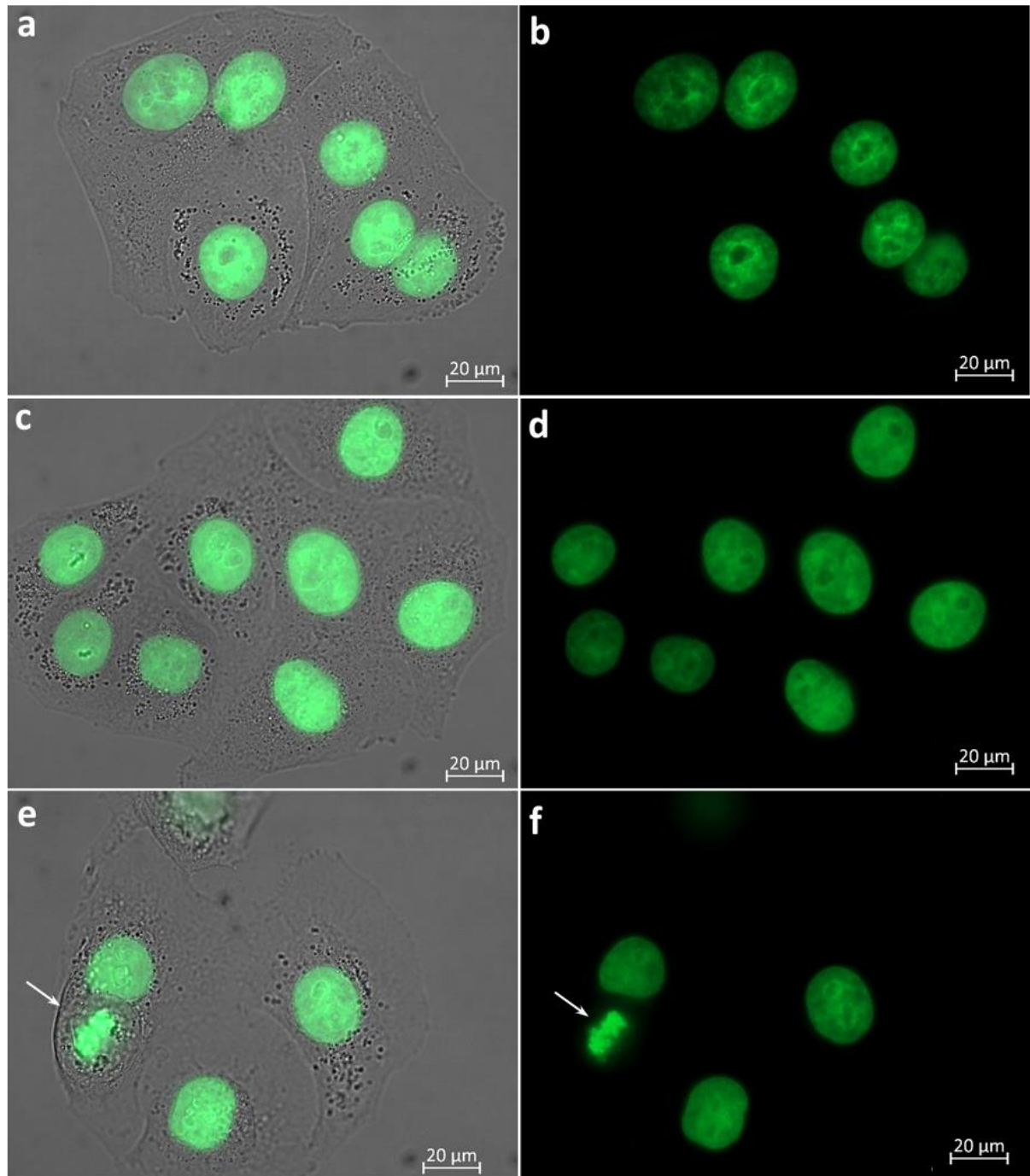
Figure 4. Cellular and nuclear morphology in living histone H2B-GFP permanently transfected He-La cells after irradiation with 10 Gy taken over 48 h; a-f – medium magnification; a, c, e - overlay of phase contrast and fluorescent images; b, d, f – same cells demonstrated in fluorescent regime only. All registered cells remain mononuclear, while nuclei maintain predominantly roundish and/or ovoid shape and smooth contours. Intra-nucleolar GFP-positive inclusions become sufficiently prominent (Figure 4. a-d). Note profound PCC surrounding nucleolus in form of solid ring (Figure 4. b). Also note presence of mitotic cell (Figure 4. e, f, arrows).
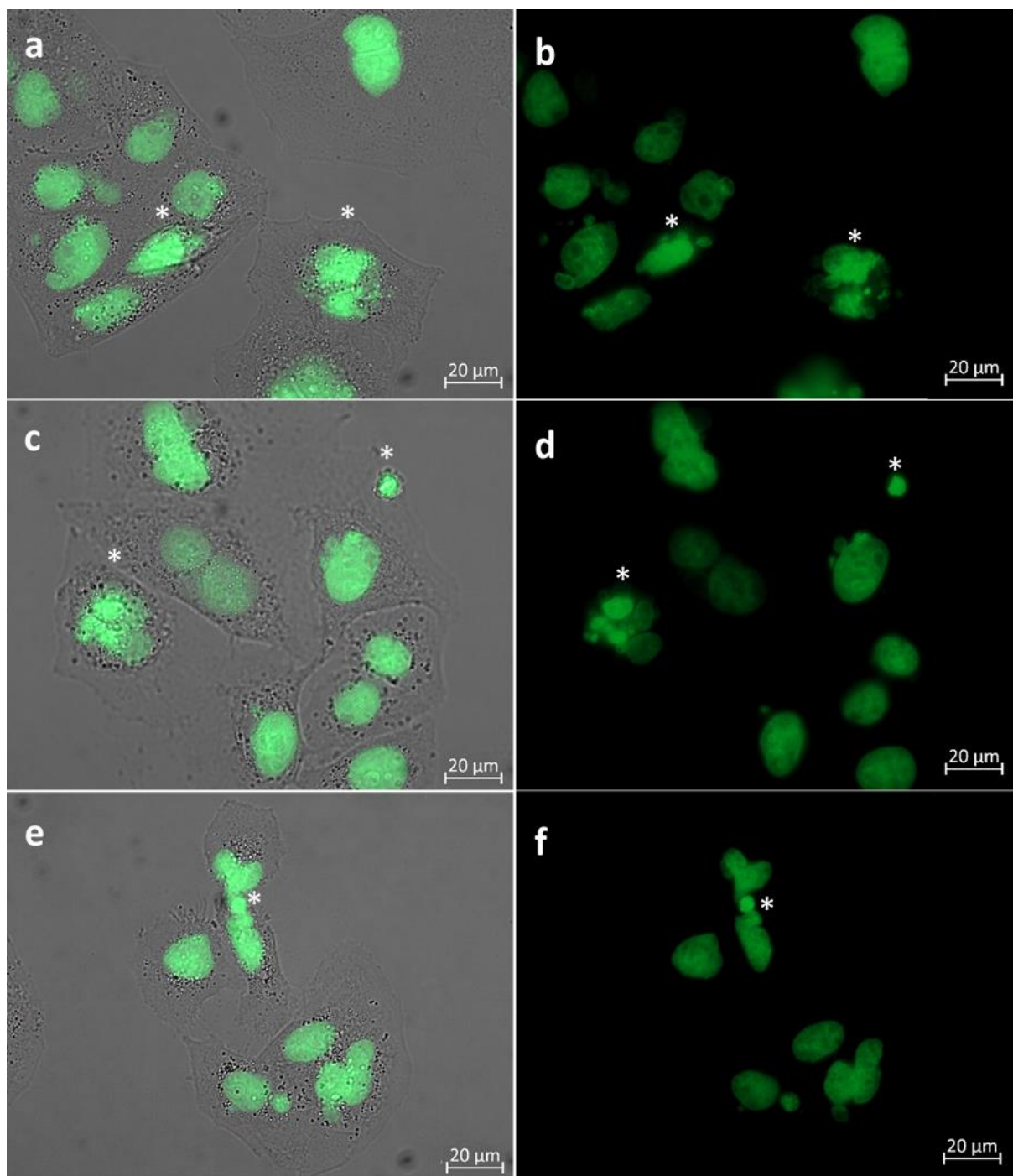
Figure 5. Drastic changes of cellular and nuclear morphology in living histone H2B-GFP permanently transfected He-La cells after irradiation with 30 Gy taken over 48 h; a-f – medium magnification; a, c, e - overlay of phase contrast and fluorescent images; b, d, f – same cells demonstrated in fluorescent regime only; a-f – initial appearance of polynuclear (Figure 5. a, c, e), apoptotic (Figure 5. c, d) and deformed (Figure 5. e) cells. Most probably Figure 5. a, b and Figure 5. e, f are mirroring the formation of cleaved and/or lobbed nuclei. Note asynchronous apoptosis of different nuclei within the same polynuclear cell (Figure 5. a-f, marked by stars).
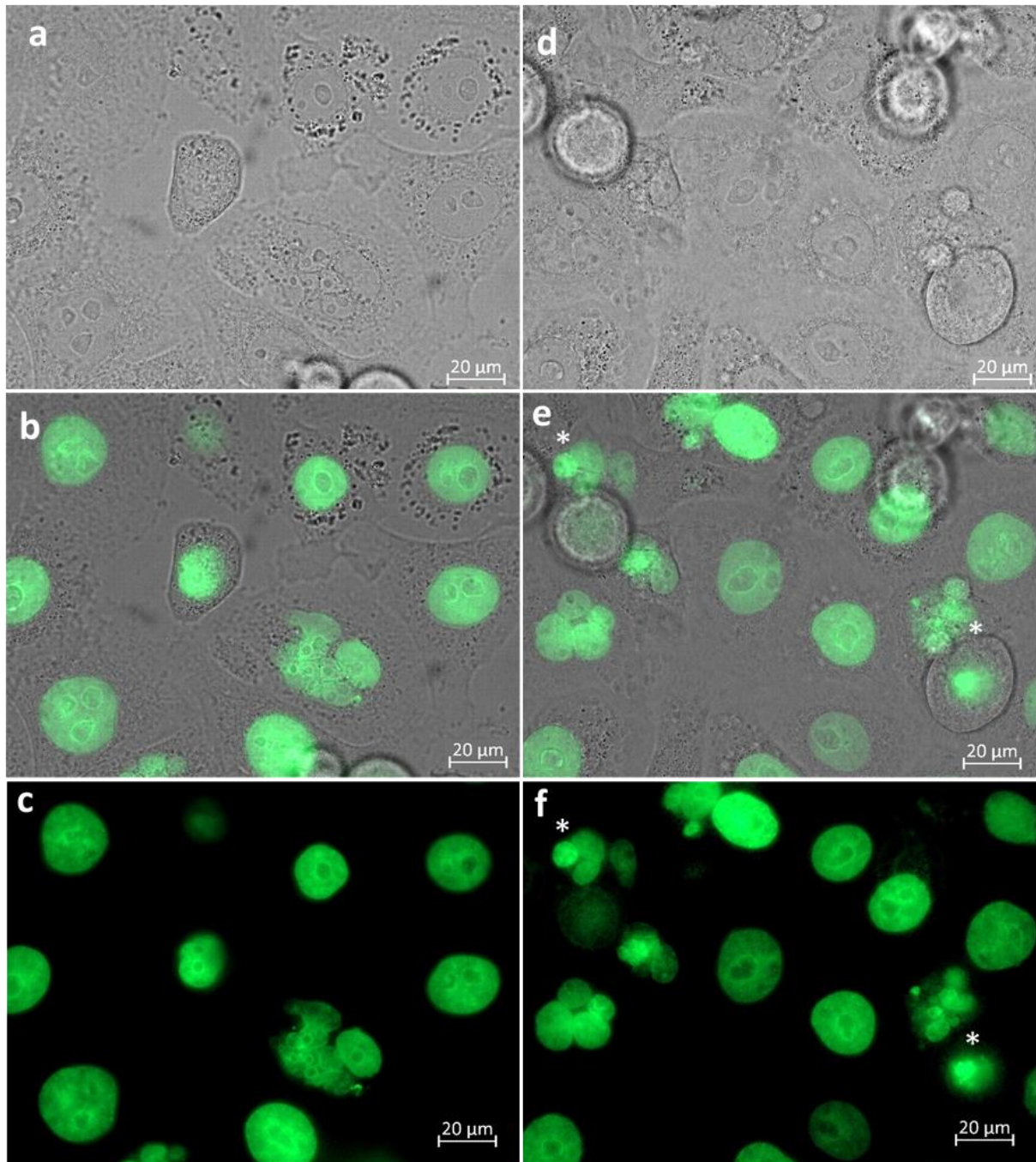
Figure 6. Drastic changes of cellular and nuclear morphology in living histone H2B-GFP permanently transfected He-La cells after irradiation with 10 Gy taken over 72 h; a-f – medium magnification; a, d – phase contrast only: appearance of intra-nucleolar light zones of different sizes; b-e – overlay of phase contrast and fluorescent images; c-f – same cells demonstrated in fluorescent regime only; b-f - the number of polynuclear and apoptotic cells dramatically increase. Asynchronous apoptosis is clearly seen (Figure 6. e, f marked by stars). Note profound PCC rings separating nucleolar territory from nucleoplasm. Even at medium magnification ICC clumps and their contact with PCC are well recognizable (Figure 6. f; see nucleus localized in the center of image).
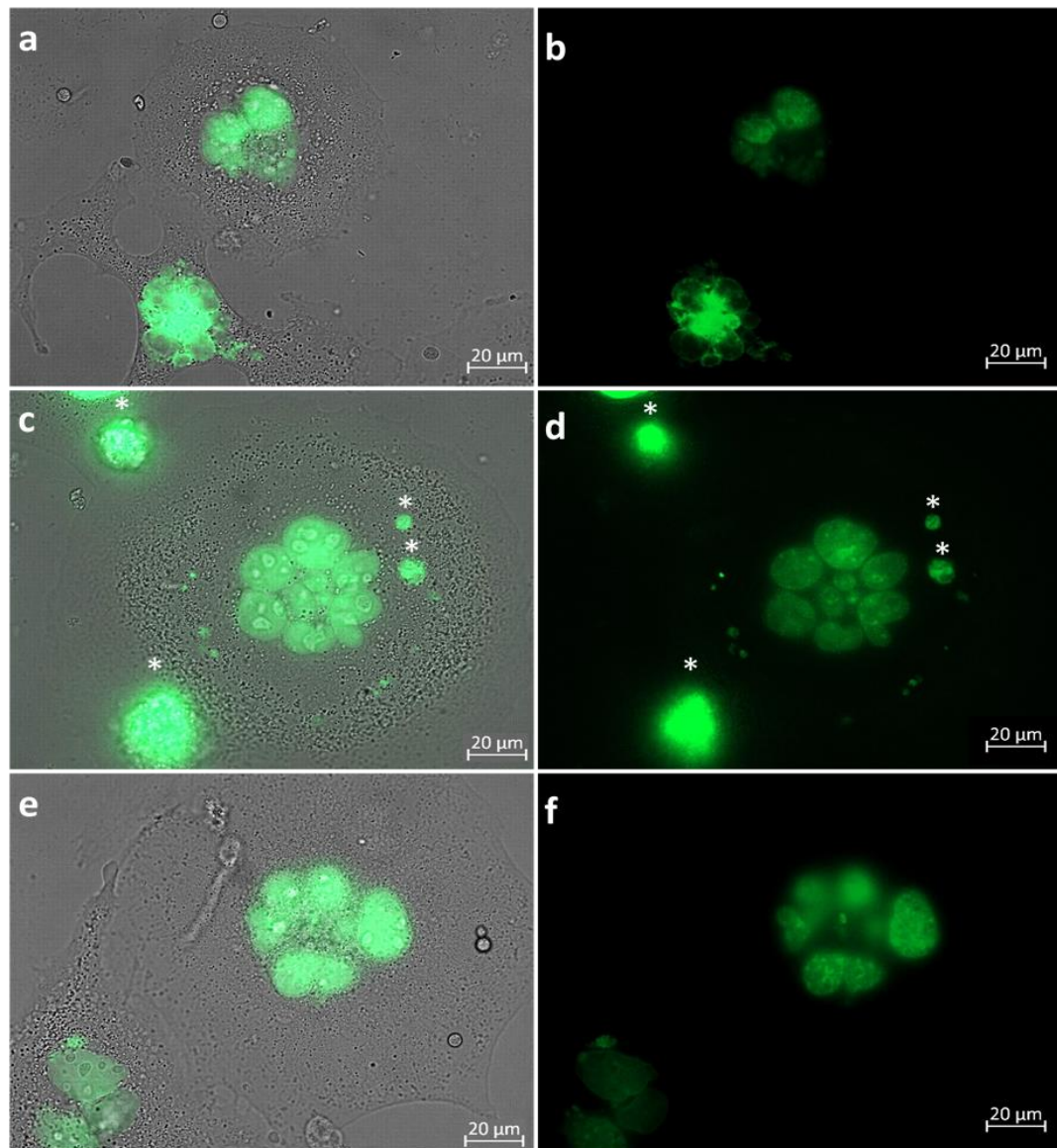
Figure 7. Gallery displaying drastic changes of cellular and nuclear morphology in living histone H2B-GFP permanently transfected He-La cells after irradiation with 30 Gy taken over 72 h; a-f – medium magnification; a, c, e – overlay of phase contrast and fluorescent images; b, d, f – the same cells taken using fluorescent regime only. This gallery shows massive appearance of giant polynuclear cells. Apoptotic cells marked by stars on Figure 7. c, d.

Through our 2D approach, we visualized: (i) gradual morphological changes and size variations in the nucleus, including deformation of nuclear contours; (ii) modifications in the nucleolar territory, involving alterations in the ICC network and PCC shell; (iii) the chronology of stages and potential mechanisms leading to polynuclear cell formation; (iv) asynchronous development of apoptosis-related changes in different nuclei of polynuclear cells. Together, it was revealed that post-irradiation, initially, ovoid nuclei transform into irregular shapes,

undergo drastic deformation or lobbying, and eventually fragment, resulting in the formation of polynucleated, dying cells. We did not find profound signs of cell division arrest, as different stages of mitosis (including its pathological forms) were also registered (**Figures 4.-8**).

According to time-dependent structural changes that develop in irradiation-damaged cells, we preferred to divide the whole period of post-irradiation time-lapse imaging into three stages: *stage 1* (0 - 24 h of the post-irradiation period), *stage 2* (24 - 48 h), and *stage 3* (48 - 72 h). Noteworthy, comparing the structural events over all three post-irradiation stages, we constantly specify much more profound changes in nuclear/nucleolar structure by treatment with 30 Gy regime than those of 10 Gy (compare Figure 4. and Figure 5.; Figure 6. and Figure 7.; Figures 8. a, b and Figures 8. b, c).
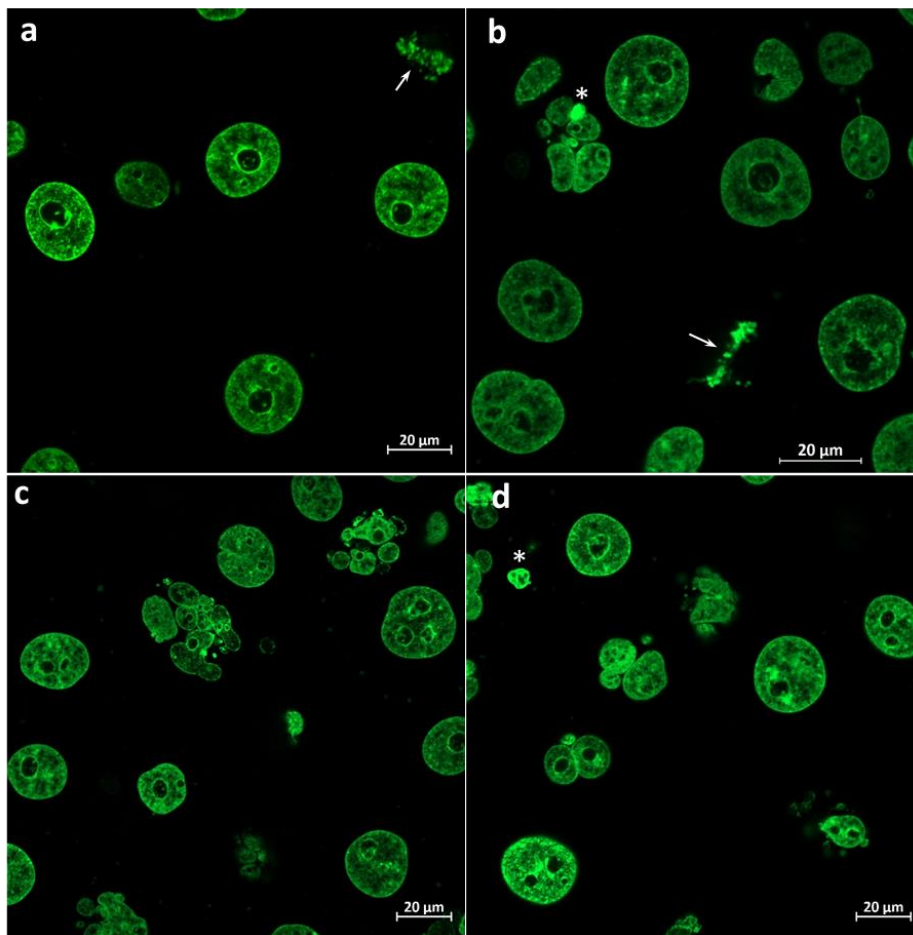
Figure 8. Changes in the structure and sizes of PCC and ICC as revealed at high magnification. a, b – fluorescent images taken using culture treated with 10 Gy over 48 h; c-d – fluorescent images correspond to treatment with 10 Gy over 72 h. Interestingly, that beside polynuclear cells (Figure 8. b-d) mitotic cells also present (Figure 8. a, b, arrows). At this stage of γ-irradiation all nucleoli contain coarse ICC inclusions that can look like clumps or reveal ring-shaped appearance (Figure 8. a, b; see upper nucleus). In all cells the PCC ring become especially prominent. Note also asynchronous apoptosis (Figure 8. b, d, marked by stars).

Stage 1: Post-irradiation changes over 24 hours. Related changes were analyzed using a 2D movie from time series at low and medium magnification. Individual LSM images reflecting different stages of post-radiation nuclear evolution were presented and analyzed in merged PC/fluorescent mode in order to better discriminate mononuclear and polynuclear cells. Correspondingly, key time points were identified and extracted for detailed analysis in galleries of individual/random sections, revealing cellular and nuclear shapes by treatment under 10 Gy and 30 Gy regimes. We concluded that during stage 1, culture maintained nuclear and nucleolar shape and structure without drastic changes over the 24-hour acquisition period, so that obtained pictures were similar to control ones. By this, mitotic cells could be detected quite often (corresponding images and movie are not shown).

Stage 2: Post-irradiation changes over 48 hours. During the 24 – 48 h post-irradiation period, the nuclear diameter progressively increased from 20.5 to 28 μm. However, the bulk of cells retain mononuclear appearance, while nuclei maintained roundish or ovoid shape with smooth outlines (Figure 4.). Mitotic cells that revealed structure very close to normal, were seen quite often (Figure 4. e, f). Over 48 h period, drastically deformed cells notably increase by treatment using 30 Gy regime, while polynuclear as well as apoptotic cells abundantly appear as displayed in Figure 5. Deformed nuclei exhibit deep invaginations, calculated from one to multiple. Apoptotic cells (including early stages) can be easily recognized due to dramatically enhanced nuclear brightness conditioned by increased chromatin compaction. Polynuclear cells can be observed very often. The number of polynuclear and apoptotic cells significantly grows to the end of imaging, i.e. after ~40 h of the post-irradiation period. In addition, different nuclei in these cells can reveal initial signs, indicating the asynchronous character of apoptotic changes. In parallel, the intra-nucleolar fluorescence becomes much brighter and more prominent than in previous samples due to the full disappearance of the ICC network and its transformation into large clumps, often being reshaped into a ring-like appearance (Figure 8. a). At the same time, we observed notable thickening of the PCC ring. Despite prominent cellular destruction, rare mitotic cells (mostly pathologic forms) could be seen.

Stage 3: Post-irradiation changes over 72 hours. The most profound effects of γ-irradiation, leading to apparent nuclear/nucleolar structural modifications and drastic changes in global cellular organization, were observed during the 48 h to 72 h period when we applied 10 Gy (Figure 6.) and 30 Gy (Figure 7.) irradiations. Consequently, a majority of the cells underwent a transformation from mono- to polynuclear forms. For example, by 30 Gy regime, massive apoptosis was detected starting from 56-60 hours into the post-irradiation period, whereas the number of wholly destructed/dead cells dramatically increase to the end of time-lapse imaging, i.e. to 70-72 h (Figure 7.). It should be specially noted that, upon comparing individual polynuclear cells, we concluded that the process of apoptosis occurs asynchronously across different nuclei within the same cell (Figures 6. e, f; 7, a, d; 8, b). At the same time, analyzing structural changes unraveled by imaging using phase contrast at medium magnification at 10 Gy regimes we registered emerging of large light zones inside nucleolus (Figure 6. a, d). At high magnification and fluorescent regime, it became clear that corresponding nucleolar modifications are concomitant with the appearance of extensive ICC zones that sometimes acquire the ring-shaped appearance. Prominent thickening of the PCC ring is also apparent (Figure 8.).

DISCUSSION

The molecular organization of the nucleolus is well documented at the molecular, genome, and proteome levels. Moreover, epigenetic mechanisms regulating r-genes expression have also been studied in detail. Consequently, over the past 30 years, the nucleolus has become recognized as a unique model for studying the spatial organization and functional state of mammalian r-genes, particularly in their functional and dynamic association with ribosome biogenesis and overall cell metabolism. Correspondingly, it is generally accepted that the sites of localization and transcription of r-genes, as well as processing of pre-RNA and pre-ribosome assembling factories organized as nucleolus, represent highly sensitive sensors of cellular stress [40-45]. Therefore, various chemical stress factors (including broadly used anticancer drugs) that inhibit different steps of ribosome biogenesis have been used as reliable tools to study structure-functional aspects of the nucleolus in compliance with cell metabolism [27, 35-39].

Conversely, while posing as an integral part of the nucleolus, the functional role of NAC still needs to be investigated despite recent data indicating its particular significance in the intra-nucleolar dynamics of NCs [27]. It is well established that, once formed, the nucleolus remains intimately associated with the physiological state of NAC. The structural remodeling of NAC can affect the spatial arrangement of active r-genes and the global organization of the nucleolar factories. For example, the contraction of NAC components drives the movement and fusion of FCs following the relocation of ICC/FC/DFC assembly from central regions to the nucleolar periphery and the incorporation of ICC into PCC [27].

Meanwhile, the structural and functional interplay between sophisticated systems, comprising giant tandems of r-genes, tightly folded and linked to unit NAC, remains completely unexplored. Most likely, NAC constituents do not contain r-genes due to the absence of specific accessory factors necessary for the maintenance of the template in an under-condensed/open state (e.g., UBTF). Hence, the absence of UBTF facilitate the keeping of the nucleosomal structure of ICC and PCC. How NAC responds to the action of DNA-damaging physical factors, particularly UV and radioactive exposure, remains largely unknown. Additionally, it is unclear how the transcriptional inactivation of r-genes, provoked by single-strand breakages, is reflected in the dynamics of nucleolar components. It seems much more problematic to understand whether NAC still retains the ability to condense and drive the movement of NCs while naDNA undergoes γ-irradiation breakage and degradation.

Therefore, the present study focuses on the reorganization of NAC, particularly ICC and PCC, under severe DNA damage induced by γ-irradiation. Accordingly, the primary goal of our study was to demonstrate the structural and functional interplay between γ-irradiation induced r-gene inactivation and large-scale modifications of intra-nuclear and intra-nucleolar structure with particular regard to possible territorial reorganization of NAC and related structures. The key findings are: (i) the dynamics of γ-irradiation-induced NAC inactivation mirror changes observed with AMD-induced rRNA synthesis inhibition. Under both irradiation regimes (10 Gy and 30 Gy), ICC structures coalesce and migrate towards PCC, forming more significant and prominent ICC clumps. This means that, despite severe naDNA damage, NAC, particularly ICC, retains the ability to contract and initiate the movement of NCs. The mechanisms underlying such a phenomenon, i.e., ICC and PCC contraction after single-strand breakage and

possible instant DNA repair, are completely obscured. (ii) As expected, a higher irradiation dose induces sufficiently rapid cellular response and more robust structural change, leading to cellular death via apoptosis. Thus, after treatment with 30 Gy, we revealed the bulk of highly deformed nuclei in both mononuclear and multinucleated cells, including apoptotic ones after 48 h. The same post-irradiation period by the 10 Gy regime shows visually nearly intact, roundish, and ovoid nuclei without any signs of nuclear deformation. In such cases, only increased nuclear diameter witnessed the influence of γ-irradiation upon cell/nuclear morphology. (iii) Post-irradiation changes over 24-72 hours enabled the revealing of the nuclear/nucleolar evolution stages and calculation of nuclear diameter changes. For this, we resorted to key time points that were identified for detailed analysis in galleries of individual sections, showing ICC and PCC changes in time. Because our study employs an approach involving both 2D LSM imaging of fixed cells and the time-lapse imaging we managed to visualize gradual morphological changes in the nucleus, modifications in the nucleolar territory (including ICC network and PCC ring), the chronology of stages leading to polynuclear cell formation, and asynchronous apoptosis-related changes. Although apoptosis in polynuclear cells was frequently registered after UV and γ-irradiation [46-51], up to date, there is no comprehensive explanation of underlying sub-cellular and molecular mechanisms. (iv) Importantly, our results demonstrate at least one of the possible sub-cellular mechanisms of polynuclear cell emergence. By this, the dynamics of this process develop in two steps. Initially, the formation of deep invaginations of the nucleus takes place that imparts a cleaved and/or lobbed shape to nuclei. During the next step, nuclei "disrupt" into separate fragments so that each lobe gives rise to individual nucleus. We observed two kinds of such a "cheeping of" process. If the lobe "engulfs" the nucleolus, nuclear disruption forms the nucleolated fragment. In opposite cases, fragments became anucleolated. Interestingly, apoptosis-associated changes develop asynchronously in both nucleolated and anucleolated nuclei. (v) Undoubtedly, one more intriguing issue worth further, more profound engagement is that even severe DNA damaging 30 Gr regime indicated the maintenance of naDNA to contract and drive nuclear and nucleolar dynamics; (vi) Another interesting nucleolus-related phenomenon deals with the emergence of large light zones known from classical studies as "nucleolini", "clear zones" etc. These changes, which can be easily registered using the phase contrast approach, were considered a reliable criterion of r-genes inactivation, regularly observed when nucleolar functions were disturbed with chemical inhibitors. Typically, these optically and electron light micro-structures correspond to 1-3 giant FCs that became significantly enlarged due to the fusion of multiple but small individual FCs [27]. However, without specific labeling of r-genes transcription sites, it is challenging to determine whether enlarged light zones correspond to FCs or NVs.

In summary, the study contributes valuable insights into the structural changes in nuclear and nucleolar structure under severe DNA damage, highlighting the significance of NAC in nucleolar organization. The observed similarities between chemical inhibition and γ-irradiation effects emphasize the role of NAC in cellular responses to different stressors.

REFERENCES

[1]. Busch, H., Smetana, K. (1970) The Nucleolus. New York, Academic Press: 1-282;

[2] Smetana, K., Busch, H. (1974) The nucleolus and nucleolar DNA. In: Busch H, editor. The Cell Nucleus. New York, Academic Press: 73-147;

[3] Hadjiolov, A. (1985) The Nucleolus and ribosome biogenesis. In: Alfert, M, Beerman W, Goldstein, L, Porter, KR, Site P, editors. Cell Biology Monographs Wien, New York, Springer Verlag: 1-263;

[4] Thiry, M., Lafontaine D. (2005) Birth of a nucleolus: the evolution of nucleolar compartments. Trends in Cell Biology, 15:194-199;

[5] Boisvert, F. M., van Koningsbruggen, S. N., Navascues, J., Lamond, A. I. (2007) The multifunctional nucleolus. Nat Rev Mol Cell Boil, 8:574-585;

[6] Hernandez-Verdun, D., Roussel, P., Thiry, M., Sirri, V., Lafontaine, D. (2010) The Nucleolus: structure/function relationship in RNA metabolism. WIREs RNA, 1:415-431;

[7] Pederson, T. (2010) The nucleus introduced. Cold Spring Harb Perspect Biol, 10:1-16;

[8] Olson, M. O. J. (2011) The nucleolus: A nuclear body full of surprises. In: Olson M. O. J. editor. The Nucleolus. Protein Reviews, New-York, Dordrecht, Heidelberg, London: Springer, 15:5-17;

[9] Tafforeau, L., Zorbas, C., Langhendries, J. L., Mullineux, S. T., Stamatopoulou, V., Mullier, R. (2013) The complexity of human ribosome biogenesis revealed by systematic nucleolar screening of pre-rRNA processing factors. Molecular Cell, 51:539-551;

[10] Farley, K. I., Surovtseva, Y., Merkel, J., Baserga, S. (2015) Determinants of mammalian nucleolar architecture. Chromosom, 124:323-331;

[11] Pollock, C., Huang, S. The perinucleolar compartment. J Cell Biochem (2009), 107:189-193;

[12] Pollock, C., Daily, K., Nguyen, V. T., Wang, C., Lewandowska, M. A., Bensaude, O. (2011) Characterization of MRP RNA-protein interactions within the perinucleolar compartment. Mol Biol Cell, 22:858-867;

[13] Misteli, T. (2005) Concepts in nuclear architecture. Bioassays, 27:477-487;

[14] Ochs, R. I., Press, R. I. (1992) Centromere autoantigens are associated with nucleolus. Exp Cell Res, 200:339-350;

[15] McKeown, P. C., Shaw, P. J. (2009) Chromatin: linking structure and function in the nucleolus. Chromosoma, 118:11-23;

[16] Bartova, E., Horakova, A., Uhlirova, R., Raska, I., Galiova, G., Orlova, D. (2010) Structure and epigenetics of nucleoli in comparison with non-nucleolar components. J Histochem Cytochem, 58:391-403;

[17] Nemeth, A., Conesa, A., Santoyo-Lopez J., Medina I., Montaner D., Peterfia B. (2010) Initial genomics of the human nucleolus. PLOS Genetics, 6:1-10;

[18] Van Konningsbruggen, S., Gierlinski, M., Schofield, P., Martin, D., Barton, G. J., Ariyurek, Y. (2010) High resolution whole-genome sequencing reveals that specific chromatin domains from most human chromosomes associate with nucleoli. Molecular Biology Cell, 21:3735-3748;

[19] Nemeth, A., Langst, G. (2011) Genome organization in and around the nucleolus. Cell, 27:149-156;

[20] Stults, D. M., Killen, M. W., Pierce, H. H., Pierce, A. J. (2008) Genomic architecture and inheritance of human ribosomal RNA gene clusters. Genome Res, 18:13-18;

[21] Floutsakou, I., Agrawal, S., Nguyen, T. T., Seoighe, C., Ganley, A. R. D., McStay, B. (2013) The shared genomic architecture of human nucleolar organizer regions. Genome Res 23:2003-2012;

[22] Grob, A., McStay, B. (2014) Construction of synthetic nucleoli and what it tells us about propagation of subnuclear domains through cell division. Cell Cycle, 13:2501-2508;

[23] Derenzini, M., Thiry, M., Goessens, G. (1990) Ultrastructural cytochemistry of the mammalian cell nucleolus. J. Histochem Cytochem, 38:1237-1256;

[24] Thiry, M., Ploton, D., Menager, M., Goessens, G. (1993) Ultrastructural distribution of DNA within the nucleolus of various animal cell lines or tissues revealed by terminal deoxynucleotidyl transferase. Cell Tissue Res, 271: 33-45;

[25] Thiry, M., Goessens, G. (1996) The nucleolus during the cell cycle. In: Landes R.G. Company editor. Molecular Biology Intelligence Unit. Austin: Chapman and Hall: 1-146;

[26] Mosgoller, W. Nucleolar, (2003) Ultrastructure in Vertebrates. In: Olson MO editor. The Nucleolus. London: Plenum Publesher: 1-11;

[27] Tchelidze, P., Benassarou, A., Kaplan, H., O'Donohue, M. F., Lucas, L., Terryn, C., Rusishvili, L., Mosidze, G., Lalun, N., Ploton, D. (2017) Nucleolar Sub-Compartments in Motion during rRNA Synthesis Inhibition: Contraction of Nucleolar Condensed Chromatin and gathering of fibrillary centers are concomitant. PLOS one: 30: 2-37;

[28] Sudpraserta, W., Navasumrita, P., Ruchirawata, M. (2006) Effects of low-dose gamma radiation on DNA damage, chromosomal aberration and expression of repair genes in human blood cells., 209: 503-511;

[29] Zlobinskaya, G., Dollinger, D., Michalski, V., Hable, C., Greubel, G. Du., G., Multhoff, B., Roper, M., Molls, T. E., Schmid. (2012) Induction and repair of DNA double-strand breaks assessed by gamma-H2AX foci after irradiation with pulsed or continuous proton beams. Radiat Environ Biophys, 51: 23-32;

[30] Nishimaki, N., Tsukimoto, M., Kitami, A., Kojima, S. (2012) Autocrine regulation of γ-irradiation-induced DNA damage response via extracellular nucleotides-mediated activation of P2Y6 and P2Y12 receptors. DNA Repair: 11: 657-665;

[31] Ghorai, A., Bhattacharyya, N. P., Sarma, A., Ghosh, U. (2014) Radiosensitivity and Induction of Apoptosis by High LET Carbon Ion Beam and Low LET Gamma Radiation: A Comparative Study. Scientifica, 2014: 1-10;

[32] Juliana, H., Osaki, Espinha, Y. T., Magalhaes, Forti, F. L. (2015) Modulation of RhoA GTPase Activity Sensitizes Human Cervix Carcinoma Cells to γ-Radiation by Attenuating DNA Repair Pathways. OxIdative Medicine and Cellular Longevity 2016: 1-11.

[33] Zhoo, H., Zhuang, Y., Li, R., Liu, Y., Mei, Z., He, Z., Zhou, F., Zhou, Y. (2018) Effect of different doses of X-rey irradiation on cell apoptosis, cell cycle, DNA damage repair and glycolysis in He-La cells. Oncology Letters, 11: 42-54;

[34] Brunner, S., Varga, D., Bozó, R., R. Polanek, R., Tőkés, T., Szabó, E. R., Molnár, R., Gémes, N., Szebeni, G. J., Puskás, J. L., Erdélyi, M., Hideghéty, K. (2021) Analysis of Ionizing Radiation Induced DNA Damage by Superresolution dSTORM Microscopy. Pathology and Oncology Research, 27: 160-173;

[35] Reynolds, R. C., Montgomery P. O., Hughes, B. (1964) Nucleolar "caps" produced by actinomycin D. Cancer Res, 24: 1269-1277;

[36] Simard, R., Langelier, Y., Mandeville, R., Maestracci, N., Royal, A. (1974) Inhibitors as tools in elucidating the structure and function of the nucleus. In: Busch H, editor. The Cell Nucleus. New York: Academic Press: 447-487;

[37] Puvion-Dutilleul, F., Mazan, S., Nicoloso, M., Pichard, E., Bachellerie, J. P, Puvion, E. (1992) Alterations of nucleolar ultrastructure and ribosome biogenesis by actinomycin D. Implication for U3 snRNP function. Europ J Cell Biol, 58:149-162;

[38] Shav-Tal, Y., Blechman, J., Darzacq, X., Montagna, C., Dye, B. T., Patton, J. G. (2005) Dynamic sorting of nuclear components into distinct nucleolar caps during transcriptional inhibition. Mol Biol Cell, 16:2395-2413;

[39] Tchelidze, P., Kaplan, H., Terryn, C., Lalun, N., Ploton, D., Thiry, M. (2019) Electron Tomography Reveals Changes in Spatial Distribution of UBTF1 and UBTF2 Isoforms within Nucleolar Components during rRNA Synthesis Inhibition. Journal Structural Biology, 208(2): 191-204;

[40] Olson, M. (2004) Sensing cellular stress: another new function for the nucleolus? Sci STKE, 10.

[41] Maggi, L. B., Weber, J. D. (2005) Nucleolar adaptation in human cancer. Cancer Invest, 23:599-608;

[42] Mayer, C, Grummt, I. (2005) Cellular stress and nucleolar function. Cell Cycle, 4:1036-1038;

[43] Drygin, D., Rice, W. G., Grummt, I. (2010) The RNA polymerase I transcription machinery: An emerging target for the treatment of cancer. Annu Rev Pharmacol, 50:131-156;

[44] Michel, J., Nolin, F., Wortham, L., Lalun, N., Tchelidze, P., Banchet, V., Terryn, C., Ploton, D. (2019) Various Nucleolar Stress Inducers Result in Highly Distinct Changes in Water, Dry Mass and Elemental Content in Cancerous Cell Components: Investigation Using Nano-Analytical Approach. Nanoteranostics, 3:179-195;

[45] Potapova, T. A., Unruh, J. R., Conkright-Fincham, J., Banks, C. A. S., Laurence, F., Shneider, D. A., Gerton, J. L. (2023) Distinct states of nucleolar stress induced by anticancer drugs. eLife, 12:1-30;

[46] Braten, M., Banreed, H., Berg, K., Moan, J. (2000) Induction of multinucleated cells caused by UVA exposure in different stages of the cell cycle. J Photochem Photobiol B: Biology, 71(5): 620-626;

[47] Salucci, S., Burattini, S., Batistelli, M., Baldassarri, V., Maltarlo, M. C., Falcieri, E. (2013) Ultraviolet B (UVB) Irradiation-Induced Apoptosis in Various Cell Lineages in Vitro. Int. J. Mol. Sci., 14: 532-546;

[48] Lee, C. H., Wu, S. B., Hong, C. H., Yu, H. S., Wei, Y. H. (2013) Molecular Mechanisms of UV-indiced Apoptosis and its Effects on Skin Residential Cells: The Implication in UV based Phototherapy. Int. J. Mol. Sci., 14(3): 6414-6435;

[49] Salucci, S., Burattini, S., Curzi, D., Buentempo, T., Martelli, A. M., Zappa, G., Falcieri, E., Battistelli, M. J. (2014) Photochem Phtobiol B: Biology,141: 1-9;

[50] Mirzayans, R., Audrais, B., Scott, A., Wang, Y. W., Kumar, P., Murray, D. (2017) Int. J. Mol. Sci.,18(2): 360-379;

[51] Azzouz, P., Khan, M. A., Sweerey, N., Palaniar, N. (2018) Two-in one: UV radiation simultaneously induces apoptosis and NETosis. Cell Death Discovery, 4: 51-78.

STUDYING THE IMPACT OF UBIQUITIN ON RADIATION-INDUCED DAMAGE TO GENES THROUGH BIOINFORMATIC METHODOLOGIES
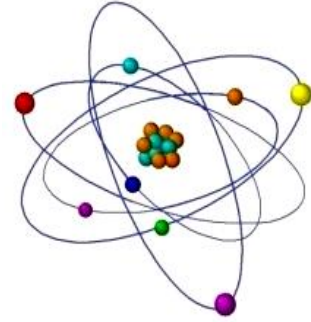
[1,2]**Irine Ioramashvili***, [2]**Rusudan Sujashvili**,
[3]**Giorgi Javakhishvili**

[1]Ilia State University, Georgia
[2]I.Beritashvili Center of Experimental Biomedicine, Laboratory of Biophysics, Georgia
[3]University of Georgia

*Corresponding author: irinejaparidze@gmail.com

ABSTRACT: *Understanding the intricacies of cellular responses to radiation exposure is crucial for advancing radiobiology and developing effective strategies against radiation-induced pathologies. The annual radiation dose, sourced from natural and human-made sources, underscores the critical nature of this problem. Ubiquitination, as a pivotal process in protein regulation, holds the potential for alterations post-irradiation, impacting cellular recovery. The unique features of ubiquitin, beyond protein degradation, position it as one of the key players in comprehending cellular responses to radiation exposure.*
Our studies, employing bioinformatic methods, have revealed the potential use of ubiquitin in the context of radiation-induced cell exposure. We conducted an analysis to assess the commonality in the genetic spectrum between genes damaged by radiation and genes associated with ubiquitin. This study utilizes RNA sequencing to identify differentially expressed genes in mice subjected to irradiation. Our investigation delves into the impact of irradiation on ubiquitin-related genes, on various functions such as chromosome segregation and organelle fission. The heightened expression of genes associated with the cell cycle suggests the foundational role of ubiquitin-related genes in organism recovery after radiation exposure. The study not only contributes to advancements in radiobiology but also offers direction for developing preventive strategies against radiation-induced pathologies.

Key words: radiation exposure, bioinformatics, cellular responses, protein regulation

INTRODUCTION

Approximately 80% of the annual cumulative dose of background radiation received by an individual emanates from naturally occurring terrestrial and cosmic radiation sources. Additionally, on a daily basis, individuals may inhale or ingest radionuclides originating from natural sources present in soil, water, and air. Human-made sources of radiation exposure cover a spectrum ranging from nuclear power generation to various medical devices, including x-ray machines and Computed Tomography (CT) scanners [1]. Radiotherapy is a prevalent treatment for over half of cancer patients, using high doses of radiation to eradicate malignant cells. However, the associated side effects are a considerable concern. Consequently, any enhancements in the field of radiotherapy hold the potential to significantly benefit many people [2]. Hence, it is crucial to investigate not only the mechanisms underlying the impact of radiation but also the potential for regulating and reducing the negative effects of radiation on the body. Exploring causative associations within the responses of living organisms to radiation

affords an enhanced comprehension of risks associated with diverse manifestations of radiation exposure.

Ubiquitination is a pivotal facet in the regulation of protein metabolism. Ubiquitylation represents a post-translational modification where ubiquitin attaches to a target protein. Ubiquitin, a 76-amino acid protein, can exist either freely or be conjugated to a protein, either as a single ubiquitin (monoubiquitination) or as multiple ubiquitins (polyubiquitination). The ubiquitination pathway involves three enzymes: Ubiquitin-activating enzyme (E1), ubiquitin-conjugating enzyme (E2), and ubiquitin-protein ligase (E3). Ubiquitin modifications intricately regulate essential cellular processes, including proteasomal degradation, activation of cell signaling cascades such as NF-κB, protein trafficking, DNA repair, maintenance of genome integrity, control of the cell cycle, and programmed cell death. A deep understanding of ubiquitination is critically important in the context of the pathobiology of various human diseases [4, 5, 6].

The versatile characteristics of ubiquitination suggest that processes involving ubiquitin may undergo alterations following irradiation, thereby influencing the recovery process subsequent to radiation exposure.

In our previous work, we identified the effect of ubiquitin administration on the proliferation of blood cells after exposure to radiation in mice, compared with intact groups [7, 8, 9, 10].

To enhance the efficiency of our investigation, we employed computational technology, using a bioinformatic approach. Bioinformatics represents the convergence of biology and informatics, offering a potent approach equipped with techniques and specialized software tools for the analysis of biological data, such as the study of the human genome [11].

Differentially Expressed Genes analysis is an effective method to identify genes implicated in disease development, allowing us to find biological distinctions between healthy and pathological states [12]. This strategic utilization of computer technology not only expedites data analysis but also affords the advantage of handling vast datasets of genomic studies, thereby augmenting the overall efficiency of our research.

Our investigation includes a comparative analysis of the spectrum of genes altered by radiation with the genetic set involved in the ubiquitylation process. The importance of such comparative study lies in the identification of damaged components, providing insights that could be used in developing strategies in radiotherapy.

MATERIALS AND METHODS

To interpret the results, we employed RNA sequencing (RNA-seq) analysis data to identify differentially expressed genes in both irradiated and non-irradiated conditions among young mice (2-3 months old). Although our working group had previously analyzed this data, we found it useful in elucidating the influence of ubiquitin on the organism post-irradiation [13, 14].

The information pertaining to ubiquitin-related genes was retrieved from an open-source database [15]. Molecular pathways identification was conducted using the David Genes bioinformatics platform and the KEGG PATHWAY database. For data processing and figure generation, statistical packages in R and Python were utilized.

RESULTS

In our prior investigation, we analyzed 322 differentially expressed genes, considering a threshold of expression levels exceeding ±1. Out of these, 212 genes associated with the ubiquitin and ubiquitination processes were identified. Based on the expression level higher than ±1.5 we identified 74 genes from this data set. The information regarding ubiquitin-related genes was sourced from the Gene Cards database [15].

According to our findings, the majority of ubiquitin-related genes are upregulated, with only three cases of downregulated genes. Notably, pronounced alterations in ubiquitin-related genes of irradiated mice were observed in chromosomes 1, 2, 7, and 11. To elucidate the gene expression patterns in this context, we conducted Gene Ontology analysis (GO) utilizing R bioinformatic packages. GO is a widely used tool to specify gene involvement in terms of cellular location, molecular function, and biological processes. For GO analysis 10 additional genes with expression levels lower than ±1.5 were used.

The biological processes (BP), molecular functions (MF), and cellular components (CC) associated with the obtained gene set are represented in Figure 1, Figure 2, and Figure 3 respectively. We chose genes with p. value < 0.0001 and the number of genes participating in the processes no less than 8.
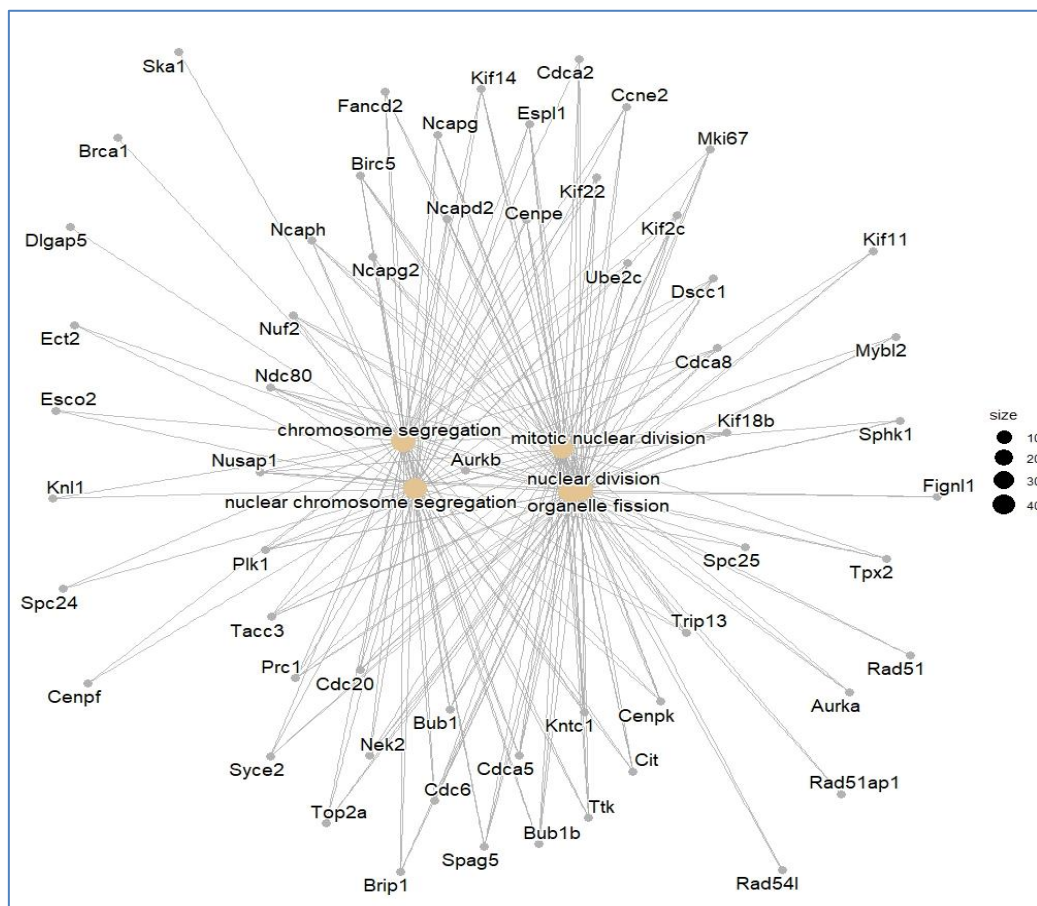
Figure 1. Biological processes (BP) associated with obtained genes set
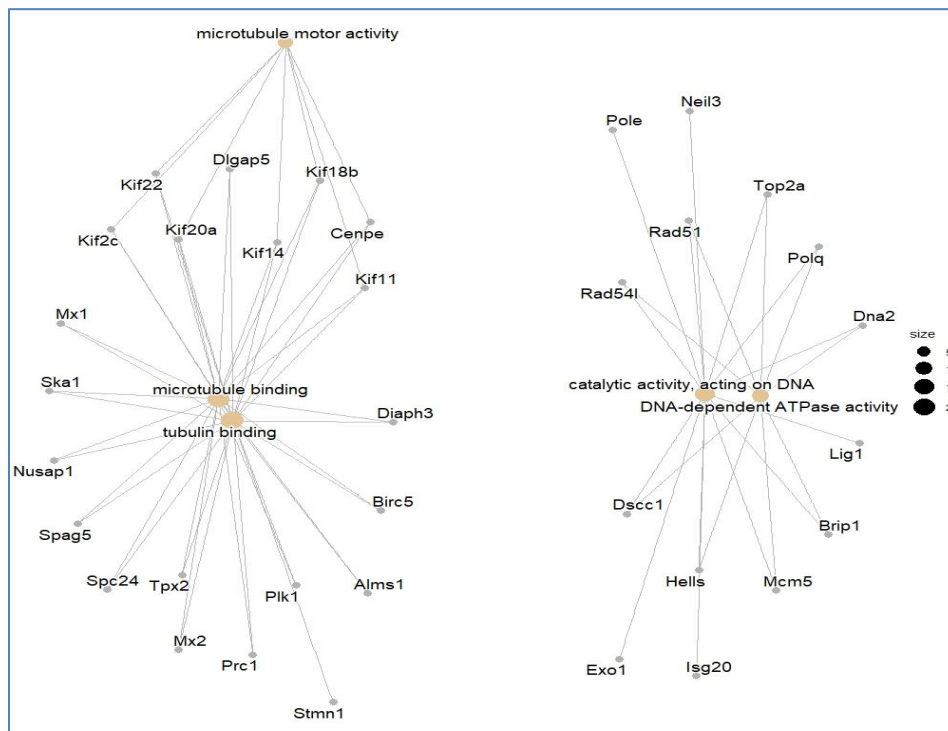
Figure 2. Molecular functions (MF) associated with obtained genes set.
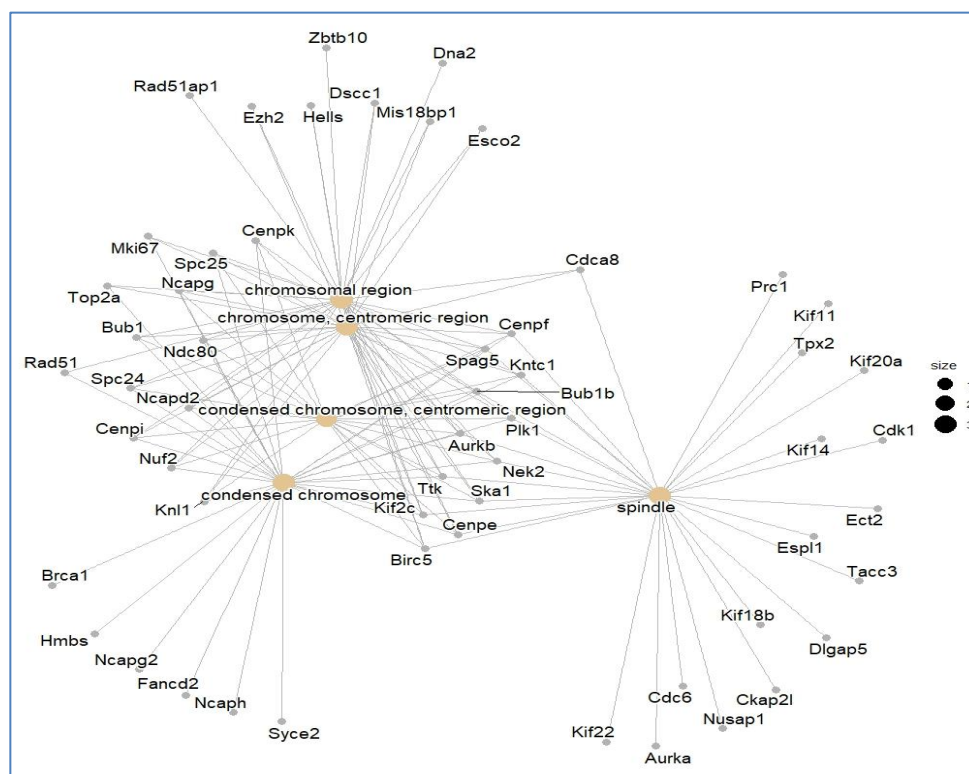
Figure 3. Cellular components (CC) associated with obtained genes set.

We quantified genes involved in biological processes (BP), molecular functions (MF), and cellular components (CC) in gene ontology analysis. Utilizing the entire gene set common with ubiquitin-related genes, regardless of their expression levels, we identified 76 genes for BP, 75 for MF, and 60 for CC. Notably, 28 genes actively participated in all three processes: 'Tpx2', 'Aurkb', 'Kif22', 'Top2a', 'Aurka', 'Kif18b', 'Ect2', 'Dlgap5', 'Ttk', 'Cdk1', 'Bub1', 'Spc24', 'Dscc1', 'Ncapg2', 'Nek2', 'Kntc1', 'Rad51', 'Nusap1', 'Plk1', 'Bub1b', 'Kif14', 'Birc5', 'Ska1', 'Kif11', 'Spag5', 'Cenpe', 'Prc1', and 'Kif2c'.

This data suggest that the pathological condition induced by irradiation leads to a disruption in the cell division process. This observation indicates alterations in protein functions, with some of their genes exhibiting atypical expression levels. A comprehensive investigation, including RNA sequencing under narrower conditions of the experiment, could provide further insights into resolving this matter.

 DISCUSSION

This bioinformatics project aimed to discern alterations in gene expression following radiation exposure, to broaden insights into the role of ubiquitin in diverse biological processes.

The unique properties of ubiquitin have positioned it as the focal point of our investigation. Beyond its role in protein degradation, ubiquitin exhibits the capability to post-translationally modify proteins, and form ubiquitin conjugates. This multifunctionality potentially exerts a profound impact on normal cellular functions [16]. Moreover, these distinctive features of ubiquitin suggest its participation as one of the contributors to cellular processes following radiation exposure.

Bioinformatics investigations of genes and Gene Ontology (GO) analysis, focusing on ubiquitin-related genes altered by irradiation, reveal significant impacts on various functions and processes. The affected biological processes include chromosome segregation, nuclear chromosome segregation, mitotic nuclear division, nuclear division, and organelle fission. In terms of molecular functions, alterations are observed in microtubule binding, tubulin binding, catalytic activity acting on DNA, and DNA-dependent ATPase activity. The changes in the expression of these genes manifest in the chromosomal centromeric region, spindle, and condensed chromosome centromeric region.

These processes are fundamental to cell formation and functionality, and their disturbances observed in this study are attributed to irradiation. The obtained information aligns with well-known effects of ionizing radiation, such as apoptosis-induced cell death and irreversible arrest of the G1/S cycle (G1/S arrest). These effects are characterized by the loss of normal nuclear structure, coupled with DNA degradation [17, 18].

   Let us delve into the intricate processes governed by genes exhibiting differential expression in irradiated mice. During the accurate segregation of chromosomes, kinetochores attach to microtubules coming from opposing poles of the spindle, forming bioriented chromosomes on the metaphase spindle. Positively expressed in our study, Survivin (Birc5) and Aurora B kinase form a chromosome passenger complex, regulating this critical process. The deubiquitylation enzyme hFAM plays a role in dissociating Survivin from centromeres, while the ubiquitin-binding protein Ufd1 is essential for the association of Survivin with centromeres.

Consequently, ubiquitin serves as a regulatory factor ensuring the precise targeting of Survivin and Aurora B (Aurkb) to centromeres [19]. Moreover, the Linear Ubiquitin Chain Assembly Complex (LUBAC) catalyzes linear ubiquitination, facilitating chromosome congression and dynamic alignment by linking the dynamic kinetochore microtubule receptor CENP-E to the static KMN network. The KMN network is a multiprotein assembly component crucial for establishing kinetochore-microtubule junctions [20]. These detailed mechanisms highlight the intricate regulatory role of ubiquitin in orchestrating fundamental processes like chromosome segregation and alignment in response to irradiation. Considering ubiquitin's potent regulatory role, changes in its functions due to irradiation may profoundly impact the above-mentioned processes.

Upon examination of obtained protein set and their alignment with KEGG pathways, specifically those related to the cell cycle (Figure 3.), it was found that 23 of the identified genes, derived from gene expression analysis, are involved in the cell cycle, including the MAPK signaling pathways. Significantly, all these genes exhibit an increased expression in our study. This heightened expression implies a potential response aimed to initiate the restoration of cells lost due to radiation-induced cell death.
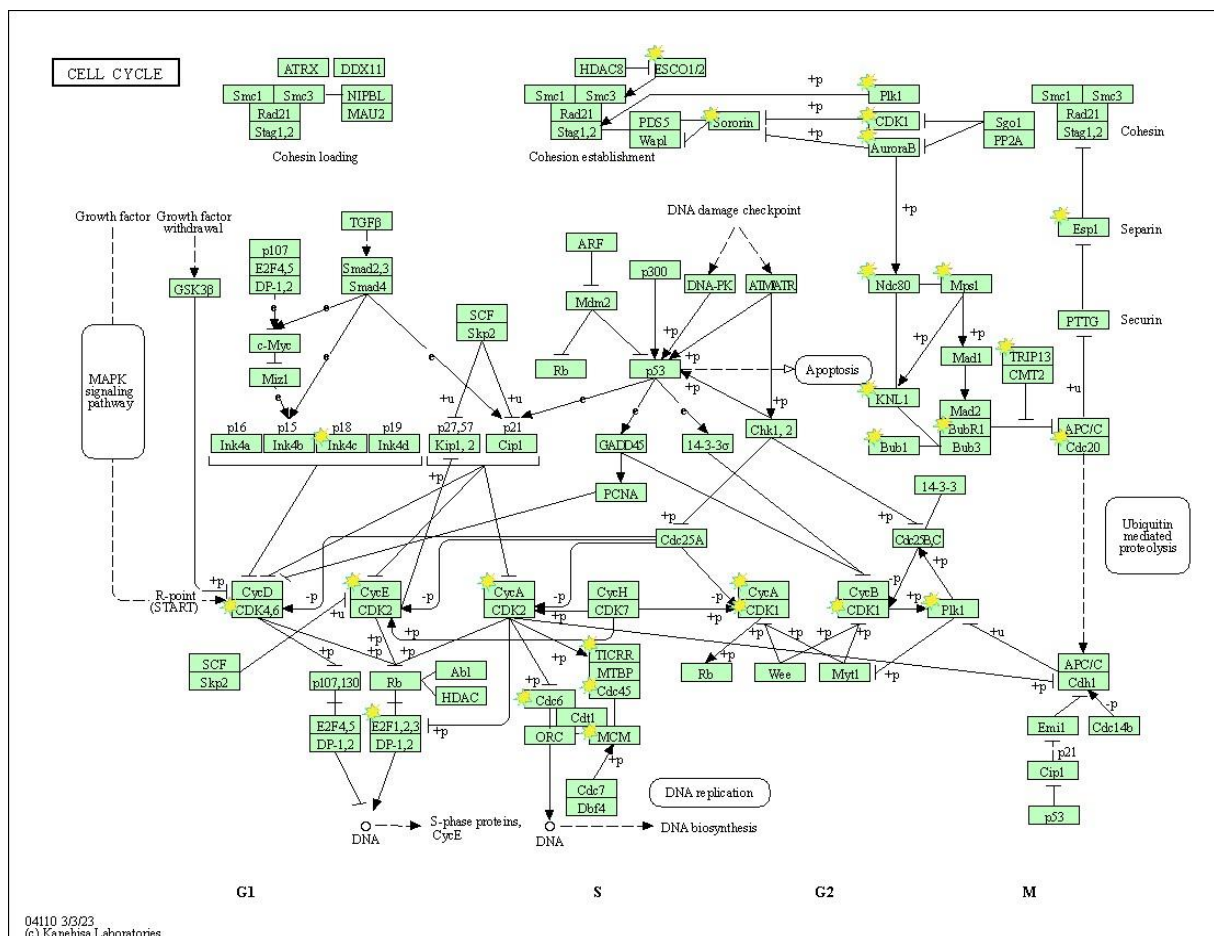
Figure 3. Cell cycle pathways. Asterisks indicate genes with the levels of expression changed by irradiation according to our study (the figure was generated based on our data using the David Genes bioinformatics platform and the KEGG PATHWAY database)

Activation of signaling pathways such as MAPK, PI3K, Wnt, and Sonic Hedgehog (SHH) is known to induce proliferation in various cell types [21]. Among these, the Ras/Raf/MAPK (MEK)/ERK pathway is a pivotal signaling cascade within the MAPK transduction pathways [22]. It is evident that the damage inflicted upon proteins involved in these signaling pathways by irradiation may be one of cases of the adverse effects of radiation on the organism.

Our investigation extends beyond the well-established effects of radiation, such as apoptosis and G1/S arrest, to propose a potential involvement of the MAPK signaling pathway. The comparative analysis and utilization of the KEGG pathways database highlight an association between irradiation and alterations in this crucial pathway governing cell proliferation and expression.

While the direct influence of ubiquitin remains unexplored in our study, it is crucial to emphasize the foundational role of ubiquitin-related genes in our computational analysis and the identification of the coincidences with known processes in which they participate. The possibility of changes in ubiquitylation and modifications of proteins under the influence of irradiation suggests a disruption in protein regulation. Our findings warrant further exploration through comprehensive studies employing advanced techniques like RNA sequencing and targeted protein quantification.

In essence, our study lays the groundwork for future research endeavors aimed at unraveling radiation-induced cellular responses and underscores the potential significance of the MAPK signaling pathway and ubiquitin-related processes in this context.

Future investigations under more refined conditions, including specific animal groupings and varied irradiation doses, hold promise for a deeper understanding of the intricate mechanisms of radiation exposure.

CONCLUSIONS

1. In accordance with our investigations, the commonality of the genetic spectrum between genes susceptible to radiation-induced damage and ubiquitin-related genes has been established. This observation pertains to 65% of the genes with altered expression subsequent to exposure to radiation. In the course of our research, 84 genes were selected, of which 74 exhibited a deviation in expression levels no less than ±1.5. Additionally, 10 genes were identified through the application of Gene Ontology (GO) analysis.

2. Gene Ontology (GO) analysis was applied to the obtained gene set, revealing insights that suggest alterations in gene expression may potentially stem from disruptions in the cellular division process and associated mechanisms. We interpret this observation as evidence of the potential of ubiquitin in mitigating the negative effects of radiation on the human body.

3. The gene set was studied using the KEGG database, allowing us to conclude that the radiation-induced disturbance in the cell cycle, considering ubiquitin-related genes, may correspond to an interference with the MAPK molecular pathway. Disruption of this molecular pathway is implicated in various pathologies.

Our investigation not only contributes to the understanding of radiobiology but also offers avenues for developing targeted interventions and preventive strategies against radiation-induced pathologies.

REFERENCES

[1]. World Health Organization. "Ionizing Radiation and Health Effects." WHO, 2023. [Online] Available: https://www.who.int/news-room/fact-sheets/detail/ionizing-radiation-and-health-effects

[2]. Jain, S. "Radiation in Medical Practice & Health Effects of Radiation: Rationale, Risks, and Rewards." J Family Med Prim Care. 2021 Apr;10(4):1520-1524. doi: 10.4103/jfmpc.jfmpc_2292_20. Epub 2021 Apr 29. PMID: 34123885; PMCID: PMC8144773.

[3]. Zhang, R.K., Lyu, J.H., Li, T. "Effects of Radiation on Protein." Journal of Nutritional Oncology 5(3):116-122, August 15, 2020. | DOI: 10.34175/jno202003002

[4]. Guo, H.J., Rahimi, N., Tadi, P. "Biochemistry, Ubiquitination." Treasure Island (FL): StatPearls Publishing, [Last Update: March 16, 2023]. [Online] Available: https://www.ncbi.nlm.nih.gov/books/NBK556052/

[5]. Damgaard, R.B. "The Ubiquitin System: From Cell Signaling to Disease Biology and New Therapeutic Opportunities." Cell Death Differ 28, 423–426 (2021). https://doi.org/10.1038/s41418-020-00703-w

[6]. Ioramashvili, R. Sujashvili, "Involvement of Ubiquitin – 26S Proteasome System in Regulation of Obesity", Proc.Georgian Nat. Acad. Sci., Biomed. Series, 2020, vol.46, N5-6. ISSN-0321-1665.

[7]. Sujashvili, R., Ioramashvili, I., Gvinadze, N., Aptsiauri, K. "Inhibition of Proliferative Activity of Bone Marrow Cells by Extracellular Ubiquitin." Proc Georgian Natl Acad Sci, Biomed Ser. 2014;40(5-6):265-270.

[8]. Sujashvili, R., Ioramashvili, I., Tsitsilashvili, S., Mazmishvili, K. "The Impact of Extracellular Ubiquitin on Regenerating Bone Marrow and Peripheral Blood Cells After Irradiation." Cold Spring Harbor meeting: Ubiquitins, Autophagy & Disease. April 23-27, 2019, New York, USA.

[9]. Sujashvili, R., Ioramashvili, I., Aptsiauri, K., et al. "Negative correlation between levels of extracellular ubiquitin and regenerating blood cell count in irradiated mice." EuroSciCon Conference on Oncology and Cancer Stem Cell. November 05-06, 2018, Paris, France.

[10]. Sujashvili R., Ioramashvili I., Mazmishvili K., Tsitsilashvili S., Gamkrelidze M., Moderation of quantitative changes of regenerating erythropoietic cells by extracellular ubiquitin, Georgian Medical News, 2020, Jul-Aug; (292-293):87-92

[11]. Iqbala, N., Kumarb, P. "From Data Science to Bioscience: Emerging Era of Bioinformatics Applications, Tools, and Challenges." International Conference on Machine Learning and Data Engineering, ScienceDirect, Procedia Computer Science 218 (2023) 1516–1528.

[12]. Boldogh, I., Pratomo, I.P., Tedjo, A., Noor, D.R., Rosmalena. "Differentially Expressed Genes Analysis in the Human Small Airway Epithelium of Healthy Smokers Shows Potential Risks of Disease Caused by Oxidative Stress and Inflammation and the Potentiality of Astaxanthin as an Anti-Inflammatory Agent." International Journal of Inflammation, Volume 2023, Article ID 4251299, https://doi.org/10.1155/2023/4251299

[13]. Ioramashvili, I., Gogebashvili, M., Sujashvili, R., & Ivanishvili, N. (2023). "Evaluation of Differently Expressed Genes in Irradiated and Intact Mice to Study Radioactive Aging Phenomenon." Radiobiology and Radiation Safety, 3(4), 32–40. https://radiobiology.ge/index.php/rrs/article/view/6290

[14]. Ioramashvili I., Gogebashvili M., Sujashvili R., Ivanishvili N., Investigation of Radiation Induced Aging Model, 5th Biennial International Symposium and School for Young Neuroscientists Brain and Neuroplasticity. Structural and Molecular Aspects, 2023, ISBN 978-9941-18-433-8

[15]. Stelzer, G., Rosen, N., Plaschkes, I., Zimmerman, S., Twik, M., Fishilevich, S., Stein, T.I., Nudel, R., Lieder, I., Mazor, Y., Kaplan, S., Dahary, D., Warshawsky, D., Guan-Golan, Y., Kohn, A., Rappaport, N.,Safran, M., and Lancet, D. "The GeneCards Suite: From Gene Data Mining to Disease Genome Sequence Analyses." Curr. Protoc. Bioinform. 54:1.30.1-1.30.33. doi: 10.1002/cpbi.5

[16]. R. Sujashvili, I. Ioramashvili, N. Gvinadze, K.Aptsiauri, N.Ivanishvili, K.Mazmishvili, "Changes of serum ubiquitin levels along with development of thrombocytopenia in irradiated mice", Digest of Beritashvili Center of Biomedicine, ISBN:978-9941-8-1339-9, 2019, 227-233

[17]. Little, J.B. "Principal Cellular and Tissue Effects of Radiation." In: Kufe DW, Pollock RE, Weichselbaum RR, et al., editors. Holland-Frei Cancer Medicine. 6th edition. Hamilton (ON): BC Decker; 2003. https://www.ncbi.nlm.nih.gov/books/NBK12344/

[18]. Jiao, Y., Cao, F., Liu, H. "Radiation-induced Cell Death and Its Mechanisms." Health Physics 123(5):376-386, November 2022. | DOI: 10.1097/HP.0000000000001601

[19]. Vong, Q.P., Cao, K., Li, H.Y., Iglesias, P.A., Zheng, Y. "Chromosome Alignment and Segregation Regulated by Ubiquitination of Survivin." Science. 2005 Dec 2;310(5753):1499-504. doi: 10.1126/science.1120160. PMID: 16322459.

[20]. Wu, M., Chang, Y., Hu, H., et al. "LUBAC Controls Chromosome Alignment by Targeting CENP-E to Attached Kinetochore." Nat Commun 10, 273 (2019). https://doi.org/10.1038/s41467-018-08043-7

[21]. Zhang, Q., Wang, L., Wang, S., et al. "Signaling Pathways and Targeted Therapy for Myocardial Infarction." Sig Transduct Target Ther 7, 78 (2022). https://doi.org/10.1038/s41392-022-00925-z

[22]. Guo, Y., Pan, W., Liu, S., Shen, Z., Xu, Y., Hu, L. "ERK/MAPK Signalling Pathway and Tumorigenesis (Review)." Experimental and Therapeutic Medicine 19, no. 3 (2020): 1997-2007. https://doi.org/10.3892/etm.2020.8454

ARE THE "LOW DOSES" TRUE LOW?

*Mikhyeyev Oleksandr[1], Lapan Oksana[2]

[1]Institute of Cell Biology and Genetic Engineering,
National Academy of Science of Ukraine, Ukraine
[2]National Aviation University, Ukraine
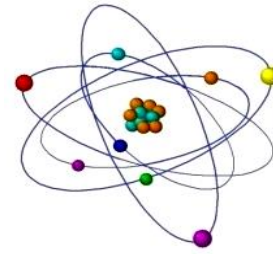
*Corresponding author: mikhalex7@yahoo.com

ABSTRACT: *The article states that the Chernobyl accident caused only a quantitative change in the pre-existing spectrum of radiobiological problems in the direction of increasing attention to the theoretical and practical issues of the effect of chronic ionizing radiation on biological objects of different levels of structural and functional organization. It is believed that chronic radiation influences biological objects in the so-called "low doses", the quantitative measure of which, however, is determined by subjectively chosen criteria. The article considers two main aspects of the problem of "low doses": firstly, to establish a relationship between these doses and subthreshold doses and, secondly, to show the role of heterogeneous tropism of biological structures in relation to their ability to absorb radionuclides from the environment, which contributes to the formation of uneven dose loads.*

Key words: "low doses", "subthreshold doses", radiocesium, radiostroncium

The relationship between the concept of "low doses" and the concept of "subthreshold doses". The resulting radioecological situation determined such characteristics of dose loads on organisms that forced radiobiologists to move from studying the predominantly effect of acute exposure at doses that cause radiation sickness or deterministic effects in the general case, to a closer study of the so-called "low doses" of radiation which are associated, as a rule, with chronic exposure conditions.

Probably the most practical definition of "small doses" would be to define them as poorly studied doses due to many methical and methodological difficulties (the complexity of dosimetry, statistical data processing, the need for large amounts of research, the complexity of interpreting the results). If we try to give a more exact definition of "small doses", it is necessary, first of all, to determine or select a test reaction by which one can judge the effect of radiation (chromosomal aberration frequency, mitotic index, average life expectancy (ALS) etc.). Obviously, most reactions will have a threshold of sensitivity and (or) resistance to radiation. In this case the only non-threshold reaction will be the ionization or excitation of atoms and molecules of the irradiated object, since the energy of quanta or particles of ionizing radiation is much greater than the ionization energy of atoms or the energy of their covalent bonds in molecules. In this regard, the question of the threshold effect of radiation at a given level of integration is removed, and in relation to these reactions it is incorrect to talk about small doses or rather it is meaningless regarding the large values of the energy of particles and quanta.

Any absorbed dose is capable of causing a response at the molecular level, and the whole problem comes down to its detection. The existence of quasi-thresholds and, accordingly, quasi-threshold doses found in the study of dose dependences of the survival of unicellular organisms testifies just in favor of the fact that these reactions are non-threshold and, therefore, are caused by damage of N-impact targets, the probability of which always exists according to the Poisson nature of the distribution primary acts of interaction of quanta or corpuscles of radiation with the target. Obviously, the degree of manifestation of the reaction (reproductive death, for example) to irradiation in each cell does not depend on the absorbed dose; therefore, such reactions are usually called stochastic. This class of reactions should also include somatic (carcinogenic, for example) and hereditary effects that arise on the basis of one damaged cell but retained the ability to reproduce cells [1].

All reactions or stages of reaction to irradiation develop within the framework of a specific structural and functional hierarchy of the biological system under study (from cells to ecosystems). If they (reactions) have a pronounced threshold character, then the dose dependence has a true shoulder [2]. Only for reactions of this kind it is expedient to speak about the existence of small doses, which are more correctly (stricter) called subthreshold. Of course, a subthreshold dose for one type of effect may simultaneously be above the threshold for another effect and vice versa. For example, subthreshold doses for insects regarding the effect of irradiation on life expectancy turn out to be sterilizing or at least disrupting gametogenesis. Probably, in this case insects "survive" due to the functioning of somatic cells that are more radioresistant to radiation. In another situation a subthreshold dose in relation to the inhibition of a function may be suprathreshold in relation to the stimulation of the same or another function. In other words, we should talk about the complex potential structuring of any studied threshold.

Studying the reactions of biological objects of any structural and functional level, one can always distinguish a range of doses called "small" which are essentially subthreshold. For instance, even subthreshold doses that are close to those that induce interphase death of plant cells and are measured in thousands of *Gy* have the right to be called small, since they are not capable of inducing a transient process in a cell ending in its metabolic death. Radiobiological reactions that have a true threshold, the degree of manifestation of which depends on the absorbed dose (delayed cell division, acute radiation sickness or loss of organ function, for example) are classified by the ICRP as deterministic [1]. Thus, only in relation to deterministic reactions it makes sense to speak of "small doses", meaning subthreshold doses by them.

Quasi-background doses. Regardless the nature of the effect induced by ionizing radiation, i.e. regardless of whether this is stochastic or deterministic, from our point of view, most of the doses received by biological objects in the territories contaminated after the Chernobyl accident should be called "quasi-background doses", emphasizing their quantitative and qualitative similarity to the pre-accident parameters of the natural radiation background (NRF). Thus, the concept of "quasi-background dose" is closer in the meaning to the concept of "exposure dose" and characterizes to a greater extent the conditions of irradiation of a biological object, regardless of the thresholds of its sensitivity or stability. In particular, this concept can be useful

in studying the nonlinear dependence of the frequency of the output of stochastic effects (aberrations, for example) in the region of doses close to the background values.

The vertical distribution of radiocesium in the main root of an aquatic culture of seedlings as an example of the conditions for the formation of heterogeneous dose loads.

Previously we studied the growth reaction of the roots of pea seedlings grown in an aqueous solution of chloride salt of cesium-137 [3]. At the specific activity of the used solutions from 1480 to 2220 *kBq/l* after a week of incubation of the plants, a complete cessation of the growth of their roots was observed. The calculation of the doses absorbed by the roots [4, 5] from external irradiation and exposure due to radionuclides incorporated into the root tissue was based on the assumption of a uniform distribution of radiocesium in the zones of the main root (meristematic zone, the zone of extension and differentiation, the zone of differentiated cells). The absorbed dose rate from internal exposure was determined by the formula:

$$P = 1,6 \times 10E^{-13} \times C \times f \times E,$$

where: *P* is the absorbed dose rate, *Gy/s*;

C is the specific activity of the sample, *Bq/kg*;

f is the output of this type of radiation to decay;

E is the energy of particles (for beta particles - average), *MeV*.

The power of external irradiation in the zone of root habitation was 5 *mlR/h*. The value of the total absorbed dose accumulated during the time of plant incubation (7 days) was about 1 *Gy*, which in no way corresponded to the observed inhibitory (lethal) effect on the root meristem. Comparing the data of these experiments with the results of studying the effect of acute irradiation and knowing that the gamma and beta radiation of cesium-137 does not differ qualitatively from the standard radiation, we assumed the heterogeneity of the vertical distribution of radiocesium in the main root with its predominant concentration in the meristematic zone.

To test this assumption a series of experiments was carried out in which the vertical distribution of radiocesium along the length of the main root was studied. For this purpose after a day of incubation of 5-day seedlings of peas of the Zelenozerny variety and corn of the Dneprovskaya 247 variety in a radiocesium solution with a specific activity of 296 and 1700 *kBq/L*, respectively, the main root was cut along its entire length into 5-mm segments, weighed, and the total activity of each segment was measured on a 1211 RACKBETA liquid scintillation counter, after making sure that the self-absorption of beta radiation in the samples can be neglected [6].

The results of this series of experiments are shown in Figures 1. a, b. One can see a sharp uneven distribution of radiocesium along the length of the root. The first segment, in which the meristematic zone is located, has the highest specific activity. This was especially pronounced in maize roots. As the distance from the root tip, the activity of the segments drops sharply, and this drop has a noticeable oscillatory character. By incubating seedlings in a solution of radiocesium until lateral roots appeared and analyzing the distribution of radiocesium along the

length of the latter, we found that the distribution of radionuclides in them had a similar character (Figure 2.). Only some features of radiocesium accumulation by lateral roots should be noted. In particular, the total level of accumulation is much lower than in the main root, because by the time the lateral roots form, the main amount of the isotope (up to 98%) [7] is absorbed by the main root. In addition, some increase in the level of accumulation in the last segments of the lateral root was noted which is probably due to the secondary redistribution of the isotope in the main root.

Figure 3. presents the results of a more detailed study of the distribution of radiocesium within the first and the second segments with a total length of 10 mm. It can be seen that the main part of the activity is concentrated in the first three millimeters of the root apical zone. This is exactly the zone where the meristem is located, which consists of the most radiosensitive cells [8].

Knowing the total activity of radiocesium in the main root, the weight of its individual segments, and the total activity of the isotope in each of them, it is possible to calculate what proportion of the total activity contains the apical part of the root and also to calculate the accumulation coefficients of the radionuclide by individual segments. It turned out that the apex 5 mm long whose weight is approximately 3% of the weight of the entire root (on the 5th-6th day of cultivation) contains up to 30% of the total activity of sorbed radiocesium. With an average accumulation coefficient for the entire root of about 800-1000, the accumulation coefficient in the apex reaches tens of thousands (27000), i.e. the concentration of radiocesium in the apical part and especially in the meristematic zone (accumulation factor 39000) is an order of magnitude higher than the average concentration of the radionuclide in the root, which means that the absorbed doses of gamma and beta radiation from incorporated radiocesium are at least 10 times higher than the initially established value, that is, it approaches a value of 10 *Gy*. This absorbed dose is already high enough to cause irreversible inhibition of growth processes. Figure 4. shows the dynamics of accumulation of radiocesium by the apical zone of the root, and in Figure 5. is shown the dynamics of the absorbed dose from external and internal exposure**.**

The heterogeneity of the distribution of radiocesium established in this way confirms our assumption and makes it possible to explain the lethal effect of cesium radionuclides incorporated into the root tissue.

Based on data on the unequal intensity of biochemical processes along the length of the main root (respiration, protein synthesis, etc.) [6] and taking into account the chemical similarity of cesium with potassium, a series of experiments was carried out to elucidate the role of active and passive sorption of radiocesium in causing the registered heterogeneity of its accumulation. In the experimental version of the experiment, the roots of the seedlings were subjected to hyperthermic treatment before planting on the radiocesium solution by heating them in a water bath for 30 seconds at 50 ^{0}C. The results of this experiment (Figure 6.) show that, at least in the apical part of the root, the recorded level of radiocesium absorption is a consequence of active physiological and biochemical processes. However, these results cannot be considered definitive proof of the role of active sorption, since hyperthermia could also disrupt the processes of passive sorption.

In addition to experiments with cesium-137, similar studies were carried out with strontium-

90. An aqueous solution of strontium-90 nitrate was used. Without going into the methodological details of experiments with radiostrontium, we only note that a lethal effect similar to that observed for radiocesium was obtained at specific activities of radiostrontium that were three orders of magnitude higher than the corresponding values for radiocesium [3]. We found the explanation of this fact by analyzing the distribution of radiostrontium along the main root of pea seedlings. It can be seen from Figure 7. that radiostrontium is concentrated mainly in the zone of elongation and the beginning of cell differentiation which ultimately leads to significantly lower dose loads from beta radiation on the meristematic zone of the apical part of the root.

In order to make sure whether the established features of the distribution of radionuclides over root zones are significant for the root systems of plants growing under soil culture conditions, it was decided to conduct a series of experiments on growing pea seedlings on soil contaminated with cesium-137 radionuclides. Soil with a specific activity for caesium-137 of 15 *kBq/kg* was used. Seedlings were removed from the soil from time to time and their main roots were cut into segments and analyzed by the method described above. The results presented in Figure 8. show a similar nature of the distribution of radionuclides along the length of the main root both in the water culture of seedlings and in the soil culture. The accumulation coefficient of radiocesium in the apical part of the root for 72 hours of incubation under these conditions was 200, and the specific activity was 3.5 *MBq/kg*. During the same period (comparatively short compared to the maximum possible duration of the growing season), the dose accumulated by the apical part under the conditions of soil culture was 0.02 *Gy* (in solution for the same period - 9.2 Gy). This circumstance once again indicates the important role of heterogeneity in the accumulation of radionuclides by different biological structures and the need to take it into account when estimating the doses absorbed by them, which may turn out to be very far from "low doses".

The heterotropy of biological structures, revealed by studying the intake of radionuclides into them, causes the formation of heterogeneity of the doses absorbed by different structures, which can (at a high level of tropism) cause inhibition effects and even lethal effects. This circumstance is of fundamental importance for explaining radiobiological effects in plants growing in areas with an increased radiation background (zones of radionuclide anomalies). In particular, the most likely cause of the stimulatory effect of radiation on plants under such conditions may be a significant inhibition of proliferative activity or even irreversible damage to the root apical meristem which, as a rule, is followed by the removal of apical dominance, increased development of lateral roots resulting in the stimulation of the development of the aerial parts of plants   .

Thus, the detected vertical heterogeneity of the distribution of radiocesium in the main root of seedlings (with its predominant concentration in the meristematic zone) makes it possible to significantly refine the amount of doses absorbed by the root meristem from incorporated radionuclides, explaining the apparent discrepancy between the calculated absorbed doses and the observed effects. In addition, the established pattern of distribution of radiocesium in the root can serve as an experimental basis for developing a method for predicting radionuclide contamination of plants by analyzing the content of radionuclides in the root apexes.
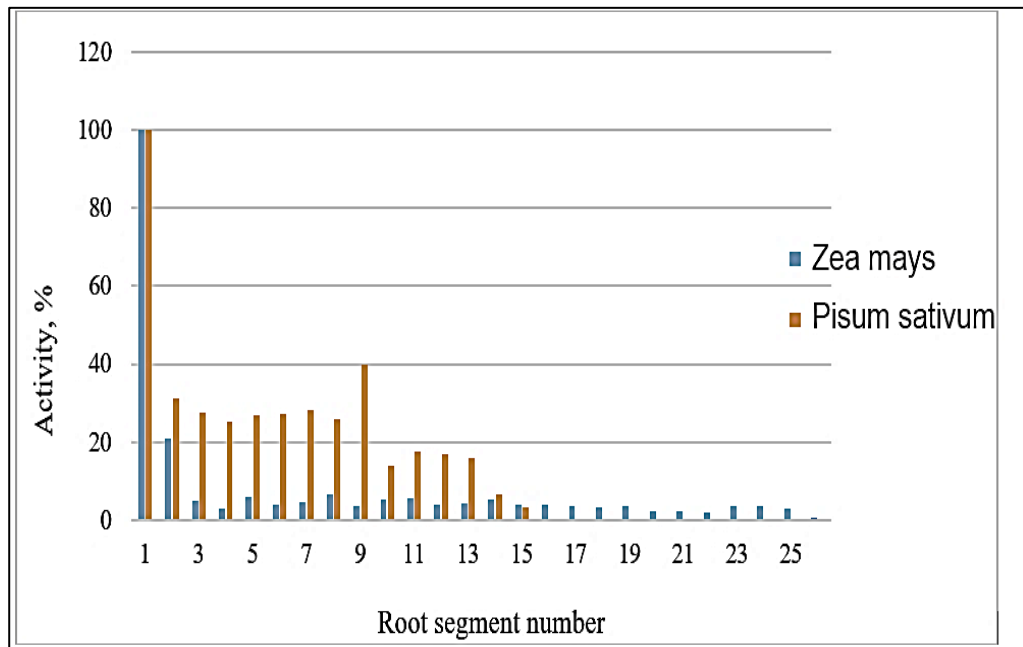
**Figure 1. Specific activity of cesium-137 in 5-mm segments
of the main roots of corn and pea seedlings, % of the activity of the apical segment**
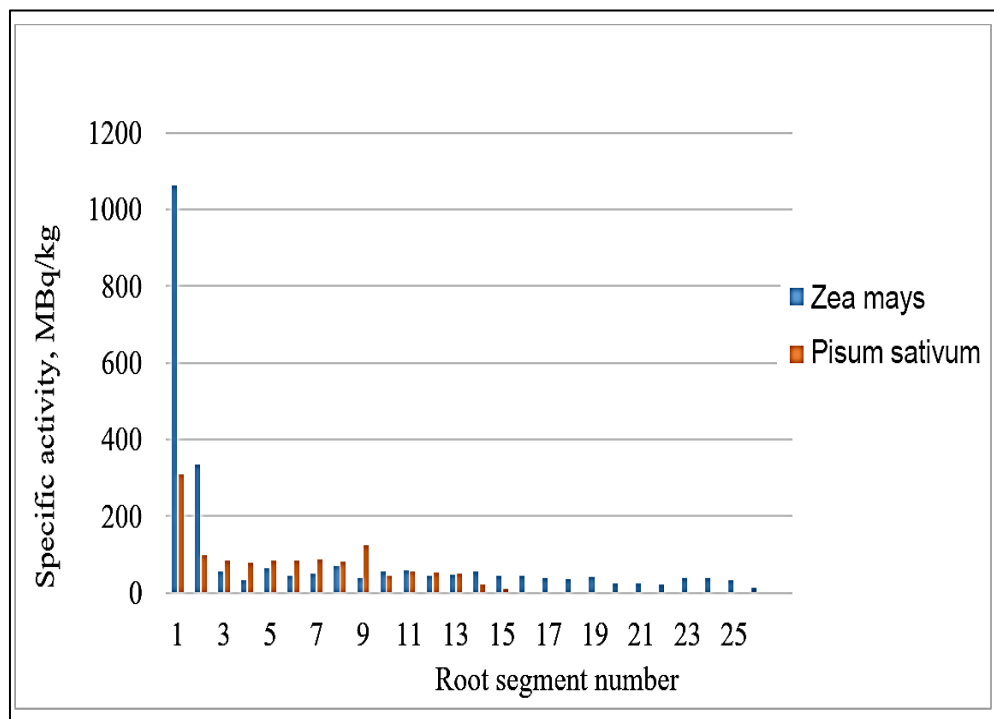
**Figure 1.a. Specific activity of cesium-137 in 5-mm segments of the
main roots of corn and pea seedlings, MBq/kg**
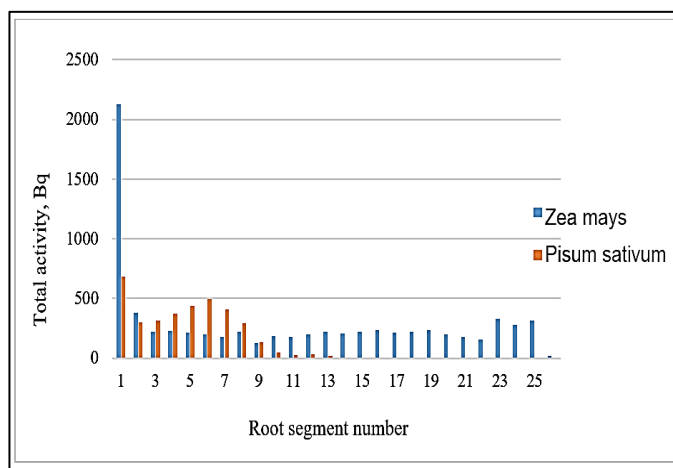
Figure 1.b. Distribution of the total activity of cesium-137 over 5-mm segments of the main roots of corn and pea seedlings, Bq

Figure 2. Specific activity of caesium-137 in 5-mm segments of lateral roots of pea seedlings, % of the activity of the apical segment

Figure 3. Specific activity of cesium-137 in root segments depending on their distance from the apex of the main root of pea seedlings grown on an aqueous solution of cesium-137 chloride with a specific activity of 1.7 MBq/l, MBq/kg
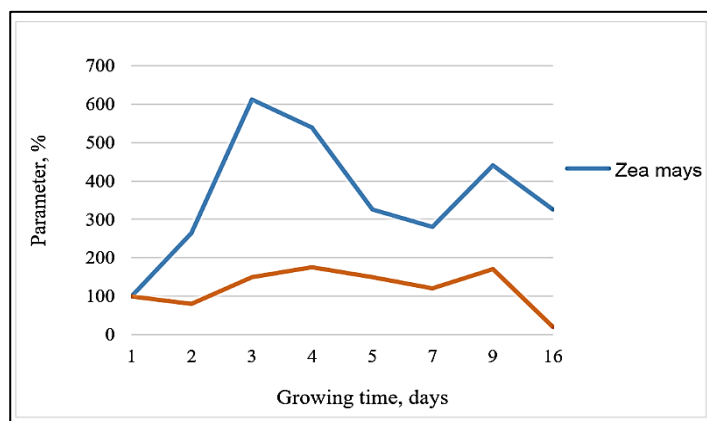
Figure 4. Dynamics of accumulation of cesium-137 by the apical part of the main root and dynamics of growth of the main root of pea seedlings grown on a solution of cesium-137 chloride with a specific activity of 1.7 MBq/l, % to the corresponding indicator for the first day
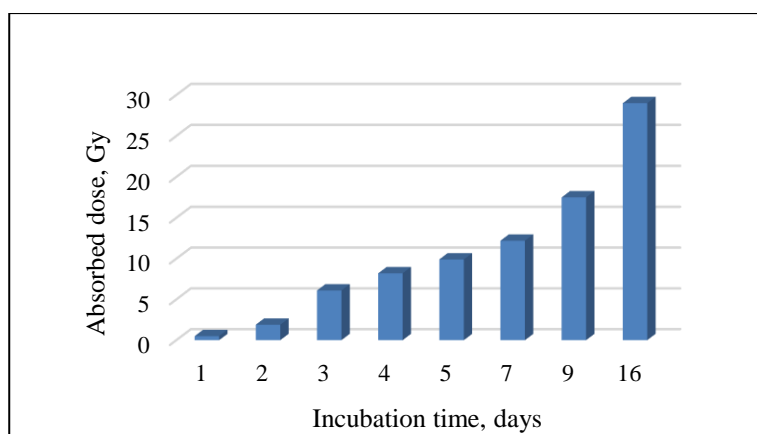
Figure 5. Dose absorbed in the 5-mm apex of the main root of pea seedlings grown on an aqueous solution of cesium-137 chloride with an initial specific activity of 1.7 MBq/l, Gy
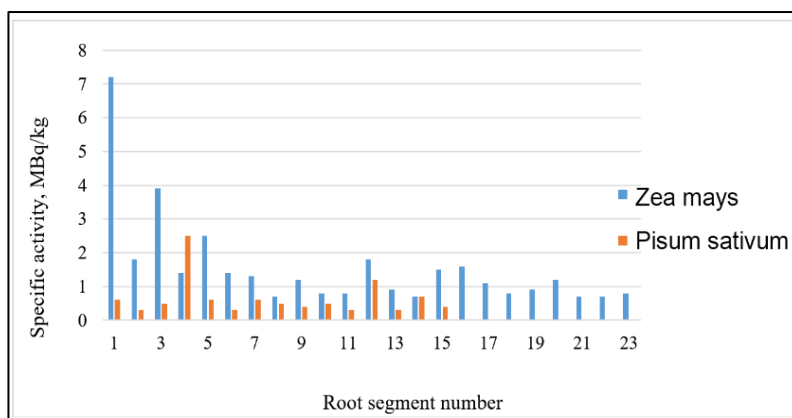
Figure 6. Specific activity of cesium-137 in 5-mm segments of the main root of pea seedlings after their hyperthermal treatment, MBq/kg
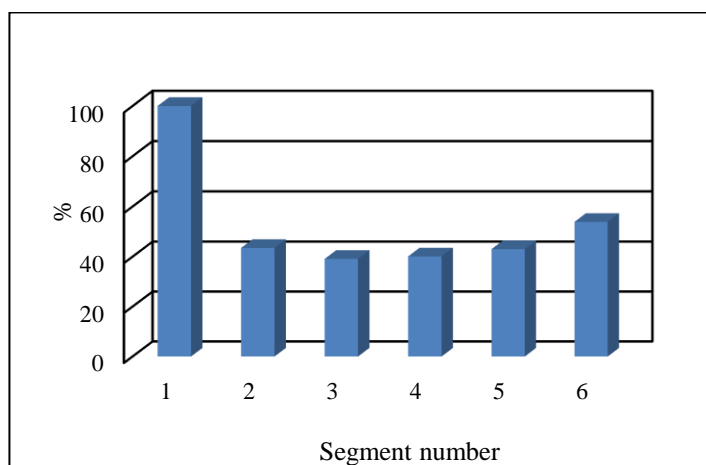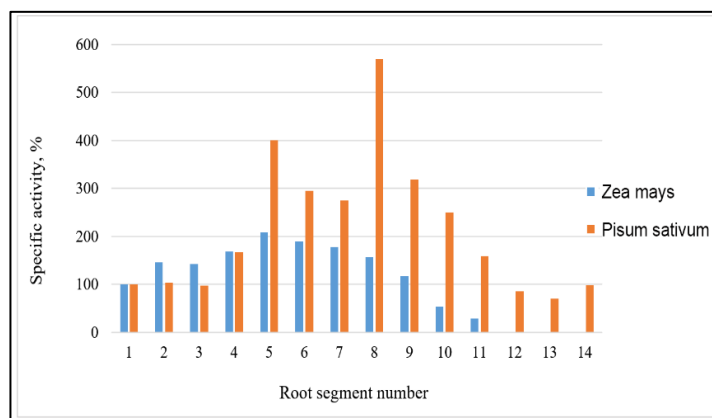
Figure 7. Specific activity of Sr-90 in segments of the main root of pea seedlings, % of the specific activity of the apical segment
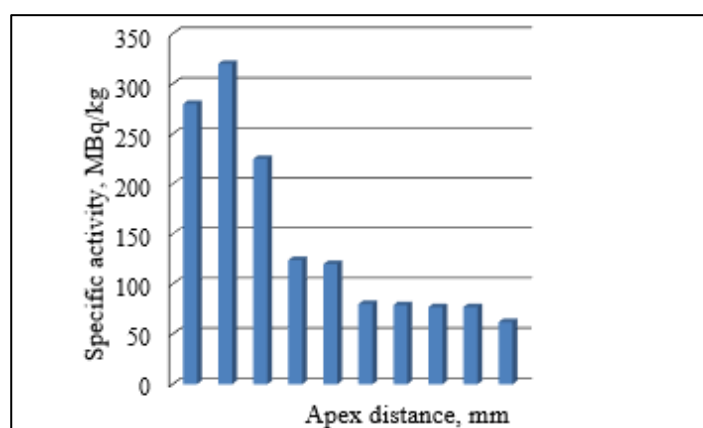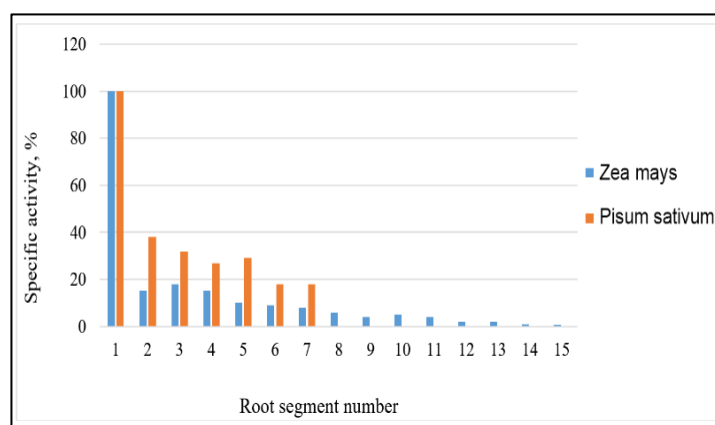

Figure 8. Specific activity in the root segments of pea seedlings grown on an aqueous solution of Cs-137 and on soil contaminated with a mixture of radionuclides of Chernobyl origin, % of the activity of the apical segment

REFERENCES

[1] Radiation safety (1992). ICRP Recommendations 1990. ICRP Publication 60. Part 1. M.: *Energoatomizdat*, 192 p. (in Russian).

[2] Akoev I. G. (1970). The problems of post-radiation recovery. M.: *Atomizdat*, 368 p. (in Russian).

[3] Grodzinsky D. M., Kolomiets K. D., Kutlakhmedov Yu.A. (1991). Anthropogenic radionuclide anomaly and plants. Kyiv: Lybid, 92 p. (in Russian).

[4] Grodzinsky D. M. (1962). Methodology for the use of radioactive isotopes in radiobiology. Kyiv: *Izdatelstvo akademii selskohozyaystvennyih nauk*, 172 p. (in Russian).

[5] Moiseev A. A., Ivonov V. I. (1990). The Handbook of Dosimetry and Radiation Hygiene. M.: *Energoatomizdat*, 252 p. (in Russian).

[6] Kozlov V. F. (1991). Radiation Safety Handbook. M.: *Energoatomizdat*, 352 p. (in Russian).

[7] Mikheev A. N., Zezina N. V., Kutlakhmedov Yu. A., et al. (1991). New phenomena and approaches in investigation of soil-to-plant radionuclide transfer. In "Proceeding of I.U.R. Soviet Branch Seminar on the Radioecology and Counter-measures" Kyiv, DOC UIR, 209–224.

[8] Gudkov I. N. (1980). The dynamics of the meristem and its radioresistance. In book. "Forms of post-radiation restoration of plants". Kyiv: *Naukova Dumka*, 82–115 (in Russian).

[9] Kolosov I. I. (1962). The absorption activity of root systems. M.: *Izdatelstvo Akademii nauk SSSR*, 388 p. (in Russian).

INFLUENCE OF Mn(II) IONS ON FROZEN AND GAMMA IRRADIATED SPIRULINA PLATENSIS

***Eter Gelagutashvili, Alex Gongadze,
Mikheil Gogebashvili., Mikheil Janjalia, Nazi Ivanishvili**

Iv.Javakhishvili Tbilisi State University,
E.Andronikashvili Institute of Physics, Georgia
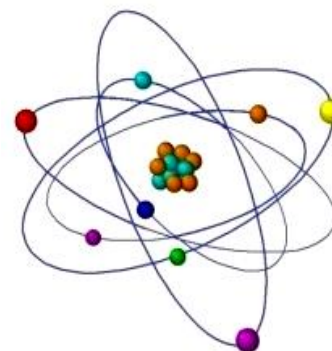
*Corresponding author: eterige@gmail.com

ABSTRACT: *The influence of Mn(II) ions on frozen Spirulina platensis at -80°C and -20°C and high-dose irradiated ^{137}Cs (400 kGy) was studied using a UV–Visible spectrometer. The absorption process was relatively fast in small concentrations of Mn(II) in the case of interaction with irradiated Spirulina platensis. However, for frozen Spirulina platensis, the absorption decrease was regarded as very slow. It was shown that the effect of Mn(II) ions on Spirulina platensis constituents (chlorophyll a, phycocyanin, carotenoids) under various conditions is different.*

Key words: *Spirulina platensis*, Mn(II) ions, gamma-irradiation

INTRODUCTION

Spirulina platensis (filamentous cyanobacteria) is a blue-green microalga with a worldwide distribution, being easily cultivated and controlled, growing naturally in marshes, reservoirs, waterways, and paddy fields. *Spirulina* has been used for food since time immemorial by tribes living around Lake Chad in Africa. The chemical composition of *Spirulina* includes protein (55-70%), carbohydrates (15-25%), essential fatty acids (18%), vitamins, and minerals. *Spirulina* also contains many photosynthetic pigments, such as chlorophylls, carotene, and phycocyanins. Chlorophyll is the most visible pigment in *Spirulina*. It releases ions when struck by the energy of sunlight. These free ions proceed to stimulate the biochemical reactions that form proteins, vitamins, and sugars in *Spirulina* cultures [1]. Carotenoids are generally responsible for the red and yellow hues seen in nature. Beta-carotene accounts for 80% of the carotenoids present in *Spirulina*, which is convertible into vitamin A [2,3]. Phycobiliproteins are a small group of highly conserved chromoproteins that constitute the phycobilisomes, a macromolecular protein complex. The most common classes of phycobiliproteins are C-phycocyanin (CPC), allophycocyanin (APC), and phycoerythrin (PE), which comprise about 20% of the cellular protein. Phycocyanins are an important source of blue pigment for use in food coloring. The photosynthetic energy transfer in the phycobiliproteins (PBPs) from phycocyanin (PC) to chlorophyll a can be influenced by different types of heavy metal ions, such as Hg [4] and Cr [5]. In cyanobacteria, metals exert toxic action mostly by damaging the chloroplast and disturbing photosynthesis [6]. In previous works [7-9], we studied the biosorption and accumulation of different metal ions in this alga and its main protein

phycocyanin in vitro and in vivo under various conditions. In this work, using UV-visible spectrometry, we studied the effect of Mn(II) ions on *Spirulina platensis* frozen at -80°C and -20°C and irradiated with high doses (400 kGy) of ^{137}Cs, and then recultivated.

MATERIALS AND METHODS

Spirulina platensis IPPAS B-256 strain was cultivated in a standard Zarrouk [10] alkaline water-salt medium at 34°C, illumination ~5000 lux, at constant mixing in batch cultures [11]. The cultivation of the *Spirulina platensis* intact cells was conducted for 14 days. The growth was measured by optical density by monitoring changes in absorption at a wavelength of 560 nm using the UV-Visible spectrometer Cintra 10e. *Spirulina* grows optimally in a pH range of 9-11. The intact cell suspension of *Spirulina platensis* at pH 10.1 in the nutrient medium was used for scanning the absorption spectra from 400 to 800 nm. The concentration of *Spirulina platensis* was determined by the instrumental data. *Spirulina platensis* suspension (100 ml) was irradiated with 400 kGy gamma radiation from April to January over 10 months using ^{137}Cs as a gamma radiation source at the Applied Research Center, E. Andronikashvili Institute of Physics (Dose rate -1.1 Gy per minute). After 14 days of cultivation, *Spirulina platensis* was frozen by stepwise freezing at 23°C, 4°C, and then separately at -20°C in one case and -80°C in another case for 48 hours. In the first case, the suspension (100 ml) after irradiation (400 kGy) and freezing (after melting at room temperature) was filled up with Zarrouk medium and then recultivated. The solutions of metal ions were prepared in deionized water with appropriate amounts of inorganic salt. The reagents MnCl2·4H2O were of analytical grade.

RESULTS AND DISCUSSIONS

The influence of Mn(II) ions on *Spirulina platensis* frozen at -80°C and -20°C and high-dose irradiated C^{137s}, and then recultivated, was studied as a function of metal concentration. **Figure 1.** shows the absorption characteristics after irradiation, freezing, and recultivation of *Spirulina platensis* cells. The peak at 681 nm is due to the absorption of chlorophyll a (Chl a). The peak at 621 nm is due to the absorption of phycocyanin (PC). The peak at 500 nm is due to the absorption of carotenoids. A peak at 440 nm is due to the Soret band of Chl a [12]. In **Figure 1.** (A, B, C) the effect of Mn(II) ions on the absorption of irradiated (400 kGy), frozen at -80°C and -20°C, thawed, and recultivated *Spirulina platensis* cells is shown. It is seen from **Figure 1.** that with increasing metal concentrations, absorption intensity decreased for all cases. As can be seen from **Figure 1.** the absorption process was relatively fast at small concentrations of Mn(II) in the case of interaction with irradiated *Spirulina platensis*, but for frozen *Spirulina platensis* the decrease is regarded as very slow. The influence of Mn(II) ions after irradiation (400 kGy) and freezing at -20°C and -80°C, and then recultivation of *Spirulina platensis* constituents (chlorophyll a (Chl a), phycocyanin (PC), carotenoids) are shown in **Figures. 2-5**. It is clear that the effect of Mn(II) ions on the absorption intensity maxima for wavelengths 440 nm, 500 nm, 621 nm, and 681 nm of *Spirulina platensis* constituents is different. In particular, at 440 nm (changes to the Soret band of chlorophyll a), with increasing Mn(II) concentration, the intensity of absorption decreases at a high dose of radiation, decreases less after freezing at

-20°C, but almost does not change at -80°C. Analogous results were received for carotenoids at 500 nm wavelengths. For the change in absorption intensity at 621 nm, which is the peak of absorption of the major protein phycocyanin in *Spirulina platensis*, the absorption intensity very efficiently decreases at a high dose of radiation but almost does not change after freezing at -20°C and -80°C. The influence of Mn(II) ions after irradiation and freezing, and then recultivation of *Spirulina platensis* at 681 nm wavelengths (changes in chlorophyll a) is similar. In the review [13], the stability of phycocyanin (pH, temperature, and light) is discussed, considering the physicochemical parameters of kinetic modeling. The optimal working pH range for phycocyanin is between 5.5 and 6.0, and it remains stable up to 45°C. However, exposure to relatively high temperatures or acidic pH decreases its half-life and increases the

A   B

C
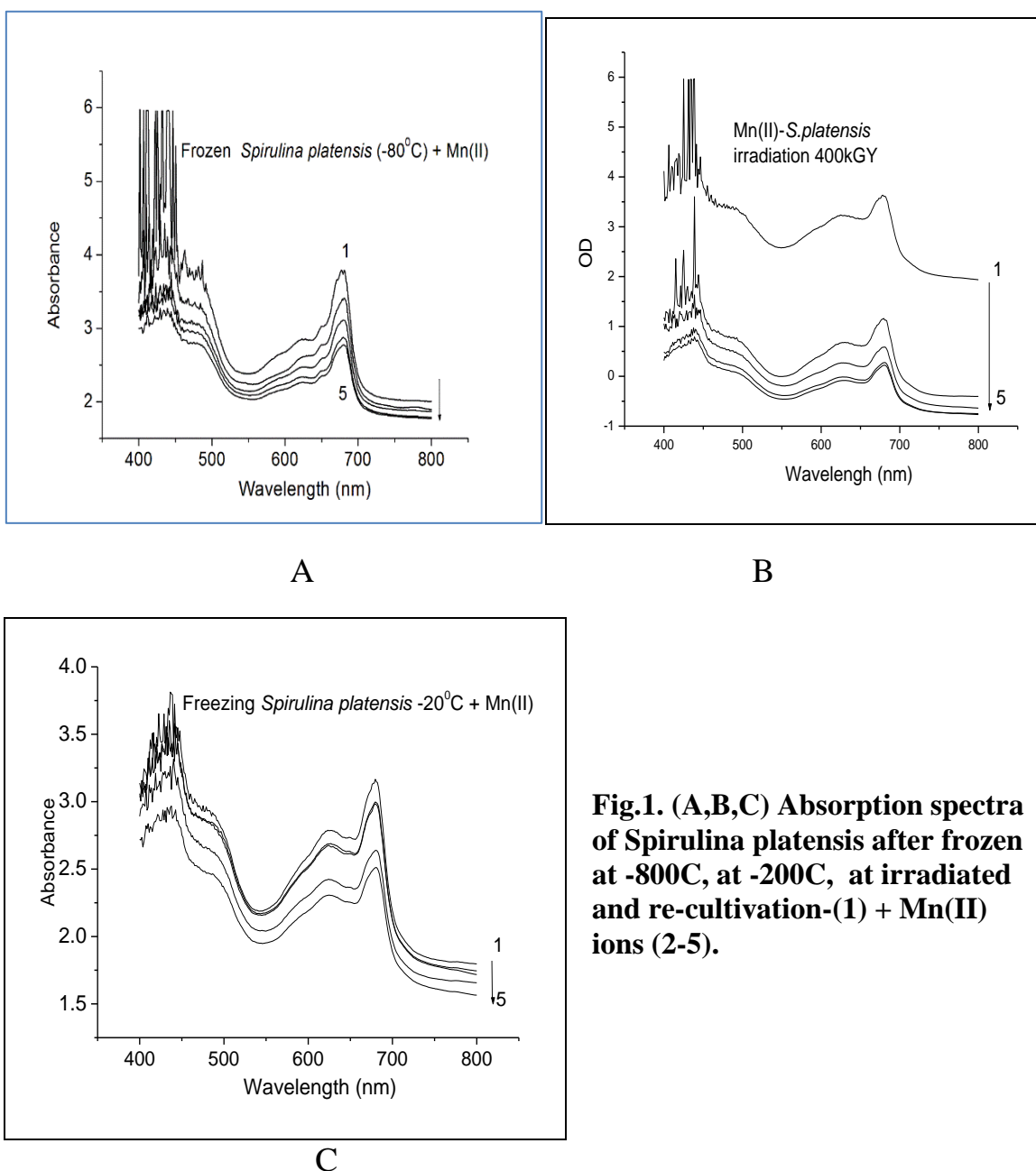
Fig.1. (A,B,C) Absorption spectra of Spirulina platensis after frozen at -800C, at -200C, at irradiated and re-cultivation-(1) + Mn(II) ions (2-5).
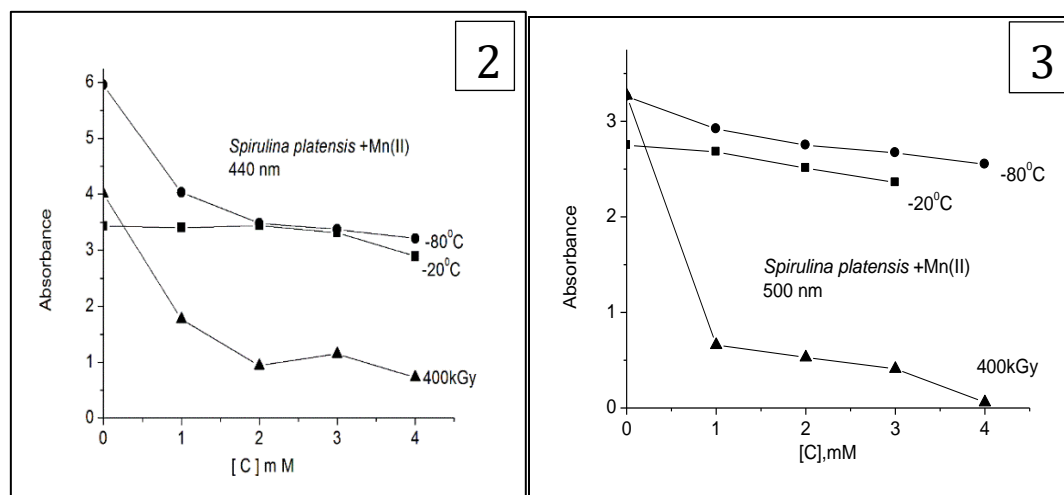
Figure 2. Influence of Mn(II) ions after irradiation (400kGy) and after frozen -20⁰C and -80⁰C on temperature and then recultivation of *Spirulina platensis* (changes to the constituent- soret band into the chlorophyll a)

Figure 3. Influence of Mn(II) ions after irradiation (400kGy) and after frozen -20⁰C and -80⁰C on temperature and irradiated and then recultivation of *Spirulina platensis* (changes in the carotenoids)
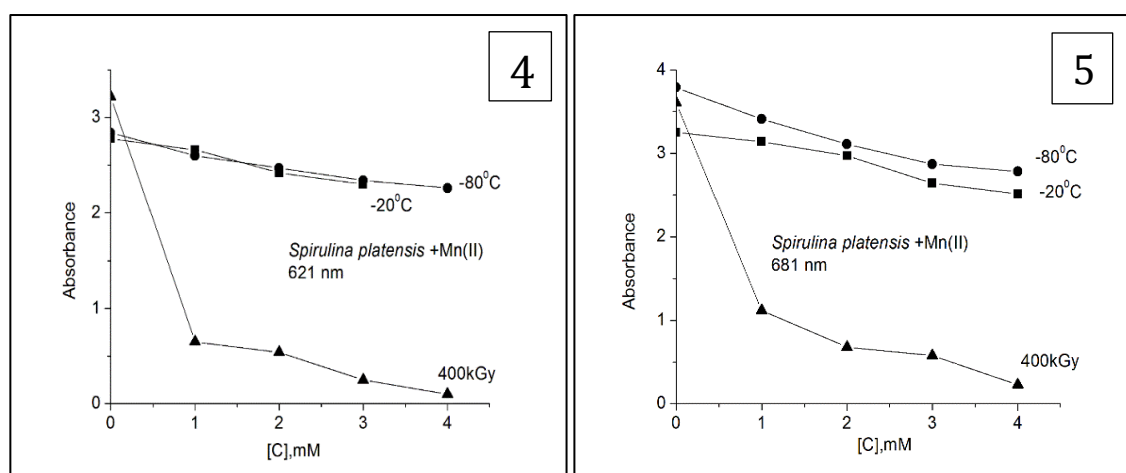
 Figure 4. Influence of Mn(II) ions after irradiation (400kGy) and after frozen -20⁰C and -80⁰C on temperature and irradiated and then recultivation of *Spirulina platensis* (changes in the basic protein -the phycocyanin)

Figure 5. Influence of Mn(II) ions after irradiation (400kGy) and after frozen -20⁰C and -80⁰C on temperature and irradiated and then recultivation of *Spirulina platensis* (changes in the chlorophyll a).

Maximum biosorption capacity of *A. platensis*, determined from the Langmuir equation, was 44.3 mg/g for Mn(II) ions [14]. The raw and enriched microalgal biomass was examined by ICP-OES to determine its multielemental analysis before and after biosorption, FTIR to indicate functional groups that participated in biosorption, and SEM-EDX to illustrate the binding of

metal ions on the surface of algal biomass. FTIR spectroscopy evidenced that biosorption of metal ions was mainly due to carboxylate groups present on the microalgal cell wall. *Arthrospira platensis* turned out to be a good biosorbent of metal ions [14].

Using optical and DSC studies, it was shown that *Spirulina platensis* irradiated with 137Cs γ 400 kGy and then stored under anaerobic conditions in the dark at 4°C remained viable despite 96.9% denaturation of its whole biomass. The DSC data showed that PBSc in the recultivated samples, which were preliminarily irradiated with 10-400 kGy doses, melted cooperatively [15]. Combined effects of ^{137}Cs gamma irradiation and heavy metal ions Ni(II), Zn(II), and Ag(I) on *Spirulina platensis* cells using UV-VIS spectrometry after three times irradiation and recultivation were discussed [16].

It was shown that the possible use of gamma irradiation together with Ni(II) and Zn(II) ions does not change the nature of the interaction of these metal ions with *Spirulina platensis*. Whereas in contrast to the ions Ni(II) and Zn(II), for silver ions, an increase in intensity is observed in both the irradiated and non-irradiated states. The combined effects of ionizing radiation and other stressors such as silver ions on *Spirulina platensis* exhibit synergistic effects for C-phycocyanin as a stimulatory agent to raise its content [16]. FTIR spectroscopy evidenced that biosorption of metal ions was mainly due to carboxylate groups present on the microalgal cell wall. SEM analysis clearly showed that biosorption occurred. While the constituents are distinct among different algal strains, it is necessary to screen the algae with high adsorption capacities for heavy metal ions by analyzing the algal components [17]. The results of field-emission scanning electron microscopy, Fourier-transform infrared, and X-ray photoelectron spectroscopy analyses of the N-containing functional groups indicated that *Spirulina platensis* was successfully immobilized on the alginate matrix [17,18].

Chronic kidney disease is a significant health problem. In work [19], the protective mechanism of *Spirulina platensis* against γ-irradiation (R) and/or thioacetamide (TAA)-induced nephrotoxicity in rats was investigated. Rats intoxicated with R or TAA showed alterations in kidney function markers, antioxidant enzymes, and several inflammatory markers. Rats also acquired apoptosis, evidenced by high caspase-3 activity [19]. The high subzero preservation of *Spirulina*: *Spirulina platensis* CMU2 and *Spirulina platensis* GD1 was performed by stepwise freezing at 25°C, 4°C, and -20°C for 30 min. Then they were preserved at -80°C for seven months with four cryoprotectants: dimethyl sulfoxide, horse serum, calf serum, and glycerol. The viability of these two strains and cell concentration was not significantly different. The survival of *Spirulina platensis* depended on the type and concentration of cryoprotectant and thawing temperature [20]. This apparent protective effect of *SP* is mediated by the regulation of miR-1 and miR-146a gene expression, preventing the release of ROS, inflammation, apoptosis, and autophagy via the AMPK/mTOR pathway. Subsequently, administration of *SP* could be a convenient food supplement for protection against R and/or TAA-induced nephrotoxicity.

Thus, as of today, the investigation of irradiated and frozen *Spirulina platensis* and the effect of metal ions on it is very relevant, both for medical purposes and as promising biosorbents for the removal of toxic metals from industrial effluents due to the presence of various free functional groups.

REFERENCES

[1]. Rangel-Yagui, O., Danesi, G., Carvalho, M. and Sato, S. 2004, Chlorophyll production from Spirulina platensis: cultivation with urea addition by fed-batch process. Bioresour. Technol., 92(2), 133–141.

[2]. Theodore, S. and Georgios, S. 2013, Health aspects of Spirulina (Arthrospira) microalga food supplement.J. Serb. Chem. Soc., 78 (3), 395-405.

[3]. Vonshak, A. 2002, Use of Spirulina Biomass, In: Spirulina platensis (Arthrospira) Physiology Filament Biology and Biotechnology. (Ed. Vonshak, A.), Taylor & Francis, ISBN, London, pp. 159-173.

[4]. Murthy SDS. 1991. Studies on bioenergetic processes of cyanobacte¬ria: Analysis of the effect of selected heavy metal ions on energy linked process.

[5]. Middepogu A, Murthy SDS. 2011, Altered energy transfer in phycobili¬somes of the cyanobacterium, Spirulina platensis under the in¬fluence of chromium (III). Journal of Pure and Applied Sciences. 19, 1-3.

[6]. Ma Z, Lin L, Wu M, Yu H, Shang T, et al. 2018, Total and inorganic arse¬nic contents in seaweeds: absorption, accumulation, transfor¬mation and toxicity. Aquaculture. 497, 49-55.

[7]. Gelagutashvili, E. 2014, Biosorption of Heavy Metals by Spirulina Platensis and their Components, invited chapter in collected book: Plants and Microbes (eds: Pankaj Goyalabhishek Chauhanpurshotam Kaushik), chapter 9, 154-174. ISBN: 9788185708300. https://www.flipkart.com/plants-microbes-an-innovative-approach/p/itmc7c3a395393f8

[8]. Gelagutashvili, E. 2013, Binding of Heavy Metals with C-Phycocyanin: A Comparison between Equilibrium Dialysis, Fluorescence and Absorption Titration, American Journal of Biomedical and Life Sciences, 1,(1), 12-16. https://dx.doi.org/10.11648/j.ajbls.20130101.13

[9]. Monaselidze, J., Gelagutashvili, E., Bagdavadze, N., Gorgoshidze, M. and Lomidze, E. 2019, Simultaneous Effects of Cd(II) and Pb(II) ions and γ-irradiation om Stability of Spirulina platensis. Eur. Chem. Bull. 8(2), 38-43.
https://www.scilit.net/article/17e0c0bbb8ac3157afa429e09e8d3e37

[10]. Zarrouk C., 1966, Contribution to the cyanophyceae study: influence various physical and chimical factors on growth and photosynthesis of Spirulina maxima (Setch et Gardner) Geitler extract. Doctorate Thesis, Faculty of Sciences. University of Paris, France. p. 146.

[11]. Mosulishvili, L., Belokobilsky, A., Gelagutashvili, E., Rcheulishvili, A., Tsibakhashvili, N. 1997, The Study of the mechanism of cadmium accumulation during the cultivation of Spirulina Platensis. Proceedings of the Georgian Acad. of Sciences, Biol. series, 23(1-6), 105-113. ISSN - 0132-6074.

[12]. Fork, DC and Mohanty, P. 1986, Fluorescence and other characteristics of blue-green algae (cyanobacteria), red algae, and cryptomonads. In: Govindjee, Amez J. and Fork DC (eds) Light Emission by Plants and Bacteria, pp 451–496. Academic Press, Orlando, Florida

[13]. Aïda Adjali, Igor Clarot, Zilin Chen, Eric Marchioni, Ariane Boudier. 2022, Physicochemical degradation of phycocyanin and means to improve its stability: A short

review, Journal of Pharmaceutical Analysis, 12(3),406-414.

    https://doi.org/10.1016/j.jpha.2021.12.005

[14]. Izabela Michalak, Małgorzata Mironiuka, Katarzyna Godlewskab, Justyna Tryndac, Krzysztof Marycz, 2020, Arthrospira (Spirulina) platensis: An effective biosorbent for nutrients, Process Biochemistry, 88, 129-137.

https://doi.org/10.1016/j.procbio.2019.10.004

[15]. Monaselidze, J., Gelagutashvili, E., Gogebashvili, M., Gorgoshidze, M., Gongadze,A., Bagdavadze,N., Kiziria,E. 2022, Survival and growth of Spirulina platensis cells and thermodynamic stability of their main proteins after recultivation following irradiation with Cs137 γ doses of 0 to 400 kGy, Algal Research, 15 November, 102900. https://doi.org/10.1016/j.algal.2022.102900.

[16]. Gelagutashvili, E., Bagdavadze, N., Gongadze, A., Gogebashvili, M., Ivanishvili, N. 2021, Effect of Ag(I), Ni(II), Zn(II) ions on irradiated Spirulina platensis, e.prints: arXiv:2102.02007 [physics.bio-ph],Cornell University.

[17]. Jinghua Liu, Changwei Zhu, Zhengpeng Li and Haoyuan Zhou.. 2022, Screening of Spirulina strains for high copper adsorption capacity through Fourier transform infrared spectroscopy, METHODS article, Front. Microbiol., Sec. Microbiotechnology, v.13. https://doi.org/10.3389/fmicb.2022.952597

[18]. Purev, O., Park, C., Kim, H., Myung, E., Choi, N., Cho, K. 2023, Spirulina platensis immobilized alginate beads for removal of Pb(II) from aqueous solutions. Int. J. Environ. Res. Public. Health. 20(2), 1106. doi: 10.3390/ijerph20021106. PMID: 36673865; PMCID: PMC9859109.

[19]. Salem AA, Ismail AFM. 2021, Protective impact of Spirulina platensis against γ-irradiation and thioacetamide-induced nephrotoxicity in rats mediated by regulation of micro-RNA 1 and micro-RNA 146a. Toxicol. Res. (Camb). 10(3),453-466. doi: 10.1093/toxres/tfab037. PMID: 34141159; PMCID: PMC8201556.

[20]. Manita Motham, Yuwadee Peerapornpisal, Sudaporn Tongsriri, Chayakorn Pumas and Panmuk Vacharapiyasophon, 2012, High subzero temperature preservation of Spirulina platensis (Arthrospira fusiformis) and its ultrastucture, Chiang Mai J. Sci. 39(4), 554-561. http://it.science.cmu.ac.th/ejournal/

A NEW APPROACH TO THE CALCULATION OF THE CARCINOGENIC RADIOGENIC RISK
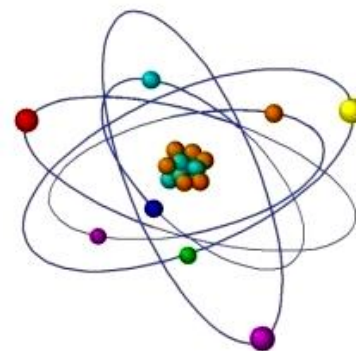
[1]**Oleksandr Mikhyeyev**[*], [2]**Oksana Lapan**

[1]Institute of Cell Biology and Genetic Engineering,
National Academy of Science of Ukraine, Ukraine
[2]National Aviation University, Ukraine

[*] Corresponding author: mikhalex7@yahoo.com

ABSTRACT: *A new method of calculating the carcinogenic risk factor (CRF) in accordance with the influence of ionizing radiation is proposed based on data concerning the level of spontaneous DNA degradation. It is shown that the CRF value can be at least 2 orders of magnitude less than the generally accepted values of this parameter. Accordingly, the costs of radiation protection can be reduced to the same extent. The specified estimates were obtained using assumptions about the non-threshold action of ionizing radiation and the linear dependence of 'dose-effect' on the parameter of carcinogenic action, and may be overestimated for this reason.*

Key words: radiation carcinogenesis, dietary risk

Currently, the expenses for radiation protection and radiation regulation on a global scale have amounted to about 10 trillion US dollars. The approach proposed in the article for assessing radiogenic carcinogenic risk will reduce the level of current expenditures for these purposes by at least two orders of magnitude.

Our interest in this problem has arisen in connection with a paradoxical situation – an extreme discrepancy between the significance of the problem of radiation safety and regulation, on the one hand, and the number of relevant studies conducted in the countries of the former Soviet Union. The problem of assessing the risk of stochastic consequences (primarily carcinogenic) of the action of ionizing radiation has two aspects. Firstly, it is a dosimetric sub-problem (the adequate assessment of the dose of ionizing radiation, its distribution over critical tissues and organs, etc.). Secondly, it is a sub-problem of assessing the kind and type of relationship among absorbed doses and the probability of stochastic effects. As far as the analysis of the Russian literature allows, the efforts of radiobiologists in the post-Soviet space are concentrated mainly on the first aspect. As for the second aspect, in risk calculations, almost everyone is guided by the recommendations of the ICRP [1, 2].

According to WHO experts, annually in the world, out of the total number of 50 million people who die, more than 5 million people have cancer as the cause of death. In the USSR, back in the years of stagnation, malignant tumors accounted for 14% of all causes in the overall structure of mortality.

From all non-accident sources of human exposure (natural radiation background (NRF), nuclear testing, nuclear power engineering, occupational exposure (NPP workers, radiologists, X-ray specialists, pilots, cosmonauts), medical exposure for diagnostic and therapeutic purposes, the use of fertilizers containing radionuclides (40K), household radiation from goods whose work is accompanied by ionizing radiation (computer monitors and televisions), the average annual individual effective equivalent dose of radiation in 1981-1985 was 5.05 mSv. 2.25 mSv of this dose was due to exposure to NRF.

According to L. A. Ilyin [3], the average per capita dose expected during the coming life due to the Chernobyl accident for the population of the former USSR will be 1.17 mSv (0.46%), including for Belarus - 10.6 mSv (4.04%), for residents of the Zhytomyr, Kyiv, and Chernihiv regions - 3.68 mSv (1.4%), for residents of the central regions of Ukraine - 1.43 mSv (0.56%), for 272.8 thousand people living in areas of strict radiation control - 197.6 mSv (43.9%).

With the accumulation of doses in human organs and tissues from units to several tens of Sv, the relationship between the dose and the incidence of tumors is linear. The difficulties in determining the dose dependence of the frequency of malignant neoplasms (MNs) begin in the dose range that exceeds the doses from NRF but is close to the background values. The radiobiology of quasi-background doses (the doses close to the background values) does not have a sufficiently powerful arsenal of methods and means for solving this problem yet, but even now we can assume that the non-threshold concept underlying the calculation of radiation risks is taken into account only for humane reasons, the basis for which is the material possibilities of the state to protect the population from the blastomogenic effects of radiation.

For the calculations in the field of quasi-background ('low') doses, the ICRP, IAEA, UNSCEAR, USSR NCRP, Russian NCRP, and Ukrainian NCRP have adopted and continue to accept as a basis a non-threshold concept, the essence of which is the assumption of a linear dependence of the frequency of malignant neoplasms (MN) on the dose throughout the dose range. It is believed that for 1 million people per cSv in addition to the background values of absorbed doses, from 100 to 1000 or more cases of fatal cancer may occur (see Table 1) [4].

Table 1. The risk of developing radiation-induced malignancies during a person's life in the population of 1 million, each member of which received a radiation dose of 1 cSv

Organization, researcher	Risk ratio
ICRP	125 (before 1984) and 600 (after 198.. (lethal cases)
United Nations Scientific Committee on the Effects Atomic Radiation (UNSCEAR) - 1977	100 (lethal cases)
John Hoffman - 1981	3333 - 4255 (neoplasms)
Rosalie Pertel – 1982 within 11 - 30 years after irradiation throughout life	369 - 823 (neoplasms) 549 - 1648

It is easy to see that the assessment of radiation risk is very vague, indicating once again the absence of a sufficiently rigorous level of scientific validity in the proposed assessments. Consequently, we have attempted to evaluate (reassess) it based on data concerning the spontaneous instability of DNA (thermodynamic, chemical).

However, firstly, let's see how the carcinogenic risk coefficients recommended for usage by the ICRP [1] work in relation to the assessment of the consequences of the Chernobyl accident. Taking into account the value of the collective dose received by the inhabitants of the "affected" regions of Ukraine, Belarus, and Russia (approximately 200,000 person-Sv according to the estimates of L. A. Ilyin and his colleagues [5]) and the carcinogenic risk coefficient proposed by the ICRP, the number of lethal cancers should be estimated at approximately 10,000 (we note, by the way, that the Chernobyl Forum estimates this value at 4,000), which is less than one percent of the spontaneous level of diseases of this type. Identifying such a relatively small "addition" to the spontaneous level is practically impossible, given the rather high level and significant annual fluctuations in the spontaneous level of carcinogenesis.

The comparison of the qualitative and quantitative ranges of spontaneous and radiation-induced DNA damage, as well as the frequency ranges of the distribution of cancer in individual human organs and tissues, has shown a high level of similarity. If we arrange the organs in ascending order of the probability of inducing cancer deaths per unit of absorbed dose, we get the following order: bone surface, thyroid gland, ovaries, liver, mammary gland, bladder, esophagus, red bone marrow, lungs, stomach.

When compared with several organs and tissues arranged according to the increase in spontaneous frequencies of induced cancer deaths (thyroid gland - ovaries - liver - esophagus - mammary gland - skin - lungs - stomach), it can be concluded that the pattern of spontaneous cancer coincides with the pattern of radiation-induced cancer. The exception is the skin, for which the spontaneous level occupies one of the first places (resulting from UV radiation).

There is also a qualitative similarity in the spectrum of DNA damage (single breaks because of depurination and/or depyrimidinization, direct breaks, and deletions of DNA, etc.) induced by endogenous factors (thermodynamic lability of the DNA molecule, DNA-modifying enzymes and agents, ROS, etc.).

Thus, it can be stated that there is no clear specificity in the carcinogenic effect of ionizing radiation compared to the spontaneous spectrum of carcinogenesis.

According to existing estimates [6, 7, 8], the rate constant of DNA degradation as a result of spontaneous single-strand breaks practically coincides in various biological objects belonging to different radiotaxa (phages, bacteria, mammals, etc.) and varies in the range $(1-9)\times10^{-11}$ s^{-1}, which is six orders of magnitude higher than the corresponding constant of DNA degradation under the action of radiation from the average natural radiation background (NRF) $(2\times10^{-17}$ s$^{-1})$.

Based on the foregoing, we assume that the frequency of spontaneous cancers (approximately 3,000 cases per 1 million people per year [9]) is directly dependent on the level of spontaneous DNA degradation and that the frequency of cancer induced by NRF is in the same direct correlation with the level of DNA degradation induced by radiation from NRF. At the same

time, the proportion of cancer induced by NRF should be 1×10^{-6}th of the level of spontaneous cancers, i.e., approximately 0.003 additional cases of diseases per year per 1 million people.

During the year, 1 million people receive from NRF radiation a collective effective dose of the order of 0.24×10^6 cSv, which, according to our assumption, is likely to induce these 0.003 additional cases of cancer. There will be 0.012 additional cases of cancer per 1 million cSv people per year. Even over a 100-year life, this risk will be 1.2. Thus, the coefficient of the carcinogenic risk due to ionizing radiation can be at least two orders of magnitude less than the generally accepted values of this parameter. It should also be considered that our estimates were obtained using assumptions about the non-threshold and linearity of the dose-effect relationship and may even be overestimated for this reason.

It would probably be appropriate to mention the phenomenon of radiation hormesis, which, although not sufficiently studied yet to base the regulation of irradiation on it, is nevertheless essential evidence of the threshold effect of ionizing radiation. At the same time, there are sufficient grounds to consider the possible anticarcinogenic effect of irradiation hormesis, which was observed in Japanese children who suffered from the atomic bombings of 1945 – the number of spontaneous (!) leukemia cases in children irradiated at doses of 5–100 mSv decreased by two-thirds [10].

Thus, taking into account the value of the collective dose received by the inhabitants of the "affected" regions of Ukraine, Belarus, and Russia (approximately 200,000 person-Sv according to the estimates of L. A. Ilyin and his colleagues [5]), the carcinogenic risk coefficient calculated by us, the number of lethal cancer cases should not exceed 20-30 cases, which is more than two orders of magnitude lower than the estimates of the Chernobyl Forum.

REFERENCES

[1]. Radiation safety. (1994). ICRP Recommendation. ICRP Publication 60. Part 1. M.: Energoatomizdat, 192.

[2]. The norms of radiation safety of Ukraine (NRBU-97); Sovereign hygiene standards. (1997). Kyiv: Department of Polygraphy of the Ukrainian Centre of State Sanitation Inspection of the Ministry of Health of Ukraine, 121.

[3]. Ilyin L. A. (1996). Realities and myths of Chernobyl. M.: "ALARA Limited", 474.

[4]. Moskalev Yu. I., Zhuravlev V. F. (1983). Levels of risk under various conditions of radiation exposure. M.: Energoatomizdat, 112.

[5]. Ilyin L. A., Kirillov V. F., Korenkov I. P. (1999). Radiation hygiene. M.: Medicine, 384.

[6]. Vilenchik M. M. (1987). DNA instability and long-term effects of exposure to radiation. M.: Energoatomizdat, 192.

[7]. Sarapultsev B. I., Geraskin S. A. (1991). Genetic nature of the phenomenon of cell radiation resistance. Radiobiology, 31 (4), 593–599.

[8]. Billen D. (1994). Spontaneous DNA damage and its significance for the "Negligible Dose" controversy in radiation protection. BELLE, 3 (1), 8–11.

[9]. Balange A. (1987). Biology of tumors. Doubts and hopes. M.: Mir., 206.

[10]. Keirim-Markus I. B. (2002). Non-constructive radiation hormesis. Med. radiol. and radiats. Security, 2, 73–76.

GIGANTISM OF PHOTOSYNTHESIZING ORGANS IN DECIDUOUS AND CONIFEROUS TREE SPECIES UNDER CONDITIONS OF ELEVATED BACKGROUND OF IONIZING RADIATION
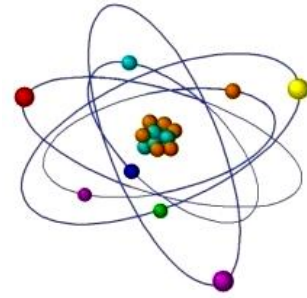
*Oleksandr Mikhyeyev[1], Oksana Lapan[2]

[1]Institute of Cell Biology and Genetic Engineering, National Academy of Science of Ukraine,
[2]National Aviation University, Ukraine

*Corresponding author: mikhalex7@yahoo.com

ABSTRACT: *The research results on the effects of indirect action of ionizing radiation on tree species according to morphological parameters are presented. The phenomenon of gigantism in the needles of Pinus silvestris and Picea excelsa was observed at absorbed doses in the range of 2-10 Gy. In this case, the shoots carrying numerous large buds were distinguished by very large needles, the length of which was 1.5-2.5 times greater than the control values. The phenomenon of gigantism in the leaf apparatus, particularly in needles, served as a basis for considering the possible role of integral reactions to irradiation, which could be expressed in the radiation modification of physiologically normal correlative interactions between different parts and organs of the plant. The assumption that radiomorphoses in the form of giant leaf blades are caused by the reproductive death of cells of individual apical meristems, resulting in disrupted trophic interactions in the irradiated plant, is justified.*

Key words: ionizing radiation, integral reactions, radiomorphoses, radiation chimeras.

After the Chernobyl Nuclear Power Plant accident, a unique situation emerged in its exclusion zone, allowing for the study of not only purely radioecological problems but also general problems of plant biology, particularly those related to the morphogenesis of plant organs. It is clear that the Chernobyl disaster could not go "unnoticed" by radiobiology and radioecology. The interest generated by this event led to a surge of publications, suggesting the emergence of a fundamentally new field requiring additional research efforts. But was this really so? Did the Chernobyl accident indeed lead to any truly unique radiobiological and radioecological phenomena and processes, differentiating them from previously known phenomena? From our point of view, the peculiarity of the accident can be discussed only in terms of its "technical" characteristics, mainly concerning the nature of radionuclide contamination of natural and man-made objects (the patchiness of radionuclide contamination of landscapes, the peculiarities of radionuclide fractionation in radioactive precipitation, etc.).   The uneven nature of the distribution of radionuclides (R.n.) in the territories adjacent to the accident zone, the presence of vertical heterogeneity in the distribution of R.n. in the soil and the presence of "hot" fuel and aerosol (condensation) particles in the habitat of plants and animals led to the fact that living

organisms in the zone of radionuclide contamination began to be unevenly influenced by sources of ionizing radiation of very heterogeneous composition and spatial distribution. However, considering that the actual radiobiological stage of interaction of the radiation factor with the biosystem begins with the penetration of R.n. into the organism or with the onset of significant external exposure from radionuclides concentrated in the environment, the "prehistory" of R.n. migration at this stage is of no significant importance for assessing the radiobiological effect, only reflecting on the kinetics of the external exposure or the dose and power characteristics of radiation from R.n. incorporation into the organism. While the power of radiation impact and the nature of R.n. distribution in tissues may change, this does not create, practically, new situations of interaction between radiation and biological objects, and therefore does not entail a qualitatively new radiobiological phenomenology. Thus, it can be assumed that at this stage, existing observations, experimental facts, and theoretical positions in radiobiology should be sufficient to explain the radiobiological phenomena ultimately caused (directly or indirectly) by the Chernobyl accident.

Nevertheless, the Chernobyl accident led to significant changes in radiobiology and radioecology. If the totality of radiobiological problems is represented as a problem spectrum with its qualitative (a multitude of problem areas) and quantitative (human, material, and time resources spent on solving a specific problem) characteristics, it can be stated that in the post-accident period it underwent only quantitative changes, and the shift in research emphasis occurred in the area of previously little studied and researched problems, such as problems of radioadaptation, radiation aging, carcinogenesis, etc. In addition, radiobiologists began to pay more attention to radiobiological and radioecological effects caused by irradiation with ionizing radiation in the range of doses and powers close to the corresponding values of the natural radiation background (NRF).

One of the radiobiological directions whose problems have gained particular relevance is the study of integral (distant, mediated, indirect) reactions of biological systems to irradiation. The complexity, multi-level nature of biological systems, and the correlated functioning of their components and structures inevitably reflect in their radiobiological reactions. Depending on the range of applied or studied doses/powers, the balance of direct and mediated reactions of biological objects to irradiation changes. In general, radiobiology faces the task of obtaining a statistical or analog model of the reaction of any biological system to irradiation, taking into account the reactions of all its constituent elements. Since biological systems are multi-level, in fact, it is necessary to build an entire hierarchy of such models, i.e., mechanisms.

The search for mechanisms of a specific observed radiobiological phenomenon for a specific structure must always be conducted with regard to the interconnectedness of the studied structure with other structures of the same level of organization that may also participate in forming its reaction to irradiation. For example, the well-known phenomenon of gigantism in spruce needles, observed in plants growing in some areas of the 30-km zone of the Chernobyl Nuclear Power Plant with an elevated level of radionuclide contamination and, accordingly, with increased (several orders of magnitude exceeding the NRF levels) doses of ionizing radiation, could be explained by considering it as a direct result of irradiation on the needles [1]. However, the strict adherence to the principles of a systemic approach, and in particular,

the requirement to describe the mechanism of the phenomenon at a specific structural and functional level, involving information about the behavior or reaction of elements directly forming this level, forces us to look for another explanation for the phenomenon of needle gigantism.

In 1986, after the Chernobyl accident, there was a significant reduction in the growth of apical shoots in common pine (*Pinus silvestris* L.) in almost all areas of the Chernobyl Exclusion Zone with absorbed doses from 3 to 20 Gr, and the shoots themselves had a curved form. In common spruce (*Picea excelsa* (Lam.) Link.), as a rule, shoots with shortened growth retained linear growth but were distinguished by a strong thickening of needles and acquired the form of a "lamp brush" [2-4]. Irradiation in 1986 and 1987 led to the increase in the quantitative characteristics of the leaf apparatus in coniferous and deciduous tree species in some cases (Fig.1).
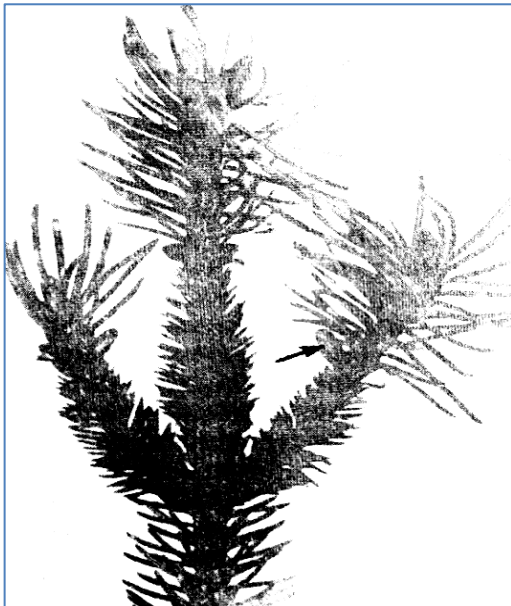
Figure.1. A lateral shoot from the top of the crown of a 25-year-old spruce with giant needles formed in 1987 under radiation exposure at a dose of 4-5 Gr. Lateral buds at the base are shown with an arrow [4]

Gigantism was also observed in the needles of *Pinus silvestris* and *Picea excelsa* at absorbed doses in the range of 2-10 Grays. Typically, shoots carrying numerous large buds were characterized by very large needles, with lengths 1.5-2.5 times, and cross-sectional areas 2.6-5.6 times bigger than the control values. The increase in needle size was generally noted at the apical part of the shoots in *Picea excelsa* and at the base of the shoots in *Pinus silvestris*. In deciduous species (*Guercus rubra* L. and *Guercus rubra* L., red and common oak, *Betula verrucosa* Ehrh. weeping birch, *Sorbus aucuparia* L. common rowan, *Tilia codata* Mill. small-leaved lime, *Robinia pseudacacia* L. white acacia, etc.), leaf gigantism was mainly observed in 1987. It was most clearly observed in *B. verrucosa* at doses of 40-60 Grays and higher, and in *G. rubra* at 8-10 Grays. The volume of needles in *Picea excelsa* in 1987 in some areas was 10-15 times bigger than that of the needles in 1986. Such giant needles were formed mainly on P. excelsa that received an elevated dose of ionizing radiation. The noted tendency towards gigantism persisted in 1988. The phenomenon of radiation-induced gigantism of the leaf apparatus and, in particular, the needles, served as a basis for us to consider the possible role of integral reactions to irradiation, which could be expressed in radiation modification of physiologically normal correlative interactions between different parts and organs of the plant. From our point of view, irradiation at comparatively low (subthreshold) doses for differentiated cells (forming the bulk of the photosynthesizing tissue), but lethal for meristematic cells (primarily, cells of apical stem meristems), led to the mass but not continuous

death of stem growth points. It can be assumed that a small number of surviving apices received an increased amount of assimilation products (primarily sugars), synthesized by a photosynthetic apparatus that has a significantly higher radio resistance [1,5], and which, thus, provided an increased amount of nutrients substances to a limited number of stem apices ("waiting" meristems) and needles embedded in their structures.   Thus, needle gigantism is probably a consequence of the disruption of correlative relationships in the irradiated plant. In any case, such an assumption should be considered first when studying the mechanism of the described phenomenon. The validity of such an approach is confirmed by data from N.I. Goltsova [6]. It turned out that the complete or partial death of terminal and lateral buds of irradiated shoots of *Pinus Silvestris L.* led to an increase in the lifespan of the old, pre-accident needles of 1984-1985. This may indicate that leaf aging is the result of complex correlative influences, in which the competition of plant organs for phytohormones (cytokinins, auxins, and gibberellins), assimilates, and water play an important role. Apparently, with the death of individual apical buds, such competition decreased, i.e., reduced or completely disappeared apical dominance, regulated by auxins and cytokinins, as a result of which cytokinins, transported upwards from the root in conditions of the death of apical buds, stimulated the growth of remaining adventitious and dormant buds. Another confirmation of the made assumption is the results of research by G.M. Kozubov and A.I. Taskaev [2], in particular, the indication that the partial volumes of tissues in the giant needles were close to the norm, i.e., the usual ratio of quantitative parameters of needle tissues was not violated. Moreover, according to these researchers, giant needles were formed practically on all trees with partially affected crowns, with the needles on pines with a higher (but not 100%) degree of radiation damage being the largest. It is also evident that the gigantism of needles could not significantly manifest in the first year after the disaster, as in the zones of sublethal radiation action, its mass influence on growth processes was not yet observed. And, indeed, gigantism was observed mainly in needles formed in 1987, i.e. in needles formed after the Chernobyl accident.

If the gigantism of the needles were a direct result of ionizing radiation, then massive changes at the cytological and histological levels would be observed. Such changes occured [7], but they were not total. Most mesophyll cells were close to normal size, and no reliable correlation was found between changes in their parameters and specific volume and the absorbed dose of ionizing radiation.

What was the reason for the increase in the size of the needles? In the giant needles of the pine, the diameter of the resin channels increased, and the cross-sectional area of the epidermis and hypodermis, as well as the cross-sectional area of the conducting cylinder, increased by 1.5-2 times. Overall, the increase in the cross-section of individual elements was parallel to the increase in the total cross-sectional area of the needles. A similar pattern was observed in the needles of spruce. In 1987, the majority of trees saw a sharp increase in all needle parameters, and vegetative shoots formed large, straight, and highly curved, thickened needles. Along with the general increase in spruce needle parameters in 1987, there was an increase in the diameters of cells in the epidermis, hypodermis, and mesophyll, with the most intense enlargement of histological elements observed in needles with the maximum cross-sectional areas (which exceeded even the pre-accident 1985 values, i.e., the absolute values were generally

proportional to the overall morphometric indicators). The relative (partial) volumes of tissues remained close to those of normal needles. An exception was the relative volume of the conducting cylinder, which reached its greatest values in the severely shortened needles in 1986 and in the giant needles in 1987. The diameters of the resin channels also increased significantly [7]. It is not by chance that we dwelled in such detail on the cytological characteristics of the giant needles. It is known that the difference in size of identical and same-aged plant organs is determined not by the number of cells but by their size [8]. The results mentioned above perfectly illustrated this point. This is most true for spruce needles, in which practically all types of cells uniformly reacted by increasing their size. The mesophyll cells of giant pine needles were practically indistinguishable from analogous control cells. Considering that hormesis (the positively stimulating effect of ionizing radiation, regardless of whether it affects the object directly or indirectly) can reveal the phenotypic (morpho-functional) potential for the growth and development of a biological object, it can be concluded that the morpho-functional potential of mesophyll cells of pine needles was more fully realized. Thus, the radiation factor can act as a factor testing the expression of gene activity at the epigenetic level of regulation [9].

Critical to the inhibitory effect of ionizing radiation on woody plants are their forming tissues - apical (top) and lateral (side) meristems. It is their reaction that determines the morphofunctional character of the remote consequences of radiation [10]. In the Chernobyl disaster zone, coniferous and deciduous trees were subjected to dose loads during active growth and formative processes, determined by a high level of proliferative activity of meristematic cells. In this state, they have increased radiosensitivity and are easily damaged by relatively low doses [11]. Acute and subsequently powerful chronic irradiation in the spring of 1986, on the one hand, affected the buds of shoots, leaves, needles and reproductive organs that were formed during the previous year, and, on the other hand, affected the primordia that were formed in the year of the disaster. What types of cellular reactions might underlie the morpho-functional disturbances induced by radiation? Firstly, they should be divided into lethal and non-lethal. The former, in its turn, are observed in the form of interphase (metabolic and apoptotic) and reproductive (proliferative) death. Metabolic death of plant cells is not associated with the genetic effect of ionizing radiation, but is caused mainly by multiple damage of membrane structures. Most likely, this type of death of differentiated cells caused the death of needles in the zone of lethal damage (lethal doses).

Another possible form of death is apoptosis, which normally is an integral part of plant development mechanisms and represents a genetically determined cell death program (programmed cell death - PCD). The implementation of this program in ontogenesis is accompanied by specific changes in cell morphology, nuclear and cytoplasmic structure, activation of caspases, nucleases, domain, and internucleosomal fragmentation of nuclear DNA. This process is observed in various plant tissues and, like cell differentiation, may be controlled by phytohormones. The apoptotic type of plant cell death can be triggered by many factors, including unfavorable ones (oxidative stress, UV, and gamma radiation, etc.). The key role in the initiation of certain types of PCD belongs to mitochondria: as in animals, the induced exit of cytochrome and other protein factors from the mitochondria triggers apoptosis in plant cells. Reactive oxygen species (ROS) can serve as trigger molecules of apoptosis, and

antioxidants suppress apoptosis in plants [12].

The reason for reproductive death of cells is lethal mutations associated with the irreversible disruption of chromosomal structure, leading to the cell's loss of proliferative ability. A cell that has died by the mechanism of reproductive or interphase death loses the ability to give rise to a cell line (stream), a necessary element of the morphogenetic process, the consequence of which can be various morphological anomalies - radiomorphoses. Does the interphase type of cell death (ID) play any role in the formation of radiomorphoses? It is known that the ID of plant cells is observed at doses exceeding those that induce reproductive death by two orders of magnitude - several hundred and several Grays respectively [13]. ID is characterized by a threshold, mass manifestation, i.e., practically 100% of irradiated cells die by this mechanism when certain absorbed doses are reached. Probably, ID of cells due to its massiveness can lead to a complete stop of growth and morphogenetic processes. Thus, if we are talking about morphological abnormalities induced by radiation, then to explain them it is enough to assume the activation of mechanisms of reproductive cell death.

Based on the above and using the results of observations of needle death and morphological anomalies, it is possible to hope that in the future a method of biological retrodosimetry can be developed based on the mentioned facts and patterns. Thus, irradiation at doses of 10-20 Grays led to the complete death of the above-ground organs of pine and spruce during the vegetation period in 1986, which indicates the metabolic type of death of the forming cells. Even if we did not know the corresponding doses, they could be restored by the nature of cell death, for which, however, additional research would be required to obtain calibration curves. Unlike interphase death, reproductive death is not a mandatory total (mass) effect when a cell population or tissue is irradiated. Cells that have lost their reproductive ability differentiate rapidly, age, but do not die immediately by the metabolic mechanism. The surrounding cells do not lose their reproductive ability and give rise to normal cell lines.

Thus, radiomorphoses are most likely caused by the reproductive death of individual cells (the result of lethal mutations) scattered randomly through the formative tissue and/or are the result of non-lethal somatic mutations affecting the physiological and biochemical parameters of the mutated cell and the surrounding cells. In the latter case, chimeric tissues consisting of genetically heterogeneous somatic cells are formed [14-15].

The real spectrum of morphological anomalies of plant organs of woody species, identified during the survey of forests in the zones of sublethal and medium damage, in the autumn of 1986 and spring of 1987, was very broad. Can the goal be set to create a semblance of the periodic system of chemical elements based on radiation-induced anomalies and find out to what extent all possible variants of anomalies were fully realized in real conditions, i.e., how fully the cells of such a "periodic system" were filled? Creating such a system would have enormous heuristic value for the theory of biological morphogenesis, as well as for the theory of radiation-induced anomalies (theory of radiomorphoses). Moreover, assuming a dependence of the qualitative and quantitative characteristics of the spectrum of induced morphoses on the qualitative and quantitative characteristics of the radiation factor, one could apply the method of generalized parameters and correspond a certain gradation of dose load to a certain expression of the characteristics of morphological anomalies. In this way, a calibration

dependence would be obtained, which could become the basis for the method of biomorphological retrodosimetry. It is obvious that such a task setting is also possible concerning functional parameters.

REFERENCES

[1] Grodzinsky D. M. (1989). Radiobiology of Plants. Kyiv: Naukova Dumka, 384 p. (in Russian).
[2] Kozubov G. M., Taskaev A. I., Abaturov Y. D. (1988). Assessment and Forecast of the State of Coniferous Forests in the Chernobyl Nuclear Power Plant Accident Area. In Chernobyl-88, Proceedings of the First All-Union Meeting on the Results of the Elimination of the Consequences of the Accident at the Chernobyl Nuclear Power Plant, Vol. 3, Part 2, Chernobyl, 21–35 (in Russian).
[3] Kozubov G. M., Kuzivanova S. V. (1990). Features of the Effect of Ionizing Radiation on the Morphogenesis of Vegetative Shoots of Conifers. In Radiation Impact on Coniferous Forests in the Chernobyl Nuclear Power Plant Accident Area. Syktyvkar: Komi Scientific Center of the Ural Branch of the Academy of Sciences of the USSR, 30–53 (in Russian).
[4] Kozubov G. M., Taskaev A. I. (1994). *Radiobiological and Radioecological Research of Woody Plants.* –St. Petersburg: Science, 256 p. (in Russian).
[5] Savin V. N. (1981). The Effect of Ionizing Radiation on the Whole Plant Organism. Moscow: Energoizdat, 120 p. (in Russian).
[6] Goltsova N. I. (1990). The Influence of Radioactive Contamination on the Structural Features of Common Pine Pinus Silvestris L. (Chernobyl). In Chernobyl-90, Proceedings of the 1st International Conference "Biological and Radioecological Aspects of the Consequences of the Chernobyl Nuclear Power Plant Accident," Vol. 1, Plant Radioecology, Radioecology of Terrestrial Animals, Radioecology of Hydrobionts. – Green Cape, 74–89.
[7] Goltsova N.I., et al. (1991). *Chernobyl Radionuclide Accident: Effect on the Shoot Structure of Pinus Sylvestris.* Ann. Bot. Fenn., Vol. 28, No. 1, 1–13 (in Russian).
[8] Bilokin I. P. (1975). *Growth and Development of Plants*. Kyiv: Higher School, 432 p. (in Ukrainian).
[9] Vakhtin Y. B. (1980). *Genetic Theory of Cellular Populations.* Leningrad: Science, 168 p. (in Russian).
[10] Gudkov I. N. (1985). *Cellular Mechanisms of Post-Radiation Recovery of Plants*. Kyiv: Nauk. Dumka, 223 p. (in Russian).
[11] Clowes F.A.L. (1963). *X-irradiation of Root Meristems.* – Ann. Bot.Vol. 27, No. 106, 343–352.
[12] Vanyushin B. F. (2001). *Apoptosis in Plants. Successes in Biological Chemistry.* Vol. 41, 3-338 (in Russian).
[13] Grodzinsky D. M., Mikheev A. N. (1984). *Patterns of Gamma-induced Interphase Death of Tobacco Callus Cells.* Academy of Sciences of the USSR, Scientific Council on Radiobiology Problems, Information Bulletin. Moscow, p. 92 (in Russian).
[14] Shevchenko V. V., Grinikh L. I. (1981). *Chimerism in Plants*. Moscow: Science, 212 p. (in Russian).
[15] Gottschalk W., Wolff G. (1983). *Induced Mutations in Plant Breeding.* Berlin, etc.: Springer-Verlag, p. 238.

STUDY OF THE RADIONUCLIDE ABSORPTION IN TO THE VEGETATIVE ORGANS OF GRAPES TO INCREASE THE EFFICIENCY OF SOIL MECHANICAL DECONTAMINATION
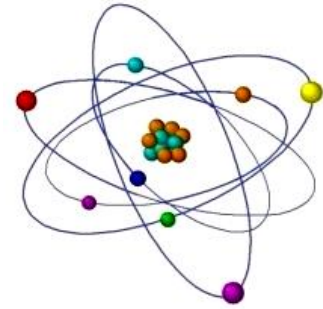
[1,2]Ivanishvili Nazi[*], [1]Gongadze Alex, [2]Kalmakhelidze Sophio, [3]Tulashvili Eremia, [1,2]Gogebashvili Mikheil

[1]Iv.Javakhishvili Tbilisi State University, E. Andronikashvili Institute of Physics, Georgia
[2]I.Beritashvili Center of Experimental Biomedicine, Georgia
[3]Iv.Javakhishvili Tbilisi State University, N. Kekelidze Materials Research Institute, Georgia

*Corresponding author: nazikoivanishvili@gmail.com

ABSTRACT: *Several man-made accidents at nuclear power plants and nuclear tests in recent years have highlighted the need to develop countermeasures that can effectively reduce the absorption of radionuclides by grape plants in viticulture. These measures should be cost-effective and easy to implement in everyday agricultural practice. To evaluate these parameters, we conducted experiments on ^{137}Cs contaminated soil. Our studies revealed the dynamics of the distribution of radionuclide contamination across the vegetative parts of the grapevine, the research also highlights the significance of vertical zone depth for the penetration of radiocesium into the plant. It was concluded that shifting the depth of the space between the rows of the vineyard by the deep plow makes it possible to move the soil layer contaminated with radionuclides into relatively deep layers, which will significantly reduce the penetration of radionuclides into the grape plant.*

Key words: Radionuclides, soil, *Vitis vinifera. L*

INTRODUCTION

In the processes of active development of various technologies in human economic activity, a large number of substances used are not found in the natural environment, and are pollutants of natural ecosystems [1]. The chemistry of the pollutants is very diverse, which makes it difficult to develop a universal technology for their utilization [2,3]. Especially radioactive waste is highly dangerous for humans and the environment. In the radioecological aspect, noteworthy are long-lived radionuclides, which can be involved in the metabolic pathways and circulation of substances in living organisms. Transfer and subsequent accumulation of radionuclides in the soil-plant continuum have gained increasing attention. Radionuclides in the soil are taken up by the plants leading to their accumulation in the organisms of food chain and represent a danger for ecosystem. This is the reason for the great interest researchers show in the selection of soil deactivation and the suitable remediation technique [4,5,6]. Over the past decade, many studies aimed at solving the problem of rehabilitating contaminated areas [7,8]. One of the most common and effective methods of soil cleaning is to remove the top layer of soil and store it in a controlled manner for a long time. However, this method generates a large amount of

radioactive waste, and the fertile layer of soil is completely removed. It is important to mention that above mentioned method is quite expensive, as it involves expenses for mechanized soil removal, transportation, and burial of large quantities of soil. The method of deep plowing of the soil is more cost-effective and useful for mechanical decontamination of soils associated with the cultivation of perennial plants, where removing the soil cover without harming the plants is technically challenging. This statement can be applied to vineyards. As the cultivation of this culture counts several decades. Our study aimed to localize radionuclide-^{137}Cs marker in the grape's vegetative organs depending on the depth of soil contamination zones. The purpose of this study was to determine if the deep plowing method can increase the efficiency of mechanical soil decontamination in vineyards.

MATERIALS AND METHODS

The object of study was the „Chinese" grape (*Vitis vinifera L*) widespread throughout the Georgian territory. Standard vine sprouts were placed in soil for rooting and then transferred to its permanent place of cultivation. The substrate was soil contaminated with radiocesium, which had been stored in sealed containers for 20 and 30 years to simulate long-term environmental exposure. For radiospectrometric analysis, the material was taken according to the plant's vegetative growth phase. The vegetative parts of the plant were dried, and fragmented in a homogenizer to standard particle sizes, and radioisotope activity was determined in a Marinelli dish.

The content of radionuclides was determined by gamma-spectrometry (Gamma-Beta Spectrometer, Atomtex-MKC-AT-1315 and Gamma-Spectrometer CANBERRA with liquid nitrogen cooled germanium detector). At the same time, the content of radioisotopes was determined in the soil used.

RESULTS AND DISCUSSION

It is widely recognized that radionuclides primarily accumulate in plant tissues via the root system, where roots absorb water along with water-soluble radionuclides, facilitating their transfer to the vegetative organs through sap flow. The level of radioactivity in plant tissues is influenced not only by species characteristics and radionuclide concentrations in soil layers but also by the interplay between soluble and insoluble fractions in these layers. The intensity of radionuclide accumulation in plants through the root system is evaluated based on factors such as shoot biomass increase, radionuclide distribution in the root system, and the availability of physical and chemical forms of radionuclides in soil profiles. Our study focused on cultivating a specific grape variety in typical soil conditions. Soil activity, determined through spectrometric analysis, revealed levels of 1250 Bq/kg for 137Cs and 980 Bq/kg for 40K. The amount of radionuclide absorbed by a plant is influenced by age-related changes in plant physiology. Each growth phase corresponds to distinct physiological processes, impacting nutrient absorption. Our investigation analyzed radio cesium content in various grape plant tissues throughout different growth stages. The distribution and localization of radiocesium in grape plant tissues vary depending on the plant's seasonal

development stages, as illustrated in **Figure 1.** For instance, during germination and growth stages (**Figure 1. a, b**), radiocesium is prominently localized in grape leaves, while in later developmental stages, including periods of physiological rest, it tends to accumulate more intensively in young tissues and sprouts (**Figure 1. c**).
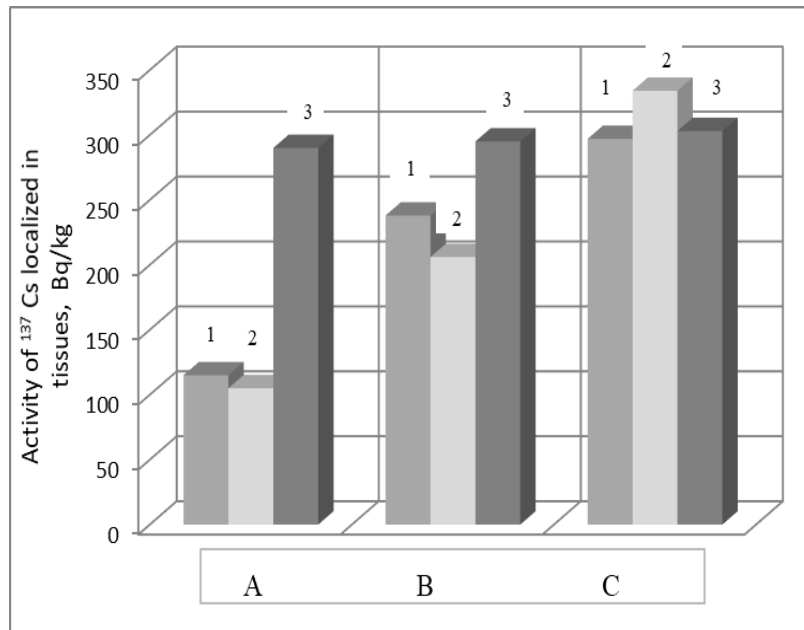
Figure 1. - Distribution of absorbed radioactive cesium in the tissues of vegetative organs depending on the stages of growth and development of grape plant.

A- Germination stage (March-April); **B**- Active growth stage (May-June);
C-physiological resting stage (September-October);
1-Leaves; 2-Sprouts of current year; 3-perineal stem

The transfer of radiocesium within the biological chain is influenced by various factors, with radioactive potassium-40K being particularly noteworthy. Radiocesium shares similar chemical properties with potassium, leading to comparable metabolic processes within biological organisms. The movement intensity of cesium and potassium in plants is approximately similar, with their absorption dependent on the total concentration of both elements and their relative characteristics relative to total concentration. Both cesium and potassium accumulate in similar organs and tissues, and their acceptable ratio is determined by their quantitative content. To explore the dynamics of radioactive potassium accumulation in plant organs alongside radioactive cesium, we determined the activity of radioactive potassium. **Figure 2.** illustrates the distribution of radioactive potassium among plant organs throughout the vegetative cycle. However, unlike radiocesium, a decrease in its activity is observed in the leaves and current-year sprouts.
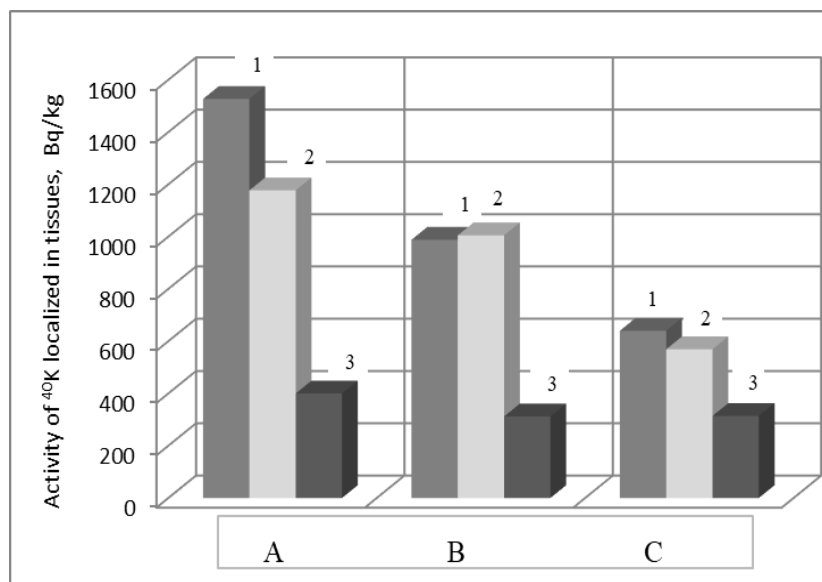
Figure 2.-Distribution of absorbed radioactive potassium in the tissues of vegetative organs depending on the stages of growth and development of grape plant
**A-**Germination stage (March-April); **B**- Active growth stage (May-June); **C**-physiological resting stage (September-October); 1-Leaves; 2-Sprouts of current year; 3-perineal stem

Potassium is a vital nutrient for plants, but unlike nitrogen and phosphorus, it is not a part of the organic matter of plants. It exists in the form of ions, soluble salts or forms unstable complexes with cytoplasmic colloids in cells. This explains why potassium is highly mobile during the various stages of plant growth and development. Potassium compounds can actively move in plant tissues, allowing for their reuse by moving from old to young tissues. The refore, this movement can result in varying levels of potassium content in leaves and stems.

The data obtained from the study show that it is feasible to use plants in the stage of physiological dormancy to study the deep distribution of radionuclides in soil. At this stage, the migration of radionuclides is almost complete and the total absorption rate of radionuclides for one season can be calculated.

In the next stage of research, we used the factor of radionuclide penetration into vegetative parts of plants by modeling the level of vertical distribution of pollution zones. The soil contaminated with radionuclides was added layers in the experimental soil and as a result, we identified three zones of radionuclide contamination in the soil:1-Superficial contamination zone (1-25 cm); 2-Total contamination zone (1-50 cm) and 3-Deep contamination zone (25-50 cm) **Figure 3. Figure 3.** shows that grapes grown in vertically contaminated soil have the greatest absorption of radionuclides in a specific zone. The first zone contains 95.8% of the total radiocesium absorption, while the third zone contains only 5.9%. However, maintaining clear boundaries between contamination zones during long-term cultivation can be technically challenging, although the pattern of radionuclide distribution into the plant's vegetative parts is evident. The obtained results show the main ways of the penetration of radionuclides into the grape plant; Namely, with air pollution of agrocenosis, radiocesium appears mainly in the upper soil layer [9,10,11,12]. which has been observed for different nature zones and the entire territory of

Georgia [13], and this value, as a rule, does not exceed 15-20 centimeters in depth. Therefore, an effective method of reducing the absorption of radionuclides into the plant is to deep plow and transfer the contaminated upper layer of soil to deeper horizons.
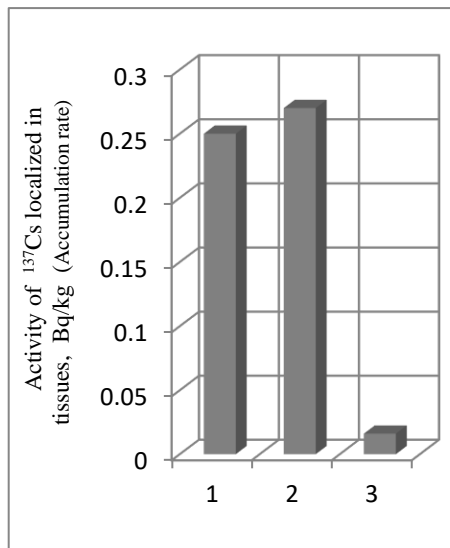
Figure 3. Three zones of cesium radionuclide contamination in the soil concerning the accumulation of radioisotopes in plants

1-Radioactive contamination zone 1-25 cm;
2-Radioactive contamination zone 1-50 cm;
3-Radioactive contamination zone 25-50 cm

CONCLUSION

Based on the conducted studies, we can conclude that mechanical cleaning of radiocesium contaminated soil surface layer significantly reduces the penetration of radiocesium into the vegetative parts of the grape plant, thereby preventing the dangers of radiation contamination in vineyards.

REFERENCES

[1]. Ranjeet Kumar Mishra, Spandana Samyukthalakshmi Mentha, Naveen Dwivedi Emerging pollutants of severe environmental concern in water and wastewater: A comprehensive review on current developments and future research. Water-Energy Nexus. Volume 6, 2023, Pages 74-95.

[2]. Vikas Kumar, Chadetrik Rout, S. Baskoutas. A review on the clean-up technologies for heavy metal ions contaminated soil samples. Heliyon, Volume 9, Issue 5, 2023, e15472.

[3]. B. Senthil Rathi, P. Senthil Kumar, Dai-Viet N. Vo, Critical review on hazardous pollutants in water environment: Occurrence, monitoring, fate, removal technologies and risk assessment. Science of The Total Environment, Volume 797, 2021, 149134.

[4]. Friederike Strebl, Sabine Ehlken, Gerald Kirchner. Behavior of radionuclides in soil/crop systems following contamination Radioactivity in the Environment, 2007.

[5]. Y. G Zhu, G Shaw. soil contamination with radionuclides and potential remediation, Chemosphere, 2000.

[6]. M. A. Edomskaya, S. N. Lukashenko, S. V. Korovin. Estimation of radionuclides global fallout levels in the soil contamination with radionuclides and potential remediation of CIS and eastern Europe territory. Journal of Environmental Radioactivity, 2022.

[7]. Neil Willey, Chris Collins, Phytoremediation of soil contaminated with radionuclides. Radioactivity in the Environment, 2007.

[8]. B.J. Merkel, M. Hoyer. Radionuclide Behaviour in the Natural Environment, Science, Implications and Lessons for the Nuclear Industry Woodhead Publishing Series in Energy, 2012, Pages 601-645.

[9]. Gerald Kirchner, Friederike Strebl, Martin H. Gerzabek. Vertical migration of radionuclides in undisturbed grassland soil Journal of Environmental Radioactivity September 2009 Journal of Environmental Radioactivity. Volume 100, Issue 9, 2009, Pages 716-720

[10]. S. Askbrant, J. Melin, J. Sandalls, G. Rauret, R. Vallejo, T. Hinton, A. Cremers, C. Vandecastelle, N. Lewyckyj, Y.A. Ivanov, S.K. Firsakova, N.P. Arkhipov, R.M. Alexakhin. Mobility of radionuclides in undisturbed and cultivated soils in Ukraine, Belarus and Russia six years after the Chernobyl fallow. Journal of Environmental Radioactivity. Volume 31, Issue 3, 1996, Pages 287-312.

[11]. P. Bouisset, M. Nohl, A. Bouville, G. Leclerc. Inventory and vertical distribution of ^{137}Cs, $^{239+240}$Pu and ^{238}Pu in soil from Raivavae and Hiva Oa, two French Polynesian islands in the southern hemisphere. Journal of Environmental Radioactivity. Volume 183, 2018, Pages 82-93.

[12]. Tengiz F. Urushadze, Dimitriy V. Manakhov. Radioactive contamination of the soils of Georgia. Annals of Agrarian Science. Volume 15, Issue 3, 2017, Pages 375-379

INVESTIGATION OF RADON RADIOACTIVE EMISSION IN NATURAL WATERS OF VILLAGE KVEMO KHVITI (GEORGIA)
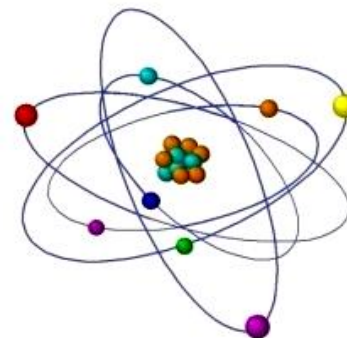
*Lela Mtsariashvili, Maia Shermadini

[1] Iv.Javakhishvili Tbilisi State University, Faculty of Exact and Natural Sciences, N.Kekelidze Materials Research Institute, Georgia
[2] Kvemo Khviti Public School, Gori Municipality, Georgia

*Corresponding author: mtsariashvili2005@yahoo.com

ABSTRACT: *In the present work it was studied the content of radioactive gas radon - Rn-222 in the number of sources of surface water located nearby to village Kvemo Khviti, (Gori Municipality) in the territory of so-called Kartli artesian basins. Research was carried out during a year once a quarter. Radon detector RAD7 was used for determining radon content. It was established, that radon content in water considerably changes depending on the source location as well as on water type too. So, for example, radon content in various sources of water was within the limits from several units of Bq/L up to 10 Bq/L. A comparison with literary data has been carried out.*

Key words: Radon, surface water, activity concentration, village Kvemo Khviti

INTRODUCTION

Radioactivity is not created by human, it is a part of the environment and is everywhere - in rocks, the surface of the earth, the atmosphere, etc. Since the 50-60s of the last century, the problem of radioactive radiation on the environment and living organisms (including humans) has been the subject of numerous studies. Scientists have determined that radioactivity affecting human health is caused by three families of natural radionuclides - Th-232, U-238 and U-235, as well as K-40. Among these radionuclides, special attention is paid to radioactive gas - radon (Rn-222), whose contribution to natural radioactivity is up to 50%.

Radon (Rn) is an element of the Mendeleev's periodic system, with atomic number 86. Radon is a colorless, odorless, tasteless, and well soluble in water, radioactive gas. It is the heaviest gas at room temperature. The most stable isotope (Rn-222) has a half-life of 3.8 days.

In nature, nuclei of radon are constantly produced during the radioactive decay of primary parent nuclei. By mass, its balanced content in the Earth's crust is 7×10^{-16}%. Due to its chemical inertness, radon relatively easily leaves the crystalline matrix of the "parent" mineral and gets into groundwater, natural gases and air. Since Rn-222 is the longest-lived isotope among the four natural isotopes of radon, its content in the environment is the maximum. The content of radon in the air depends, first of all, on the geological structure (for example, granites, which contain a lot of uranium, are an active source of radon, while the radon content on the surface

of the seas is very small), as well as on the weather (during rains, microcracks through which radon enters the soil are filled with water; snow cover also prevents radon from entering the air). An increase in radon concentration in air is observed before earthquakes, probably due to higher active exchange of air due to microseismic activity in the ground. The solubility of radon in water is 460 ml/l; the solubility in organic solvents and in human adipose tissues is tens of times higher than the solubility in water [1].

Radon is a naturally occurring, radioactive, noble gas that is ubiquitous in soil, air, and water. Radon continuously flows from the Earth's rocks as a result of the fission of the uranium (U-238) nucleus. The amount of uranium in the earth's core is low (for example granite, phosphates), so the loss of radon is constantly compensated and there is always a certain equilibrium concentration of it in the atmosphere. The released radon dissolves in the groundwater and rises with it to the earth's surface [2]. If radon-containing water is used for domestic use (shower, dishwashing, etc.), radon released from the water accumulates in living spaces. Radon accumulated in the indoor air of buildings can pose a health risk [3, 4].

If the groundwater is used for drinking purposes, the radon content of the water must be taken into account. According to the USA Environmental Protection Agency (EPA), radon dissolved in drinking water causes an average of 168 cancer deaths each year, 89% of which are lung cancer (caused by radon released from water) and 11% stomach cancer (caused by radon content in drinking water) [5]. Since drinking water is a necessary element for life, relevant institutions have developed recommendations on the content of radon in drinking water. According to the recommendation of the European Commission, the level of radon in drinking water is 100 Bq/L, and if the activity exceeds 1000 Bq/L, then safety measures should be taken [6], and the level suggested by EPA is 11.1 Bq/L [5].

Systematic studies of the state of radon distribution in water resources of Georgia is an actual problem. The work presents the results of the research of radon activity in the surface waters of the village of Kvemo Khviti (Gori municipality, Georgia), together with the students of the public school.

 PROBLEM STATEMENT

There are several artesian basins in East Georgia some of which are used for reception and supply of the population by drinking water. These artesian basins feed the numerous springs located on the whole territory of the region. Research of their natural radioactive activity represents doubtless interest from the scientific point of view as well as from the practical point of view.

The objective of the work was studying of features of radon content distribution depending on geographical factors in surface sources of water, located in Kartli artesian basin. In the present publication, there are given and generalized all results of the carried out researches for the period of winter and spring.

RESEARCH OBJECTS

The object of the study was the surface and drinking water of the territory of village Kvemo Khviti and the surrounding areas (Gori municipality, Georgia), where the radioactive gas radon

research was planned. For the research, there were selected 10 control points, located in Kvemo Khviti village and surrounding areas. The list of control points is given in Table 1.

Table 1. List of control points selected for radon research

№	Control point	Characteristics of the sample	Location of the control point
1	WT-1	Central tap water	v. Kvemo Khviti
2	WT-2	Drinking water from the reservoir	"--------"
3	WR-1	River (Liakhvi) water 1	v. Pkhvenisi
4	WW-1	Drinking water from the well	v. Variani
5	WSp-1	Drinking water from the spring	"--------"
6	WR-2	River (Liakhvi) water 2	v. Pkhvenisi
7	WT-3	Central tap water	v. Kvemo Khviti
8	WT-4	"--------"	v. Kvemo Khviti
9	WW-2	Drinking water from the well	v. Variani
10	WSp-2	Drinking water from the spring	v. Variani

Notes: WSp – spring water; WW – well water, WR – river water, WT – Tap water.

METHODOLOGY

Sampling - Sampling was carried out in special glass containers; the volume of the container is 250 mL. Containers were filled with water up to the top and densely closed by a cover. Then the selected water samples were transported to the laboratory for analysis.

Of the three isotopes of radon, the subject of research is Rn-222, because the half-lives of Rn-220 and Rn-219 are much shorter, and they decompose before migrating into soil and rocks, and their amount in the air is insignificant. Electronic radon detector RAD7 was used for the determination of radon content in water. The RAD7 device uses a method for the registration of radon decay products, namely alpha particles Po-218, Po-2014 and Po-210 (which are formed as a result of decay), based on the use of a solid semiconductor sensor.

Detailed information on measurements and processing of results can be found in the literature [7].

RESULTS

Four expeditions were carried out, during which a total of 40 water samples were taken based on the instructions given in advance to the students. Results of carried measurements are given in Table 2.

Table 2. Average minimum and maximum values of radon activity in different types of water samples taken from Kvemo Khviti village and surrounding areas

value	Water type											
	WSp			WW			WT			WR		
	aver	min	max	aver	min	max	aver	min	max	aver	min	max
A_{av}, Bq/L	4.9	2.9	6.2	5.8	4.6	7.3	4.7	3.7	6.0	0.1	0.03	0.3

Apparently from the received results, it is possible to note that the highest content of radon was observed in artesian well water with an average of 5.8 Bq/L, and the lowest with an average of 0.10 Bq/L in river water.

Table 3 shows a comparison of the received results with some literary data. Apparently from the data, the results received in the present work lay within the values received in other publications.

Table 3. Radon content in surface water in different countries

№	Country (region)	Water type	A, Bq/L			Lit.
			ave.	min.	max.	
1	Lebanon (Beirut, Mount Lebanon, Beqaa, etc)	WSp	29.0	9.8	49.6	[8]
		WW	7.3	0.9	19.9	
2	India (Rajasthan)	WUn	3.3	1.6	5.4	[9]
3	Iran (Mashhad)	WSp	16.1	12.6	20.6	[10]
4	Turkey (Tokat city)	WSp	-	0.13	1.20	[11]
5	Georgia (village Kvemo Khviti)	WSp	4.9	2.9	6.2	Present work
		WW	5.8	4.6	7.3	
		WT	4.7	3.7	6.0	
		WR	0.1	0.03	0.3	

ANALYSIS

Relatively high values of radon concentration in groundwater (artesian, well, spring waters) are due to the fact that these waters are saturated with radon, which is formed in the deep layers of the soil, rises up and dissolves in the groundwater.

Relatively low concentration of radon in surface waters (the water of the Liakhvi River) is related to the process of radon degassing, i.e. the process of passing from water to the atmosphere.

In the drinking water, collected by the students, the obtained values of radon concentration do not exceed the threshold level recommended by the US Environmental Protection Agency (US EPA) for drinking water (11 Bq/L) [12].

Thus, the conducted studies have shown that the radon content in the tested drinking water samples is not extreme, and from the point of view of radiological safety, consumption of these waters does not represent a health hazard.

CONCLUSIONS

According to the radon activity in the surface water samples, most of the the examined control points belong to the groups of low (0.3 - 1.0 Bq/L) or higher than typical (3 - 10 Bq/L) radon activity groups.

The obtained results were compared with the literature data. The average values are significantly lower compared to the data of other countries.

REFERENCES

[1] https://ka.wikipedia.org/wiki/radon

[2] http://www.ncdc.ge/Pages/user/LetterContent.aspx?ID=72269971-c496-4f20-802b-51042d712ebb

[3] J. Nikolov, N. Todorovic, S. Forkapic, I. Bikit, D. Mrdja, Wld. (2011). Acad. Sci., Eng. Tech., 52, 307–310;

[4] Roba C. A., Codrea V., Olah Ş., Niţă D., Cosma C., (2012). Geothermics, 4, 32–46;

[5] EPA (U. S. Environmental Protection Agency), 64. Federal Register, Washington, 9559–9599 (1999);

[6] E.C. (European Commission), 2001/982/Euratom, L344/85-88;

[7] Jakhutashvili T., Tulashvili E., Khikhadze N., Mtsariashvili L. (2009). Measurement of radon contents with use of modern mobile alpha-spectrometer RAD-7. *Georgia Chemical Journal*, Vol. 9, No. 2, pp. 179-182;

[8] Abdallah S.M., Habib R.R., Nuwayhid R.Y., Chatila M., Katul G. (2007). Radon measurements in well and spring water in Lebanon. *Radiation measurements*, vol. 42, no. 2, pp. 298-303;

[9] Duggal V., Mehra R., Rani A. (2013). Analysis of radon concentration in drinking water in Hanumangarh district of Rajasthan, India. *Radiation Protection and Environment*, Vol. 36, Is. 2, pp. 65-70;

[10] Mowlavi A.A., Binesh A. (2006). Radon concentration measurement in some water sources of Mashhad Region in Iran. *IFMBE Proceedings*, Vol. 14/1, pp. 498-499;

[11] Yiğitoğlu I., Öner F., Yalim H. A., Akkurt A., Okur A. and Özkan A. (2010). Radon concentrations in water in the region of Tokat City in Turkey. *Radiation Protection Dosimetry*, 142 (2-4), pp. 358-362;

[12] Federal Register. July 18, 1991. Part II. Environmental Protection Agency. 40 CFR Parts 141 and 142. National Primary Drinking Water Regulations; Radionuclides; Proposed Rule. (56 FR 33050);

Requirements for Authors

- The article should be submitted to the A4 format in the text editor Microsoft Office Word;
- Areas: upper - 20 mm; Left - 30 mm; Right -20 mm; Bottom - 20 mm
- Font: Times New Roman. Interval -1,0
- In the article formulas must be typed in the formula's editor Equation
- Drawings and illustrative materials should be inserted in the JPEG or TIFF format
- Write the article title (14 Pt, Bold) on the first line
- Bypassing the line - the surname and first name of the author(s) (11 Pt, Bold)
- One of the authors will need to be identified as the corresponding author (*), with their full name and email address displayed.
- Full name of the organization on the next line, with indicating the country or residence (11 Pt, Bold, in case of participation of different organizations in the article should be used „1")
- Skipping of two lines - abstract (11 Pt, Italics, not more than 500 words)
- Maximum 5 Key words (11Pt)
- Contents of the article (11Pt) by skipping the line

- Bypassing two lines – references (10 Pt). Used literature should be numbered according the sequence it is used in the main text (when citing inside the text, the number of the source should be written in square brackets). Use the following example while creating the reference list:

  [1] Author(s') surname(s) and initial(s). (Year of publication). Article name. *Journal in which the article is published*, *issue*, pages.

  [1] Derwing, T. M., Rossiter, M. J., & Munro, M. J. (2002). Teaching native speakers to listen to foreign-accented speech. *Journal of Multilingual and Multicultural Development*, *23*(4), 245-259.

- Electronic version of the article must be sent to the e-mail: radiobiologia2020@gmail.com
- The file must be named by the last name of the author

The editorial board is responsible for the topics of the materials submitted for publication in the journal, and the authors' responsibility relies on the content of the article, the results and conclusions. The publisher is not responsible for possible damages, which could be a result of content derived from this publication and any liabilities arising from them remain the responsibility of the authors. Articles incompatible with the above-mentioned requirements or incompatible with the theme of the article are not considered for publication. Materials are published by the author's editorship.